

Aerodynamic Shape Optimization of Axial Turbines in Three Dimensional Flow

Mohammad Arabnia

A Thesis
in
The Department
of
Mechanical and Industrial Engineering

Presented in Partial Fulfillment of the Requirements
for the Degree of Doctor of Philosophy at
Concordia University
Montréal, Québec, Canada

March 2012

© Mohammad Arabnia, 2012

CONCORDIA UNIVERSITY
School of Graduate Studies

This is to certify that the thesis prepared

By: **Mohammad Arabnia**

Entitled: **Aerodynamic Shape Optimization of Axial Turbines in Three
Dimensional Flow**

and submitted in partial fulfilment of the requirements for the degree of

Doctor of Philosophy

complies with the regulations of the University and meets the accepted standards
with respect to originality and quality.

Signed by the final examining committee:

_____ Dr. L.A.C. Lopes (Chair)

_____ Dr. Azzeddine Soulaïmani (Ext. to School)

_____ Dr. Ali Dolatabadi (Examiner)

_____ Dr. Hoi D. Ng (Examiner)

_____ Dr. Fariborz Haghighat (Ext. to Program)

_____ Dr. Wahid S. Ghaly (Supervisor)

Approved by _____
MIE Department Chair or Graduate Program Director

_____ 2012 _____
Dean, Faculty of Engineering and Computer Science

ABSTRACT

Aerodynamic Shape Optimization of Axial Turbines in Three Dimensional Flow

Mohammad Arabnia

Aerodynamic shape optimization of axial gas turbines in three dimensional flow is addressed. An effective and practical shape parameterization strategy for turbine stages is introduced to minimize the adverse effects of three-dimensional flow features on the turbine performance. The optimization method combines a genetic algorithm (GA), with a Response Surface Approximation (RSA) of the Artificial Neural Network (ANN) type. During the optimization process, the individual objectives and constraints are approximated using ANN that is trained and tested using a few three-dimensional CFD flow simulations; the latter are obtained using the commercial CFD package Ansys-Fluent. To minimize three-dimensional effects, the stator and rotor stacking curves are taken as the design variable. They are parametrically represented using a quadratic rational Bézier curve (QRBC) whose parameters are directly and explicitly related to the blade lean, sweep and bow, which are used as the design variables. In addition, a noble representation of the stagger angle in the spanwise direction is introduced. The described strategy was applied to optimize the performance of the E/TU-3 axial turbine stage which is designed and tested in Germany. The optimization objectives introduced the isentropic efficiency and the streamwise vorticity, subject to some constraints. This optimization strategy proved to be successful, flexible and practical, and resulted in remarkable improvements in stage performance.

ACKNOWLEDGEMENTS

Throughout this thesis writing I was thinking this section is the easiest part to write. But I realized it is the most difficult one as I can not deliver my heart message with the words.

I do not have enough words to express my gratitude to my professor Dr. Ghaly for offering me this opportunity, sharing his expertise, and providing guidance throughout this research project. I would like to thank him for all his invaluable moral, ethical and off course technical training.

I am grateful to my adorable parents who have always sacrificed their life for me so that I can accomplish my life goals. I also thank Mrs. Dourudian and her family who made this journey happen and helped me a lot in Montreal.

Special thanks to my lovely wife for her significant support and patience which were a great help in finishing this work.

I greatly appreciate the direct and indirect help of ENCS staff and Mechanical and Industrial Engineering department and specially Technical Support of IT group.

I cannot finish without expressing my heartfelt appreciation to all my friends especially Raja Ramamurthy, Temesgen Mengistu, Kasra Daneshkhah, Shahin Ghomeishi, Vadivel Kumaran and Benedikt Roidl for their support and for the many informative discussions that I had with them.

TABLE OF CONTENTS

LIST OF FIGURES	ix
LIST OF TABLES	xii
LIST OF SYMBOLS	xiii
1 Introduction	1
1.1 Gas turbine flow	2
1.2 Turbine blade design	3
1.3 Multi-disciplinary optimization	4
1.3.1 Genetic algorithms	6
1.3.2 Artificial neural networks	8
1.4 Previous investigations	9
1.4.1 Aerodynamic optimization	9
1.4.2 3D effects and parameterization	9
1.5 Present work	12
1.5.1 Thesis outline	13
2 Numerical tools and optimization methodology	15
2.1 Geometry modeling and grid generation	15
2.1.1 Geometry modeling	16
2.1.2 Grid generation	18
2.2 Flow analysis	19
2.2.1 Turbulence modeling	22
2.2.2 Mixing plane	24
2.2.3 Averaging	25
2.2.4 Assessment of flow solver	25
2.3 Optimization method	27

2.3.1	Design of experiment	31
2.3.2	Surrogate modeling	31
2.3.3	ANN accuracy improvement	33
2.3.4	Genetic algorithms (GA)	38
2.4	Simplified structural model	40
2.4.1	Structural model for blade	40
2.4.2	Bending moment: Beam with arbitrary area	42
2.4.3	Stress distribution computation	44
3	Blade shape parameterization	45
3.1	Blade shape representation	45
3.2	Quadratic rational Bézier curve (QRBC)	46
3.3	Stacking curve parameterization	47
3.3.1	Stacking curve design variables	49
3.3.2	Stacking curve design variables range	52
3.3.3	Sensitivity analysis of stacking curve design variables	54
3.4	Blade stagger distribution parameterization	55
3.4.1	Design variables range	56
4	Single point optimization	59
4.1	E/TU-3 axial turbine stage	59
4.2	Optimization Objectives	61
4.3	Blade row stacking optimization	63
4.3.1	Stator optimization	64
4.3.2	Rotor optimization	65
4.3.3	Structural analysis of the turbine blade	69
4.4	Stage optimization using stacking and stagger angle	70
4.4.1	Case 1: Performance optimization using stacking line	71

4.4.2	Case 2: Performance optimization using stacking and stagger .	74
4.4.3	Case 3: Performance optimization using stacking and stagger with a different objective function	84
4.4.4	Physical implications of the optimized stages	85
4.5	Conclusion	92
5	Multi-point optimization of a gas turbine stages	93
5.1	Objective function	93
5.2	Optimization at multiple points	95
6	Conclusion	108
6.1	Summary	108
6.2	Concluding remarks	108
6.3	Contributions	110
6.4	Future work	111
	Bibliography	113
	Appendix	119
A	Quadratic rational Bézier curve (QRBC)	120
A.1	Definition	120
B	Governing equations	122
B.1	Reynolds averaged Navier-Stokes equations	122
B.2	Spalart-Almaras turbulence model	124
B.2.1	Description of the model	124
C	Some notes on surrogate modeling	126
C.1	Universal approximation theory	126
C.2	Used generic functions	127

C.3 ANN accuracy	127
----------------------------	-----

LIST OF FIGURES

1.1	3D boundary layer in turbomachinery flows	3
1.2	Typical turbomachinery aerodynamic design system (Taken from Casey [1])	5
1.3	GA algorithm	7
2.1	Illustration of the computation domain and grid topology generation	17
2.2	Turbine blade grid generation	20
2.3	Initialization of the computational domain based on 1D calculations .	22
2.4	Comparison of Spalart-Almaras and $K-\omega$ turbulence models for a turbine case	23
2.5	Comparison of stage exit profiles with E/TU-4 data at design conditions (Courtesy of [2])	26
2.6	Assessment of numerical results with experimental data of E/TU-3 single stage turbine [3]	28
2.7	The aerodynamic shape optimization process with evolutionary method based on surrogate modeling	29
2.8	A multi-layer ANN network architecture	33
2.9	Error distribution of ANN approximation based on testing patterns (Taken from a single point single objective optimization using one ANN model per objective function)	35
2.10	Early stopping applied on training of two generic functions (Appendix C) with ANN	37
2.11	Derivation of blade volume into distributed mass	41
2.12	Bending of unsymmetrical cross section ([4])	43
3.1	Stacking curve parameterization with QRBC	48

3.2	Design variables for stacking curve	50
3.3	Illustration of lean angles and compound lean (a: acute angle, o: obtuse angle)	53
3.4	The sensitivity of the total pressure loss coefficients to the stacking curve design variables	55
3.5	Stagger angle parameterization with QRBC	57
4.1	E/TU-3 single stage turbine case [3]	60
4.2	Optimum stator blade stacking	65
4.3	Pressure, temperature and velocity profiles at rotor inlet boundary . .	66
4.4	Optimum rotor blade stacking	68
4.5	Stress contours of the listed cases in Table 4.5	69
4.6	Distribution of listed cases in Table 4.5	71
4.7	Case 1: Optimum blade stacking (wire frame depicts the original geometry)	73
4.8	Case 1: Stator blade pressure distribution at hub and tip	75
4.9	Case 1: Rotor blade pressure distribution at hub and tip	76
4.10	Case 2: original and optimum blade shapes	79
4.11	Cases 2 & 3: Stator pressure loading for the original stage	80
4.12	Cases 2 & 3: Rotor pressure loading for the original stage	81
4.13	SS flow separation and sonic surface for the original and optimum stators	82
4.14	Effect of stagger angle change on the throat area	83
4.15	Case 3: original and optimum blade shapes	86
4.16	Spanwise variation of mass flux in the original, Case 2 and Case 3 stages	88
4.17	Spanwise Mach number distribution in the original stage, Case 2 and Case 3 stages	89
4.18	Spanwise radial velocity and incidence angle distribution for the original stage, Case 2 and Case 3 stages	90

4.19	Spanwise variation of stage loading and reaction in the original stage, Case 2 and Case 3 stages	91
5.1	E/TU-3 turbine performance curve at design speed	96
5.2	Individual objectives at the four pre-selected points	98
5.3	Original and optimum stator and rotor blades (wire frames refer to original geometry)	100
5.4	Mach iso-surfaces of stator blade at OP4	102
5.5	Reduction of corner stall in stator SS-TE region at OP4	103
5.6	Isentropic mach across stator blade at OP3	104
5.7	Pressure coefficient for rotor blade at OP3	105
5.8	Streamwise vorticity at rotor trailing edge at OP4	106

LIST OF TABLES

3.1	List of QRBC parameters and possible design variables	51
3.2	Stacking curve design variables range for stage	54
3.3	Stagger angle design variables range	58
4.1	E/TU-3 single stage turbine specifications	60
4.2	E/TU-3 single stage turbine design point specifications	60
4.3	Stator optimization: The design variables, their range of variations and efficiency of original and optimum stages	66
4.4	Rotor optimization: The design variables, their range of variations and efficiency of original and optimum rotors	67
4.5	Studied cases for stress distribution	68
4.6	Case 1: Boundary condition (Rotor profiles are given in Fig. 4.3)	73
4.7	Case 1: Single objective optimization of stacking in stage	73
4.8	Design variables and their optimization range	77
4.9	Original, Case 2 and 3 stage aerodynamic characteristics	84
5.1	Different coefficients in objective function equation	95
5.2	Optimum design variables proposed by ANN	96
5.3	Design speed line operating points	97
5.4	Original and optimum values of design variables and their range of variation	99
5.5	Comparison of single and multipoint optimization	101
C.1	Rosenbrock function approximation with ANN: Predicted value vs. ac- tual value of testing sample points	128

LIST OF SYMBOLS

$2D, 3D$	Two-dimensional, Three-dimensional
CG	Center of gravity
Cp	Coefficient of pressure = $\frac{p-p_{in}}{\frac{1}{2}\rho_{in}V_{in}^2}$
GA	Genetic algorithm
LE, TE	Leading edge, trailing edge
M	Mach number
p	Pressure
PS, SS	Pressure side, Suction side
PT	Penalty term in the objective function
V	Flow velocity
Y	Total pressure loss coefficient = $\frac{P_{0,in}-P_{0,out}}{P_{0,out}-P_{out}}$

Greek symbols

Ω^*	Dimensionless streamwise vorticity = $\frac{\vec{\Omega} \cdot \vec{V}}{2\omega_r \vec{V} }$
α	Lean angle, Absolute flow angle ($^\circ$)
β	Sweep angle, Relative flow angle ($^\circ$)
η_{ts}	Total to static efficiency = $\frac{1 - \left(\frac{T_{03}}{T_{01}}\right)^{\frac{\gamma-1}{\gamma}}}{1 - \left(\frac{P_3}{P_{01}}\right)^{\frac{\gamma-1}{\gamma}}}$
η_{tt}	Total to total efficiency = $\frac{1 - \left(\frac{T_{03}}{T_{01}}\right)^{\frac{\gamma-1}{\gamma}}}{1 - \left(\frac{P_{03}}{P_{01}}\right)^{\frac{\gamma-1}{\gamma}}}$
ω	Rotation speed
θ	Associated angle to compound lean
ζ	Stagger angle

Subscripts

0	Total (or stagnation) quantity, Related to control point P_0
1, 2	Related to stator inlet and outlet, Related to control points P_1 and P_2
3	Related to stage outlet plane
h	Blade hub
in, out	Blade row inlet and outlet

<i>is</i>	Isentropic
<i>r</i>	Rotor, relative to the rotor blade, e.g., relative total temperature
<i>s</i>	Stator
<i>t</i>	Blade tip

Acronyms

ANN	Artificial neural network
AOA	Angle of attack
CFD	Computational fluid dynamics
CFL	Courant-Friedrich-Lewy number
CPU	Central processing unit
DOE	Design of experiment
GRMSE	Generalization root mean square error
LHS	Latin Hypercubic sampling
RANS	Reynolds number averaged Navier-Stokes
RMS	Root mean square
rpm	Revolutions per minute
QRBC	Quadratic rational Bézier curve

Chapter 1

Introduction

Gas turbines have strong impact on human life since its introduction in the twentieth century. It has been used mainly for power generation and later on in aircraft propulsion. After more than half a century of creative development, it is still a challenge for engineers of all disciplines to achieve the ever increasing and more demanding design requirements. Focusing on the design of gas turbines, aerodynamic features, structural integrity, vibrational aspects, combustion, cooling, acoustics and environmental effects are the subject of active research and development.

The flow features are complicated and may be divided into compressor and turbine aerodynamics in gas turbines. Compressor aerodynamic design is challenging due to the stability specially when the maximum efficiency is within the surge margin. On the other hand, turbine aerodynamics is also a challenge due to high inlet gas temperature, secondary flow, separation and transonic flow and their interactions.

The turbomachinery design has benefited from numerical methods and increasing computing power in the last decades. The CFD tools with their developing ability in predicting the flow features are now an essential part of design system. Their application in design is economically and logically justified. Nevertheless, the experimental validation is still a necessary step. These tools have reduced rather significantly the

design system and allowed for reducing the number of experimental cases required to verify a given design.

The drive for increased efficiency, enhanced reliability, decreased noise and cost of gas turbines especially in aerospace industry is getting stronger than ever particularly with the rise in fuel prices and stricter environmental standards. Application of optimization methods involving CFD flow simulations is a practical strategy that helps in reaching these goals.

The two dimensional and quasi-three dimensional design of turbine blades have evolved into three dimensional design. Aerodynamic optimization requires a practical parameterization which can control the flow features. Its practical development requires experience and is actually a key for performance improvement.

In the next section the important 3D aspects of the turbine stage is reviewed. Then different optimization approaches, in particular evolutionary algorithms combined with response surface approximation are discussed. This is followed by the review of literature with the focus on parameterization and optimization approaches are investigated. Finally, the work performed in this thesis is outlined in the last section.

1.1. Gas turbine flow

The flow in turbomachinery is highly complex as it is three-dimensional, inherently unsteady, compressible. This high speed flow involves laminar/transition/turbulent flow regimes, stator-rotor interactions, vortical flows, compressibility, flow separation, shocks, heat transfer etc. There are some physical features in turbomachinery aerodynamics that are purely three dimensional and cannot be completely accounted for by 2D and even quasi-three dimensional flow simulation such as secondary flow, tip leakage and 3D boundary layer (See Fig. 1.1). Rotation, curvature, radial pressure

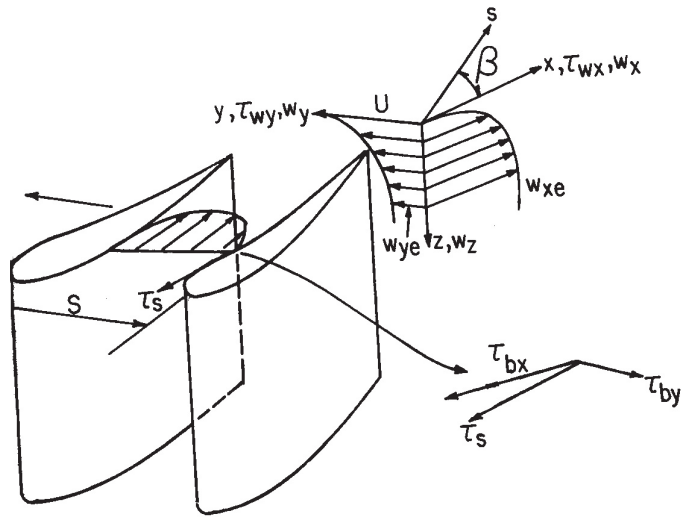


Figure 1.1: 3D boundary layer in turbomachinery flows

gradients are introducing highly 3D flow where the losses cannot be predicted with acceptable accuracy using cascade models.

Secondary flows combined with the passage vortex can move the wall flow into the main stream and add further complexity to the flow field especially in a multi-stage turbine. The interaction of tip leakage flow, annulus boundary layer and secondary flow would enhance turbulence and augment mixing which obviously ends up in higher losses. The mentioned features imply using of 3D design optimization of blade shape. In turbines for instance, secondary flow is stronger than that occurring in compressors due to higher flow turning [5]. The studies suggest that their reduction would improve the efficiency.

1.2. Turbine blade design

Design process is reviewed in brief to indicate the role of optimization in the design system. A typical aerodynamic design process in turbomachinery is indicated in Fig. 1.2. The difficulty in reaching a "good" design is to meet many criteria in different disciplines simultaneously. Empirical and analytical methods can perform

an acceptable design but there is still room for improvement. The numerical methods can also be used for flow analysis and evaluation of the design parameters. However, the complexity of design space suggests that optimization technique can provide the designer with information and conclusions that would be otherwise difficult to reach.

There are two conventional design optimization techniques: Inverse design and design optimization. In the inverse design approach [6], the blade performance is prescribed and the corresponding geometry is obtained as part of the solution. In the optimization approach, the blade performance is described quantitative is terms of a set of objectives restricted to constraints and significant engineering parameters are chosen as design variables to be optimized for best performance. Inverse design is very efficient however needs an experienced designer to prescribe a "good" target design variables. Although this method is very straight forward however the choice of target values is very challenging in 3D flow design. On the other hand, the optimization approach provides flexibility to choose objectives and constraints that the designer wants. Application of this method in multi-point optimization or multi-disciplinary optimization is straight forward, however, the required computing resources are larger than those required by inverse design method. Also they can be applied for 3D blade optimization and in general for problems with large design space. They also need the designer experience in setting up a good optimization strategy.

1.3. Multi-disciplinary optimization

The turbine blade design is multi-disciplinary and challenging. The high gas temperature requires a thermal and structural analysis. A thermal, structural and aerodynamic optimization of a micro gas turbine was carried out for a cooled turbine blade by Versteade [7].

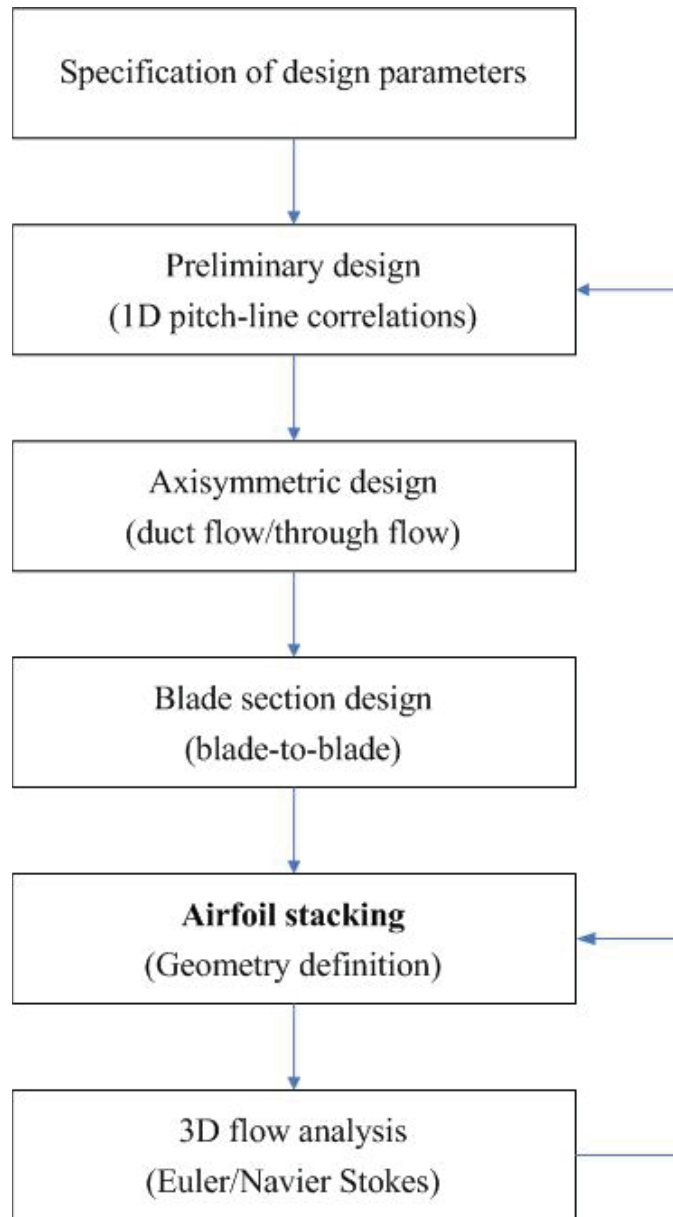


Figure 1.2: Typical turbomachinery aerodynamic design system (Taken from Casey [1])

Generally optimization methods can be divided to deterministic (like gradient-based methods) and stochastic methods (like evolutionary methods). The first method is faster but it can be trapped in local minimum especially in nonlinear functions. The latter is robust for finding global optimum due to the use of random operators. Genetic algorithm has been used extensively for optimization. In this research work for single and multi-point objective optimization GA combined with surrogate modeling similar to that developed by Mengistu [8] will be used. The GA and surrogate modeling are briefly described in the following sub-sections.

1.3.1 Genetic algorithms

The difference between GA and gradient-based methods is said very well in Goldberg [9] as: "GA works with a coding of the parameter set, not the parameter themselves. GA searches from population of points not a single. GA uses objective function not derivatives. GA uses probabilistic transition rules not deterministic rules." These features make it robust and attractive to nonlinear aerodynamic applications. GA can be coded in binary or continuous operators. Continuous method is simpler to implement and also preferable when high precision is required. In binary method when high precision is needed for chromosomes the number of bits would be large which is not good. GA algorithm is inspired from evolution processes observed in nature. The algorithm is shown in Fig. 1.3. GA will be discussed in more details in Chapter 2.

Non-Dominated Sorting GA (NSGA II) introduced by Deb [10] is used for multi-objective optimization. The initial population is initialized randomly within the design space and the fitness in each generation is based on the non-domination level and a niche count factor, which depends on the number and proximity of neighboring solutions. All sets in the first non-domination level are assigned a maximum value of equal dummy fitness and this value may be reduced based on the factor called niche

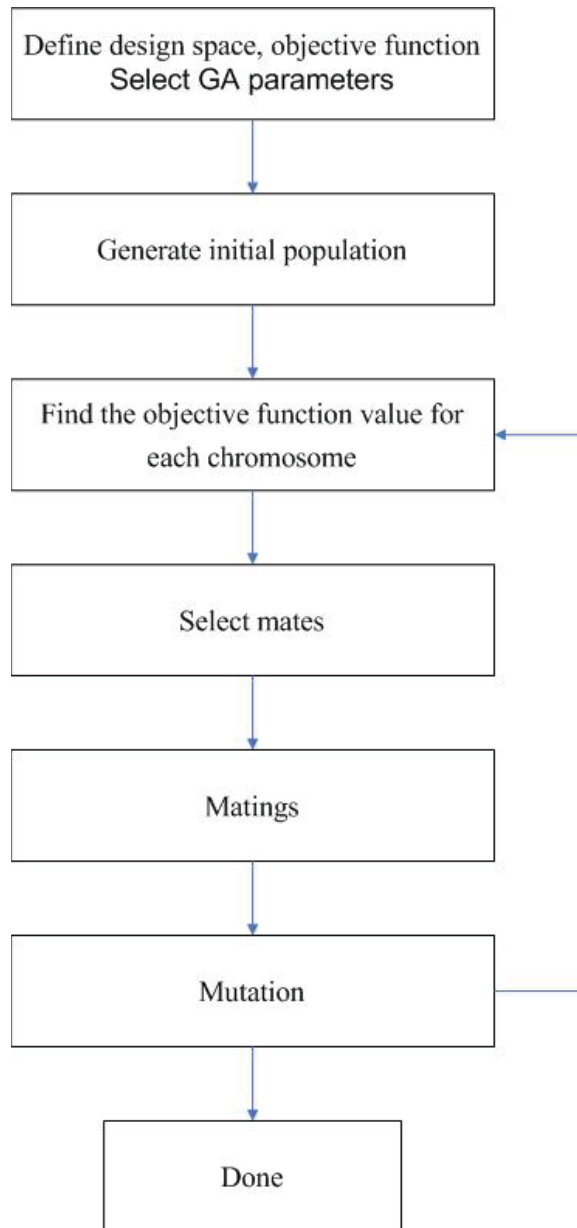


Figure 1.3: GA algorithm

count if that solution is located in a dense region of solution space.

The population in the second non-domination level is assigned a dummy fitness, which is smaller than the smallest fitness value of the previous front. The same kind of fitness reduction is carried out based on the niche count. These procedures are repeated until all the individuals are assigned a fitness value. The genetic algorithm operations like selection, crossover, mutation, elitism and reproduction are then carried out on the individuals to provide a search direction towards the Pareto-optimal region and the solution becomes well diversified due to the inclusion of a niche count factor.

1.3.2 Artificial neural networks

The use of response surface models (RSM) to approximate the objective function starting from a database reduces computation time considerably. In this work an artificial neural network ANN is modified and improved so as to approximate the objective function at a relatively low computing cost and with an acceptable accuracy. The construction of an ANN model involves two steps: training and testing of the ANN model. The steps in designing the ANN model are in brief choosing the type of ANN network, training the model to determine its parameters and finally testing the resulting ANN model to assess its accuracy.

The multi-layer feed forward network was chosen. It has an input layer that consists of the design variables and the last layer is the output layer that returns the network output. In between lies one or more hidden layer(s) where the computational process of the network is concentrated. ANN training is discussed in more details in Chapter 2.

1.4. Previous investigations

In recent years a large research activity for optimization of turbomachinery performance in both 2D and 3D analyses have been done. Overview of 2D and 3D optimization techniques, 3D design parameters (sweep, lean, bowing and end-wall contouring), geometric representation is discussed in the following paragraphs respectively. The review of these papers was helpful to introduce new parameterization method of stacking curve and understanding of 3D design parameters' effects on flow physics.

1.4.1 Aerodynamic optimization

Global optimization methods have extensively used in aerodynamic shape optimization [9], [11]. Mengistu [8], [12] has successfully implemented GA and SA as evolutionary algorithms combined with surrogate models for multi-point and multi-objective shape optimization of 2D axial compressors and turbines. ANN model as surrogate model has been trained to substitute CFD in the course of optimization. This significantly reduces computation time. The accuracy and generalization capacity of surrogate models is a subject of research and development. The effectiveness of surrogate models [13] and evolutionary algorithms [14] in aerodynamic optimization still needs further research.

1.4.2 3D effects and parameterization

In a review paper by Vad [15] among 26 documents, the physical effects of sweep and lean particularly for low-speed axial compressors are discussed and the effects of non radial stacking on loading, reaction and local total pressure loss are explained. An excellent reference for previous works done on sweep and lean effects is given by Gallimore *et al.* [16]. It presents sweep and lean effects on design of multistage low and high speed axial flow compressors of Rolls-Royce gas turbines.

In Denton [17] and Harvey [18], end-wall contouring and sweep for axial turbines have been studied experimentally. Transonic compressor has been studied for the effect of sweep by Amano [19]. The results showed that the sweep redistributes the flow and reduces the secondary flow loss, depending on the baseline. It was shown that the forward sweep reduces the tip loading in terms of the static pressure coefficient. The comprehensive study of sweep effect on the flow is given by Potts [20]. Experimental results for compressor cascades are given by Sasaki and Breuglemans [21]. Sweep in transonic compressor reduces shock losses by reducing the meridional Mach number. In general, blade sweep seems to have a strong effect on efficiency in transonic compressor to reduce shocks Kim *et al.*[22]. Multi-disciplinary optimization of compressor blade where lean and sweep are included as design variables was done by Pouzadoux [23].

Influence of lean on turbine linear cascades loss has been studied experimentally by Harrison [24]. The blades have a low aspect ratio. The physical reasons to improve loss due to leaning is explained well in terms of velocity, blade surface boundary layer transition, end wall boundary layer transition and mixing losses. A detailed experimental and numerical study of end wall profile for cascades has been studied by Atkins [25]. He found that end wall contraction has no significant improvement in nearly 2D velocity distribution of cascade flows. Rose [26] showed that end-wall profiling can reduce pressure gradients downstream of blade and prevent the mainstream from going to cavities between stationary and moving end-walls. Non-axisymmetric turbine end wall design by Harvey *et al.* [27] has been studied numerically and experimentally. It was found that the effect of end wall profiling is remarkable and comparable to leaning and skewing. Denton gathered a comprehensive review of 3D effects in Denton [28]. Other papers regarding 3D effects and design are Pierret [29]. Bagshaw *et al.* [30] have introduced smart idea for efficiency improvement by combining end-wall contouring and negative compound lean. Negative compound lean

will load the end-walls but unload the mid-span. This will decrease mid-span profile loss but increase loss at end-walls. On the other hand by end-wall contouring and reduction of secondary loss the end-wall losses are decreased.

There are relatively fewer papers for turbine blade optimization that address 3D flow effects. In Lampart *et al.* [31] 3D blading of a high-pressure and low-pressure steam turbine stage is optimized with direct optimization but on a coarse mesh. Finally it is verified on a finer mesh. Among the optimized parameters are stator and rotor blade numbers and stagger angles, rotor blade twist angle, stator blade sweep and lean, both straight and compound. The blade sections (profiles) are assumed not to change during the optimization. There are constraints imposed on the design parameters, including the mass flow rate and stage reaction. Usually, 3D blade stacking in HP turbines does not mean largely increased efficiencies [31].

There are some other papers that studied the 3D flow effects on turbine losses. however, no attempt was made to optimize the blades Wallis *et al.* [32]. Examples of optimization of stator blade linear twist, lean and sweep and rotor blade twist for a high-load HP gas turbine stage and optimization of stator blade compound lean at hub and tip with optimized rotor blade twist for a low-load HP steam turbine stage, performed by Yershov *et al.*[33] show stage efficiency improvements as considerable as 0.8%. It was shown by Lampart and Yershov [34] that stator blade lean can serve as a means of improving the LP exit stage efficiency from low to nominal load, with the most spectacular efficiency gains for low loads, by far exceeding efficiency gains for the nominal load for which the stage was optimized. However, efficiency reduction is possible here for high loads. The effects of 3D blading in high-pressure (HP) turbine cascades and stages were previously investigated by Potts [20], Harrison [35], Singh *et al.* [36], Wang [37].

Concerning parameterization of stacking curve, parabolic or quadratic curves

have been used by linking sweep, skew and lean angles to curve parameters. Generally, the curves don't have continuous curvature distribution and are multi-segments. Also there is not one parameterization tool to integrate all design variables. These observations in the reviewed papers are suggesting a scope for more work on parameterization of the stacking curve.

3D aerodynamic shape optimization of blade is extremely time consuming and virtually impossible with direct optimization methods such as GA. However by means of surrogate models this would be possible. Research on surrogate modeling is expected to decrease the error. There are some other techniques to reduce the computational time of the optimization process. Akmandor [38] has optimized a compressor blade with less high-fidelity calculations by means of multi-level GA. Another example is the work of Clarich [39] where he applied statistical analysis to measure the impact of many initial design parameters of axial compressor optimization on objective function in order to reduce the number of design variables. In addition, efficient geometry parameterization can also be helpful to save computational time as indicated by Ghaly *et al.* [40]. So methodology improvement is still required for turbine blade optimization.

1.5. Present work

This work was initiated with the objective of focusing on three dimensional flow analysis and shape optimization.

The first motivation for this work is to develop knowledge in 3D shape optimization. The traditional 2D blade design cannot capture some physical features of the flow which need to be considered in the design. Secondary flow, separation and turbulence are genuinely 3D phenomena. The success of 2D design tools relied on empirical correlations obtained from experiments. However, the correlations are

limited to a particular family of turbines which would become outdated after several years. Moreover, the experiments needed for deriving the correlations are exorbitantly expensive. These facts have necessitated the development of reliable 3D numerical analysis tools. 3D Navier-Stokes analysis has become a common tool in the last decade due to the exponential progress in computer technology and the maturity of CFD methods. Thus tremendous research work is now going on in 3D flow design and optimization using 3D simulation tools.

The second motivation is to come up with a practical and efficient blade stacking parameterization for turbine blades. Stacking of the profiles is an important 3D design parameter. The literature review identifies a shortage of work on stacking parameterization in particular for turbine blades and its quantitative impact on the design. The topic is so new that only recently it appeared in the context of a book chapter by Chen [41].

The third motivation is to come up with an optimization strategy where engineering knowledge is coupled with mathematical optimization tools to formulate the aerodynamic shape optimization problem of a turbine stage with the least number of design variables for a given performance improvement.

This research work tries to address the above mentioned motivations. The focus of the work is on the development of an efficient optimization strategy using a practical and innovative parameterization techniques for turbine blade so as to minimize the adverse effects of 3D flow on the turbine losses and hence improving the blade performance in 3D flow.

1.5.1 Thesis outline

This thesis is organized as follows. Chapter 1 introduces the scope, review, motivation for this work. The geometric modeling, flow analysis, optimization methodology which include the GA, ANN training and structural analysis are discussed in Chapter

2. The stacking curve parameterization and spanwise variation of stagger angle are described in Chapter 3. Chapter 4 presents a single-point optimization of an axial turbine stage using the optimization tools developed in Chapter 2 and the shape representation described in Chapter 3. Then the multi-point optimization of the same turbine stage is presented in Chapter 5. The last chapter concludes and summarizes the research findings, it also points out some outstanding challenges and recommends possible future work.

Chapter 2

Numerical tools and optimization methodology

In this chapter, the numerical tools used for flow analysis are presented. The geometrical modeling and grid generation approach are presented first. Then the CFD flow simulation is described and assessed for accuracy. It is followed by the optimization methodology. Also the major contributions of this thesis in terms of methodology is presented in this chapter. In the last section a simplified structural model for turbine blades is introduced.

2.1. Geometry modeling and grid generation

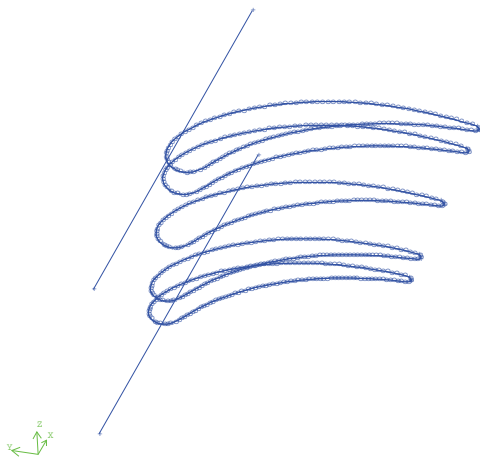
The geometrical model preparation and the grid generation are both done in Gambit 2.4, which used to be the ANSYS-Fluent pre-processing tool. The geometrical model consists of the blade geometry and the flow passage surrounding the blade, which represents the computational domain. The details of the geometric model and structured grid generation are described in this section.

2.1.1 Geometry modeling

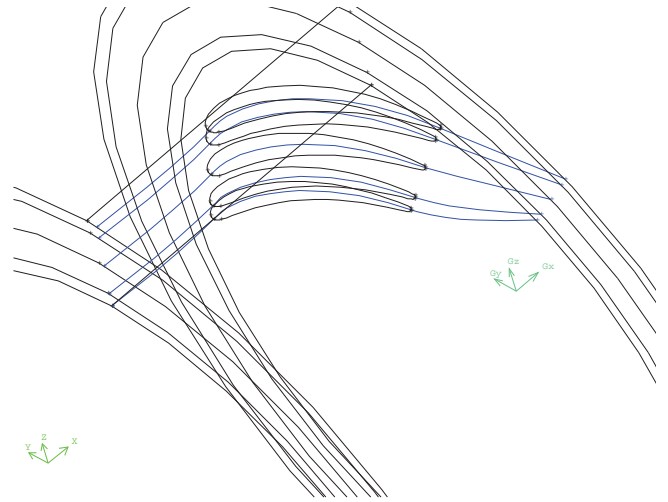
The flow passage is obtained by means of Turbo Toolbox in Gambit. It is defined by turbine blade and hub and tip profiles. The turbine blade is defined by 5 airfoils, each is given by a set of x , y and z available coordinates; These airfoils are defined at different spanwise locations from hub to tip. The blade profile is then obtained by fitting a B-spline through the given points as shown in Fig. 2.1.a. Only passage-to-passage domain can be generated with Turbo Toolbox; i.e. the blade is always centered in the computational domain and cannot be placed at periodic borders. The number of blades fixes the pitch at each radial location. The medial curves that divide the profiles equally, go through the leading and trailing edges of each profile. The two end points of the medial curves as shown in Fig. 2.1.b can be moved on the circles at the inlet and outlet. This can help in aligning the computational domain with the wake shed from the blade TE. Finally a surface is swept through these medial curves to shape the periodic surface. This surface is then rotated in both directions by half a pitch to create the periodic surfaces that are shown in Fig. 2.1.c.

Eventually, the blade volume is obtained by a skinning process [42] on the profiles. The computation domain is attained as the surrounded volume among the hub, casing, inlet, outlet and periodic surfaces as indicated in Fig. 2.1.c.

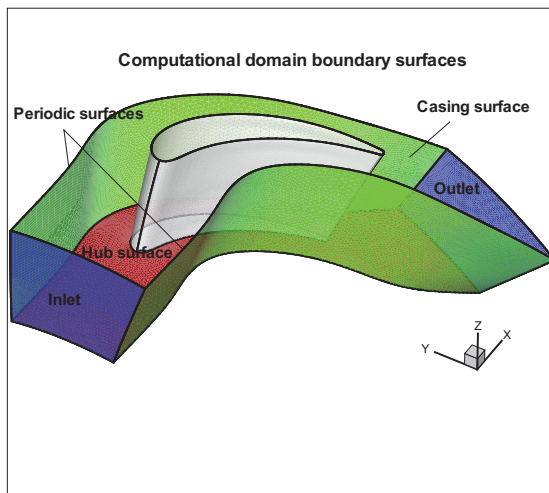
The computational domain is then decomposed to reach the desired topology for structured grid generation. The passage volume is initially divided into four blocks. The blocks consist of inlet, pressure side, suction side and outlet blocks as shown in Fig. 2.1.d. This is usually known as an H-topology. Each block is divided into two sections by means of the mid-span plane which brings the total number of blocks up to eight. This is discussed further in the following section.



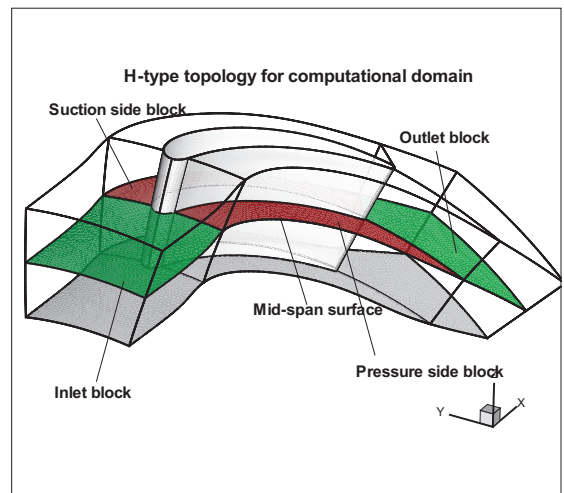
a. Fitting B-spline to the points on profiles



b. Skinning process for surface generation



c. Computation domain



d. Grid topology

Figure 2.1: Illustration of the computation domain and grid topology generation

2.1.2 Grid generation

A "good" mesh is essential to resolve adequately all the flow physics implied in a given flow, while alleviating the propagation of the numerical errors into the final results. Therefore a grid sensitivity analysis, is necessary to find an optimum grid size so as to obtain sufficiently refined grid. However, finer grid increases the computational time and the possibility of having highly skewed cells especially in unstructured grids.

It is not usually easy to achieve a grid with satisfactory level of refinement and quality particularly with highly twisted turbine blades. In addition, the two periodic boundaries require exactly the same surface mesh which cause further restrictions and less freedom to achieve a high quality grid. These are some of the challenges encountered in generating a "good" mesh.

Both unstructured and structured grid capabilities as well as a hybrid grids are evaluated to address the above-mentioned challenges. The Fluent former pre-processor, Gambit, has been used to generate the grid. Unstructured grid can be used for inviscid calculation but it is not a good choice for boundary layer calculations. In Gambit, there is a pretty helpful feature that allows using a hybrid grid, i.e. structured O-type grid around the blade and unstructured grid anywhere else. The structured block around the blade as shown in Fig. 2.2.a allows the solver to resolve the flow in the boundary layer.

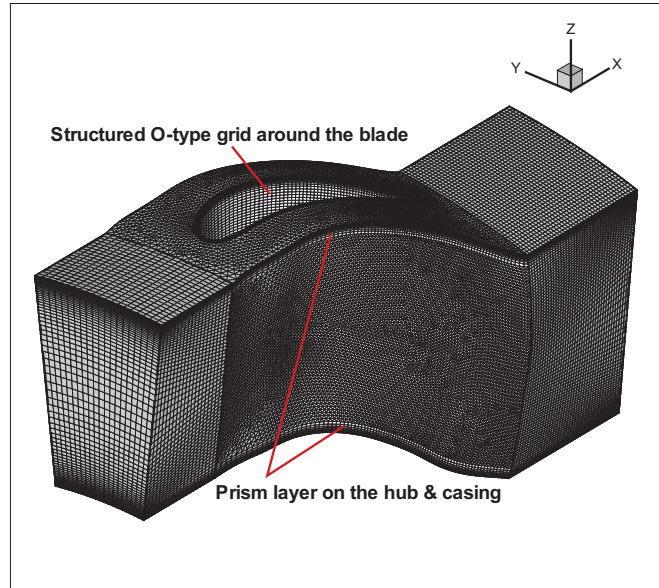
However, there are two major problems with hybrid grids in Gambit. Firstly, Gambit is not always able to provide a mesh with a $y^+ \simeq 1$. The boundary layer tool does not perform successfully as the mesh is refined for fully integrated boundary layer calculations. Secondly, the unstructured algorithm is not robust enough for unstructured volumetric grid generation. Even though the surface mesh is reasonably good, the volumetric grid generation sometimes fails for encountering negative volumes some where inside the volume. Therefore, this type of grid is not chosen as the fundamental grid generator for optimization.

Multi-block structured grid is then used although it does not have the flexibility of unstructured grids for irregular geometries such as highly twisted turbine blades. Originally the passage is divided into four blocks as shown in Fig. 2.1.d. The number of blocks can be increased to give more flexibility to grid generator to have different edge mesh spacing so as to avoid highly skewed cells. This division gives more flexibility and independence for meshing the individual blocks to achieve a higher mesh quality. Therefore, a reasonably robust and sufficiently refined grid can be achieved with this topology.

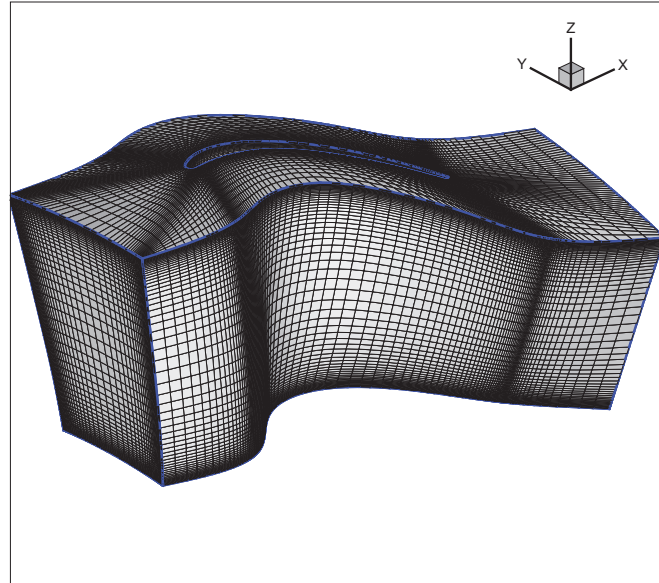
In order to keep the numerical error level to minimum in optimization, all the different geometries are meshed with the same edge spacing scheme. i.e. having identical number of mesh points and clustering method for respective edges. The mesh points are clustered near LE and TE. The number of mesh points on the LE and TE are 16 and 8, respectively. The number of mesh points in streamwise, spanwise and azimuthal directions are 140, 60 and 52, respectively. Fig. 2.2.b shows the multi-block structured mesh used in the optimization cases presented in Chapters 4 and 5. In order to resolve the boundary layer flow, more mesh points can be clustered near the walls (blade, hub and casing). The first cell adjacent to the wall gives $y^+ \simeq 30$ which is suitable to be used with wall functions explained in the next section.

2.2. Flow analysis

The CFD has matured during the last two decades to be an integral part of the design process. Specifically, the Reynolds averaged Navier-Stokes (RANS) equations coupled with different turbulence models were extensively used in aerodynamic design and analysis. This analysis requires relatively large computer resources. The precision and computational time required for the analysis depends directly to the spacial discretization. Usually a fine grid is required to capture all 3D flow features with



a. Hybrid grid



b. Structured grid

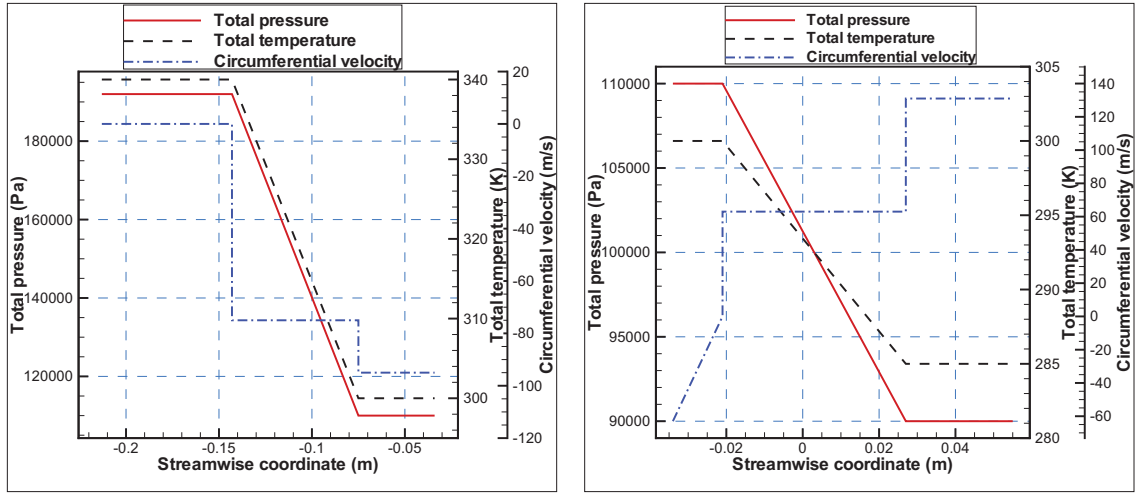
Figure 2.2: Turbine blade grid generation

an "acceptable" level of accuracy. This implies a considerable computational time. The concern in aerodynamic optimization problems is to reduce the computation time, since the optimization requires a "large" number of flow simulations. There are some techniques that facilitate the analysis such as parallel computation, multi-grid method, implicit schemes and the initialization with rough estimation.

These features are available in ANSYS-Fluent 6.3. They have been used in the present work. The RANS model is used to simulate the flow using second order upwind discretization of the coupled compressible Navier-Stokes equations. Spalart-Allmaras turbulence model with wall functions where y^+ varies between 30 and 100 is used as closure. The code was run for both explicit and implicit formulations with CFL of 200 and 1, respectively. The implicit formulation was found to converge faster than the explicit one as it takes one hour wall clock time on 4 CPUs compared to 10 hours for the explicit formulation. However, implicit scheme, "which generally is unconditionally stable" [43], with the CFL number as high as 200 would take one hour wall clock time for a similar case running on four CPUs.

The inlet boundary conditions are given as a spanwise distribution of total pressure, total temperature, two flow angles and the turbulent intensity and hydraulic diameter. The outflow boundary condition is given by the static pressure that would satisfy the radial equilibrium equation at the exit boundary. The mixing plane approach, discussed later, is used to exchange boundary conditions at the stator-rotor interface. For all cases presented in this work the flow is subsonic at both inlet and exit boundaries.

An initial guess of the pressure, temperature and velocity field for both stator and rotor can be obtained from a 1D stage calculation. Assuming constant axial velocity and zero radial velocity, the circumferential velocity can be calculated based on zero incidence and deviation angles for stator and rotor blades. The total pressure and temperature are assumed to vary linearly as shown in Fig. 2.3a. and b. This



a. Initialization of the flow field for stator domain

b. Initialization of the flow field for rotor domain

Figure 2.3: Initialization of the computational domain based on 1D calculations

would help to have a quicker convergence.

The root mean square of the residuals for all the equations are monitored for convergence check. However, the mass flow rate is taken as the stopping criterion of the analysis. The solution procedure starts with first order upwind discretization and then switches to second order discretization. The CFL number is increased after specific number of iterations step by step, until it reaches its max which is usually above 100 with implicit discretization. The maximum CFL is case dependent and sometimes cannot exceed 100.

2.2.1 Turbulence modeling

The turbulence modeling is the subject of research and there are still many unanswered questions. Selection of a model is case dependent. It can be chosen rationally based on many factors such as application, accuracy, computational cost, etc.

Spalart-Allmaras [44] and standard $k - \omega$ turbulence models are usually used in internal flow steady applications. The first one is a one- equation model and the

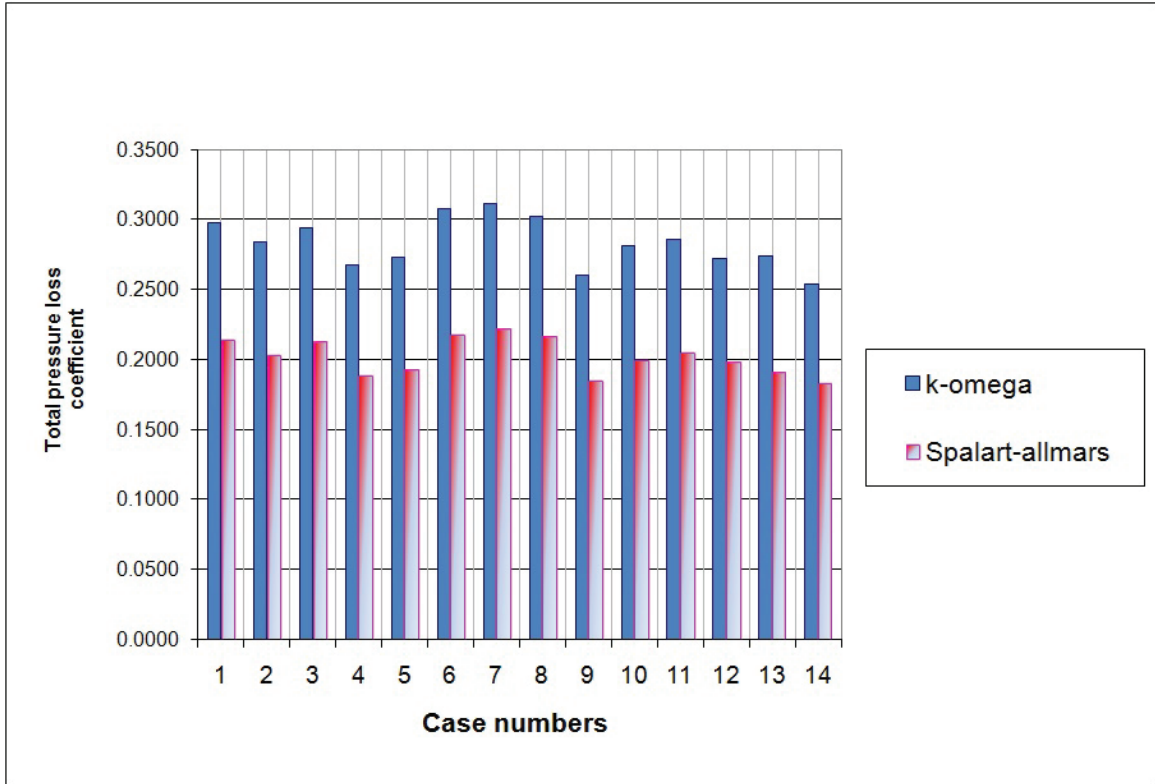


Figure 2.4: Comparison of Spalart-Almaras and $K-\omega$ turbulence models for a turbine case

second one is a two-equation model. They are competitive in accuracy, nonetheless, they can predict different results for some specific flow conditions. Therefore, the two models are studied in the present work.

Several different rotor blades, which are obtained as part of the optimization process discussed in section 4.3.2, are chosen for this study. Both Spalart-Allmaras and $k-\omega$ turbulence models are used with the same boundary conditions and exactly the same mesh to solve the steady Navier-Stokes equations. Since the interest is in loss prediction, predicted total pressure loss coefficients of the two models are compared to each other as shown in Fig. 2.4. According to this result, the two models are indicating the same trend which is critical in optimization. Moreover, the absolute value of the loss is different by almost the same amount for all the tested rotors, see Fig. 2.4.

The precise prediction of the total pressure loss for individual blade row and isentropic efficiency for the stage is technically challenging. It is possible to predict more precise absolute values for them provided that more refined meshes and more sophisticated turbulence models are used. This comes with the expense of more computational cost [16].

Spalart-Allmaras is therefore chosen not only because it is less computationally expensive but also because of its accuracy. "The Spalart-Allmaras model was designed specifically for aerospace applications involving wall flows and has been shown to give good results for boundary layers subjected to adverse pressure gradients. It has also become popular in turbomachinery applications. It has been implemented to use wall functions when the mesh resolution is not sufficiently fine." More discussion is given in [45].

2.2.2 Mixing plane

The numerical analysis of a stage requires the exchange of boundary data between stator and rotor blade rows. Mixing plane approach has been introduced [46] to allow for steady calculations. Otherwise, the time accurate simulation of the inherently unsteady flow in a turbomachine stage is so expensive. The mixing plane implementation accommodates non-conformal interface between stator and rotor blade rows.

Basically the stator and rotor computational domains are solved independently. Then flow properties such as velocity, static pressure and temperature are circumferentially averaged at stator outlet, as well as the rotor inlet. The averaged profiles are then exchanged between the two blade rows after several iterations. The mixed-out averaging formulations can be found in [47].

The mixing plane approach assumes that the flow leaving one blade row is mixed out in the circumferential direction before entering the next blade row [48]. As a result of this mixing process, entropy is generated and total pressure decreases

abruptly through mixing plane. In the present work, the mass averaging is used for stage analysis. Theoretically the mass and energy is conserved through the mixing plane but there is a sudden drop in total pressure level.

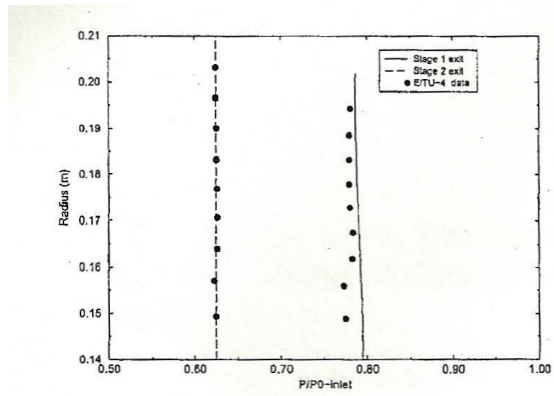
2.2.3 Averaging

The aerodynamic performance of the blade and stage is measured by total pressure loss coefficient and isentropic efficiency. The averaged flow properties such as pressure and temperature must be averaged properly in order to calculate the performance criteria. Usually they are averaged at inlet and outlet stations on the circumferential planes. The mass averaged method is used to calculate flow properties.

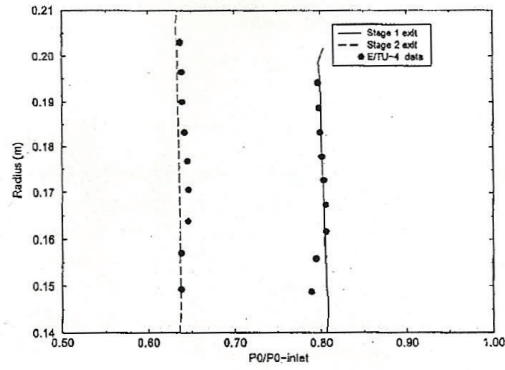
2.2.4 Assessment of flow solver

The assessment of ANSYS-Fluent numerical results in particular for turbine stage flow analysis is discussed in [2] which is a published paper by Fluent. A four stage turbine, E/TU-4 [3], is modeled with unstructured mesh. The Navier-Stokes equations with $k - \epsilon$ turbulence model are solved with explicit scheme at the design and at off-design conditions. The circumferentially averaged spanwise distributions of temperature and pressure show relatively acceptable agreement with the experimental data. These results, as shown in Fig. 2.5, are a proof of mixing plane model capability in regard to multi-stage flow analysis.

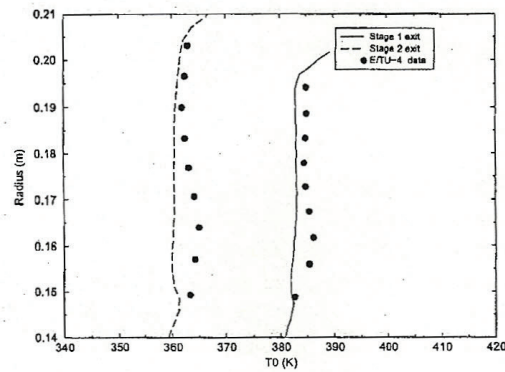
In addition, a single stage turbine, E/TU-3 [3], is analyzed at different conditions at the design speed. The analysis was carried out as described in this section. In fact with the given set of boundary conditions, the mass flow rate and total enthalpy drop are unknown. The performance curve of the turbine at design speed is numerically predicted as shown in Fig. 2.6.a. The experimental data and numerical prediction follow the same trend and agree rather well towards the two ends of the curve.



(a) Static pressure ratio



(b) Total pressure ratio



(c) Total temperature

Figure 2.5: Comparison of stage exit profiles with E/TU-4 data at design conditions (Courtesy of [2])

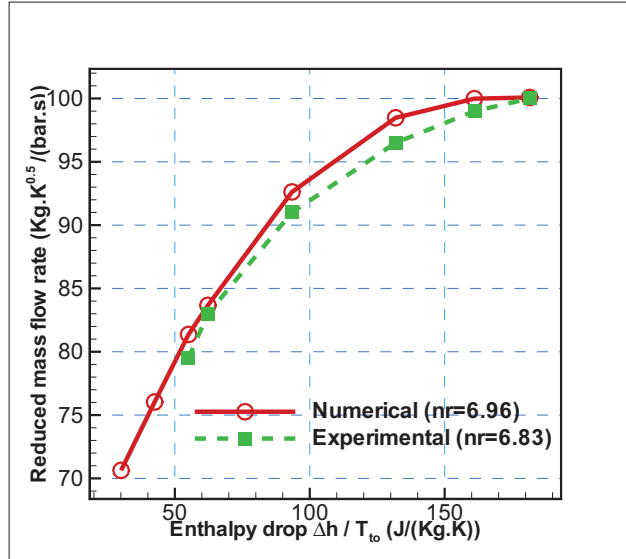
The efficiencies of the operating points in Fig. 2.6.a are also calculated and compared with the experimental data. The numerical results are following the same trend as the experimental data as shown in Figs. 2.6.b. The numerical results are offset both in mass flow rate and the efficiency. This is also observed by Gallimore *et al.* [16] and is basically related to the model accuracy. The precise prediction of efficiency requires extremely refined mesh and high fidelity turbulence model. The solution of such a model is essentially more expensive and demanding. An expensive model is not a practical choice for the optimization method explained later in this chapter. In fact, a relatively accurate model being capable of capturing the efficiency trend is adequate for optimization purpose. Because the objective is to find the location of peak efficiency in the design space rather than determining its absolute value. The Fig. 2.6.b ensures that the flow solver is adequately accurate for the optimization application.

2.3. Optimization method

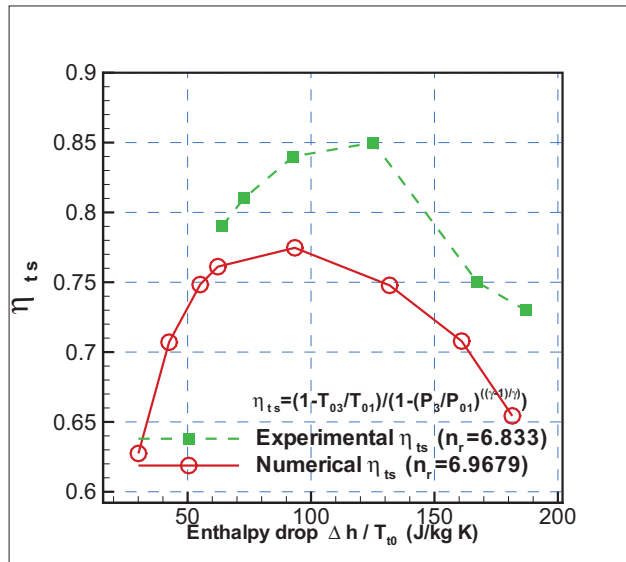
The optimization method used in this work is based on evolutionary algorithms (EA). Evolutionary algorithms, inspired from biological systems, is a population-based heuristic method that can be used in optimization.

There are several EA methods namely Genetic Algorithms (GA), Differential evolution (DE), Particle swarm Optimization (PSO) and Evolutionary Strategy (ES).

One of the most popular EA optimization methods is Genetic algorithm (GA). The heuristic feature of GA, discussed later, makes it a practical method for aerodynamic applications. Generally, aerodynamic optimization requires solving non-linear equations with many design variables. The solution is multi-modal and difficult to resolve. Therefore a gradient-based optimization can most probably be trapped in a local extremum. However, GA uses a random operator and the probability of getting



a. Turbine performance curve at design speed



b. Total-to-static efficiency

Figure 2.6: Assessment of numerical results with experimental data of E/TU-3 single stage turbine [3]

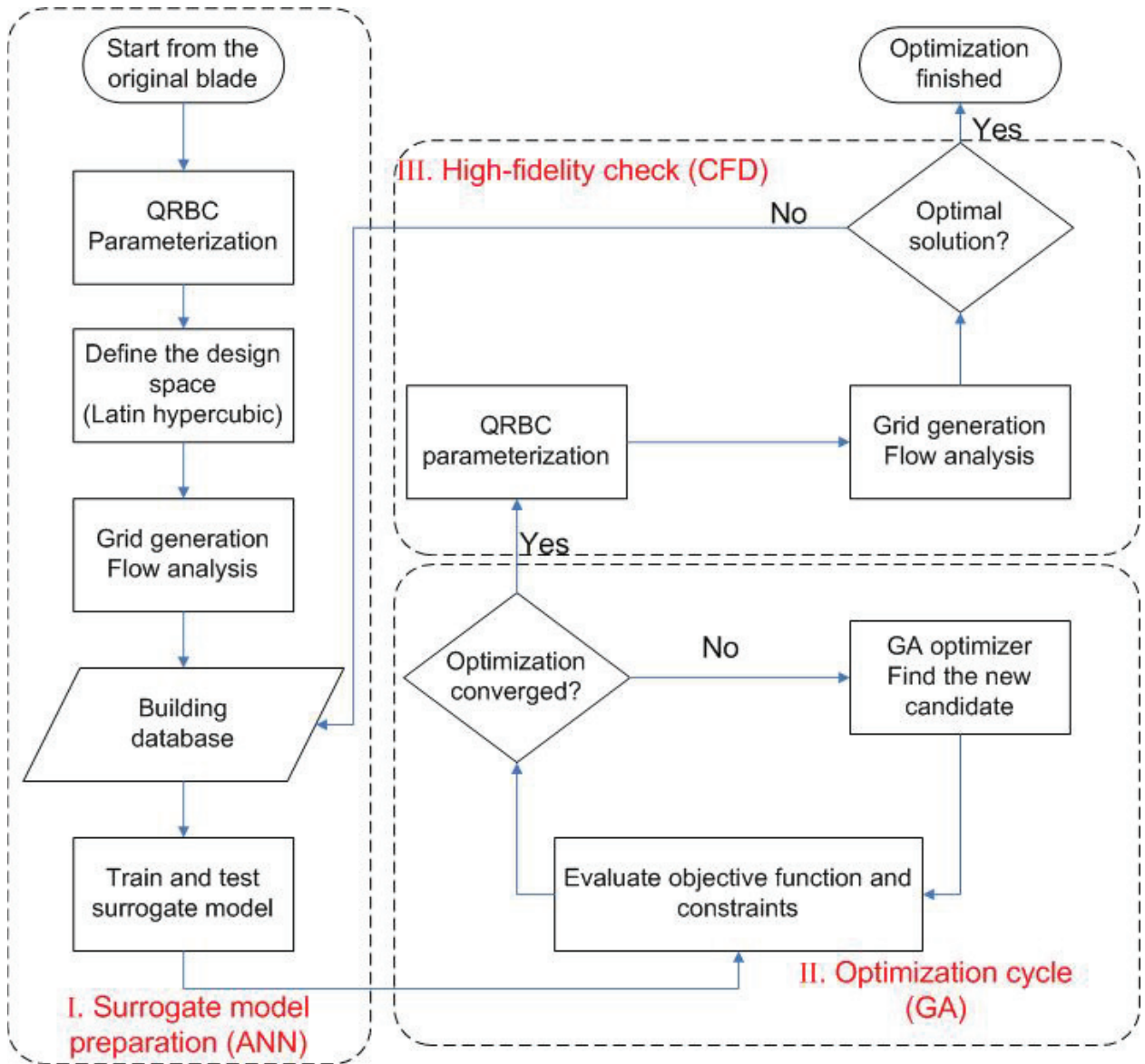


Figure 2.7: The aerodynamic shape optimization process with evolutionary method based on surrogate modeling

trapped in a local extremum is avoided, which makes it a global optimizer within the chosen design space.

However, the GA requires extremely large number of function evaluation. Its implementation is not practical with the current computer power. For instance, fifty Navier-Stokes analyses would be required in each generation (iteration) for a typical three dimensional aerodynamic shape optimization problem. Each analysis consists of grid generation and flow field solution. Assuming at least hundred generations to find the optimal answer, 5000 geometries are required to be analyzed. In brief, the aerodynamic optimization with GA is generally impractical. In order to circumvent this problem, a surrogate model is used to make the method feasible and reduce the computation time. Therefore, the first phase of the process starts with training an acceptable surrogate model. The procedure is indicated in Fig. 2.7.

Once the geometric parameterization is developed, the design space is defined. Then a design of experiment (DOE) is applied to several candidates that are evenly distributed into the design space. Usually the minimum number of candidates are two to five times the number of design variables. Then the candidates are geometrically modeled. Each model is meshed with exactly the same grid topology and spacing. The next step is to solve the flow field in order to predict the aerodynamic losses. Any high fidelity analysis such as structural analysis can be done at this step. Finally, the data are collected into a database which contains the design variables and their corresponding aerodynamic performance. A surrogate model is then built from this database. This part is critical as training an accurate model is really challenging. This is discussed in the following section.

The optimization is now fast because the functions are evaluated using the surrogate models which takes a few seconds to evaluate the objective function but is less accurate than the Navier-Stokes simulations. GA is sorting the fitness value of each member in the population and produces the next generation of candidates. The

details of GA is discussed later in this chapter. This optimization method was originally implemented by Mengistu [8]. It was considerably modified in this work and adapted for 3D aerodynamic shape optimization. The major modifications are discussed in Section 2.3.3. Eventually, the optimum candidate is analyzed with the high fidelity model. If the performance is optimum in the design space the optimization is successfully done. Otherwise, the database is enriched by addition of the optimum candidate. Then a new surrogate model is trained and tested. The optimization cycle is ran again until an optimum shape is achieved.

2.3.1 Design of experiment

The design of experiment is an extensive field with many applications mainly in statistics and in experimental work. The Latin hypercubic sampling method [49] is used in the present work. It is a statistical method to collect samples in a multi-dimensional space so that all the design space is evenly covered by the chosen sampling points.

2.3.2 Surrogate modeling

Various surrogate models namely artificial neural networks (ANN), radial basis function (RBF), wavelet and self-organization maps are used for aerodynamic applications. The appropriate choice of model is case dependent. Artificial neural network with back propagation training algorithm was used for the current work [50].

A multi-layer ANN network architecture is indicated in Fig. 2.8. The first row of nodes is the input layer that accepts the user input and the last row is the output layer that returns the network output back to the user. Between the input and output layers, lies one or more hidden layer(s) where the computational process of the network is concentrated.

The signal of input variables go through the synaptic links between the input

and hidden layer. Then each node in the hidden layer receives the signals and gets stimulated. Similarly the flow of signals go to the output layer through the synaptic links between the hidden and output layer. Finally the output node gets stimulated and sends the output signal. The amplitude of the output signal depends on the input signal and the sensitivity of the node to the input signal. The mathematical model of a network with one hidden layer is derived in Eq. 2.1. The input signals, $y_i(n)$ are the input variables. The synaptic links are modeled by the set of weights, w_{ji} , between each layer. The degree of stimulation is also modeled by so called activation function, $\varphi(v_j)$. The non-linear activation function enables the network to model the complex input-output pattern. There is always a bias neuron with unit value at each layer.

$$y_k(n) = \varphi_k\left(\sum_{i=0}^{m_1} w_{kj} \cdot \varphi_j\left(\sum_{i=0}^{m_0} w_{ji} y_i(n)\right)\right) \quad (2.1)$$

Where the activation functions used are:

$$\varphi_j = \begin{cases} 1. \frac{1}{1+e^{-v_j}} & : \text{Sigmoidal function (Logistic function)} \\ 2. \frac{e^{2v_j}-1}{e^{2v_j}+1} & : \text{Tan hyperbolic} \end{cases}$$

Training the network

The ANN network shown in Fig. 2.8 must be trained by a set of input-output examples collected by high fidelity aerodynamic simulations in a database. This means the weights have to be adjusted so as to associate to the right output for a given input vector. The back-propagation algorithm is used to find the weights. It uses two passes of signals to adjust the weights at each iteration n . The first pass of signal flow is from input to the output layer. The network is exposed to the input vector to find the value of the network output for the given initial set of weights. The error is calculated as the difference between the network output and the real value. Then the

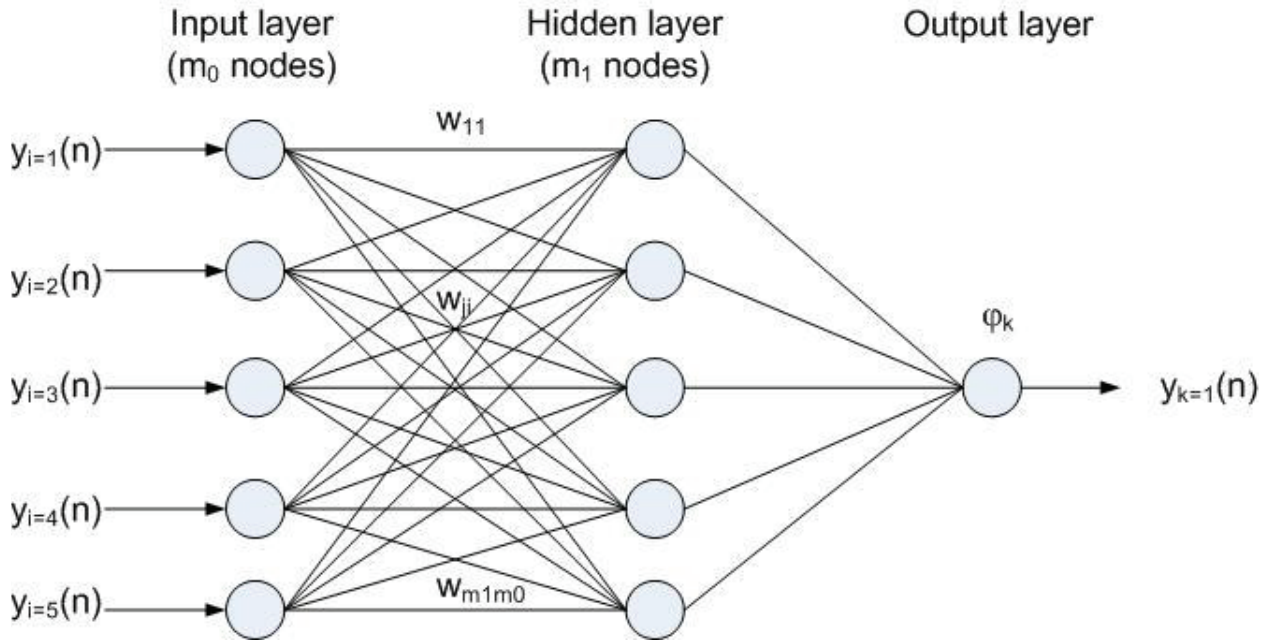


Figure 2.8: A multi-layer ANN network architecture

error signal is back-propagated so as to adjust the weights accordingly. This cycle is repeated until the error converges to a minimum value.

Assuming N number of input patterns in the database, an epoch is defined as N presentation of input vectors to the database. The weights can be updated after one epoch (batch mode training) or after each time an input vector is presented to the network (sequential mode of training). The mode of training is sequential in the present method. The input vectors are randomly selected from the database and then presented to the network during each epoch. The stochastic feature of this random behavior in sequential mode, makes it less likely for the back-propagation algorithm to be trapped in a local minimum [50].

2.3.3 ANN accuracy improvement

In the optimization loop, the surrogate model is used to evaluate an approximate value of the objective function, hence the optimum candidate will be as accurate as

the surrogate model can be. The successful results of the optimization by this method, surrogate-based optimization, proves the practicality of this method. Appendix C provides information concerning universal approximation theory. This is an existence theorem which mathematically justifies the existence of a network which is able to approximate any arbitrary continuous function with desired level of accuracy. This is similar to the existence of an approximation with any degree of accuracy by means of Fourier series for any continuous function.

An ANN network can be trained practically so as to accurately approximate the output value of a set of input vectors in a database. However, what makes the ANN training a challenge is the generalization feature of the network. It is important that ANN can generalize on a new input vector which is not presented to it during the training. This feature is essentially important for optimization. Cross-validation discussed in the following section could enhance this ability. Also the number of hidden nodes is another parameter which can reduce the approximation error if chosen properly.

An ensemble of surrogates was proposed [13] to take advantage of several surrogates simultaneously. ANN, RBF and ensemble of both were used for the evaluation of turbine isentropic efficiency. The accuracy of the last two methods are not any better than ANN. Usually RBF performs better with a high number of design variables. The ensemble of surrogates does not necessarily improve the accuracy. This is also observed by Haftka *et al.* [13].

The accuracy of the ANN model is indicated in Fig. 2.9 in terms of average relative error between high fidelity and ANN output among testing patterns. This is based on one of the cases presented in Chapter 4. This plot shows that the ANN model is reasonably accurate for estimating the isentropic efficiency for candidates that were not involved in the training process.

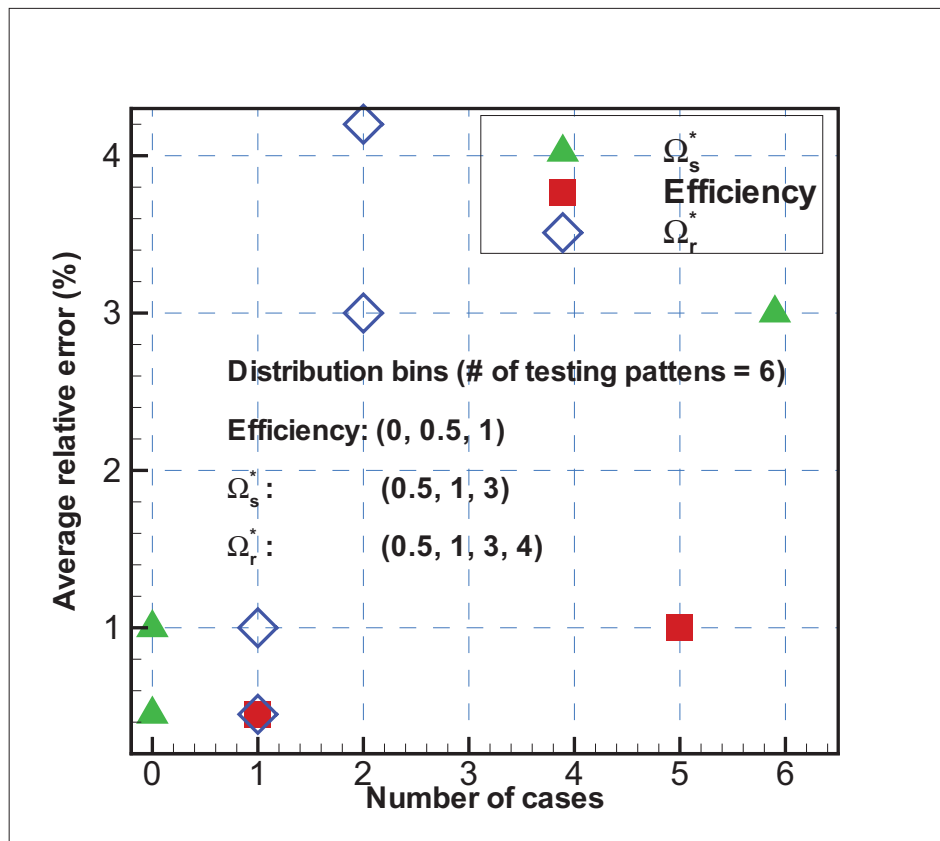


Figure 2.9: Error distribution of ANN approximation based on testing patterns (Taken from a single point single objective optimization using one ANN model per objective function)

The code developed by Mengistu [8] for ANN training was used for 2D aerodynamic optimization. In order to use it for 3D optimization, some improvements to enhance the accuracy of the model are achieved in the course of this research work. These contributions are discussed in the following sub sections.

Single output architecture

In the course of this work it was found that a single output architecture has advantages over multiple output architecture. This is discussed in [51]. The first and foremost advantage is the improvement in accuracy. Having an individual network per output, permits more chance to change the network architecture to reduce the errors as it involves only one unknown vector so that any change would not impact the approximation of any other output since the networks are separate. On the other hand, single output architecture gives more flexibility for multi-disciplinary optimization, since adding another discipline, would require the addition of new networks to the already trained ones.

Cross-validation and early stopping method

The mean-square error decreases in back-propagation algorithm as the learning continues to progress in epochs. However, there is a chance that the weights of the network get overfitted and consequently the network gets too stiff to be able to generalize. Therefore, the database is divided into the training and validation subsets for cross-validation. The training subset is used to evaluate the network weights, while the testing set is used to assess the generalization error of the network. There is an onset where the weights are overfitted. The validation error starts to increase at the onset. If the training process stops at that point, the network won't get overfitted. This is called early stopping method and is implemented in to the current algorithm in the present work. It is recommended when the number of patterns (N) is less than

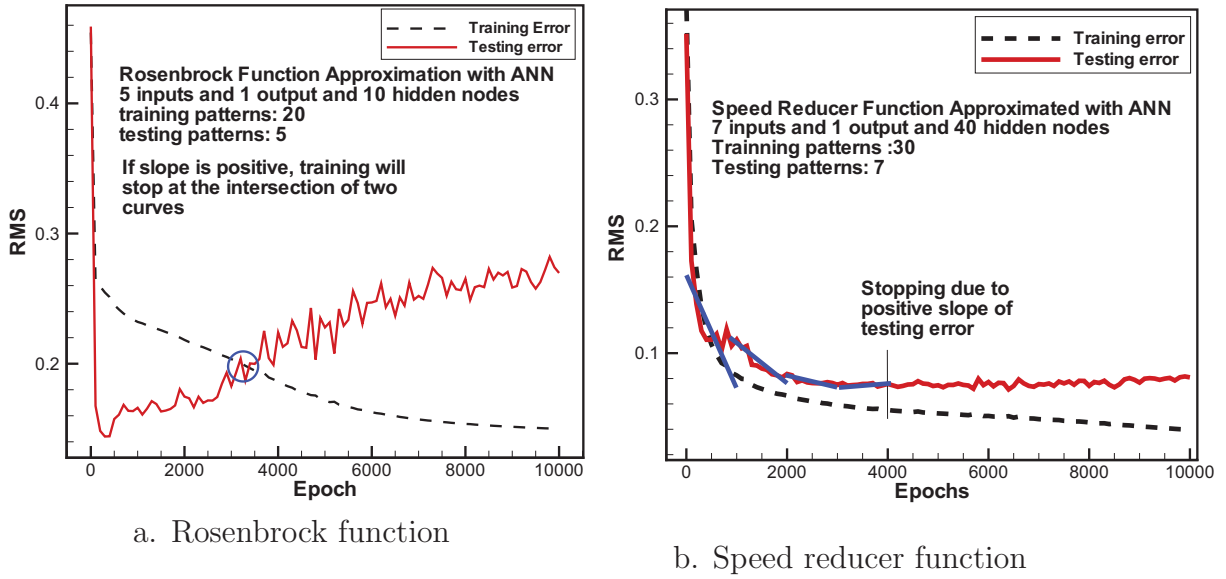


Figure 2.10: Early stopping applied on training of two generic functions (Appendix C) with ANN

the number of weights times thirty ($N < 30W$) [50]. The application of this method is shown on two generic functions in Fig. 2.10; The functions are defined in Appendix C. After certain number of epochs, which is a user input, the slope of the testing error curve is approximated by least square method. The training stops after some more number of epochs if the slope is positive. The training stops at the later of either a positive slope or intersection of training and testing curves.

As the number of patterns in the database is less than the number of the weights in the network, early stopping is necessary for improving the generalization performance [13]. The training subset is 70% to 80% of the number of patterns in the database, while the remaining patterns are used as a testing subset.

Network architecture optimization

There are several parameters related to ANN training such as the number of hidden nodes, type of transfer function and the learning rate which affect the accuracy of the network. The combination of mentioned parameters sum up to many possibilities and

so hard to find out the best by user interaction. Therefore, a method is implemented in the present work to verify all the given possibilities automatically and report the best combination in terms of minimum testing (generalization) error.

A range of variation is given for number of hidden nodes (usually 5 to 30), learning rate for input to hidden layer (usually 0.5 to 0.9) and hidden to output layer (usually 0.01 to 0.04). Then the network is trained for each case and the RMS testing error is calculated. Because the database may be split differently into training and testing subsets for each case, the comparison of testing errors would not be fair between each case. Therefore an unbiased generalization error measurement is needed for the whole network.

K-fold cross-validation is used for calculating the generalization root mean square error (GRMSE) [52]. The database is divided into k subsets of approximately equal size for each combination mentioned earlier. A surrogate model is constructed k times, each time leaving one of the subsets out of the training set, and using the removed subset to compute the error measure of interest. The GRMSE is then computed using the averaged value of the k error measures obtained.

2.3.4 Genetic algorithms (GA)

In this work, a real coded genetic algorithm GA is used where the design parameters are represented using a floating-point representation so that any individual is characterized by a vector of real numbers. The GA algorithm that was developed by Mengistu [8], involves the four basic operations namely, selection, crossover, mutation and elitism [53]. The initial population is initialized randomly within the design space and the fitness in each generation is evaluated by the surrogate model. Usually fifty individuals are used in each generation.

Selection

Next generation of candidates (children) are obtained by reproduction from the current pool of candidates (parents). There are several selection methods to select the pair of parents. Roulette wheel method is used in this work. All individuals are ranked based on their fitness function. They assign a portion on the wheel which is proportional to their fitness values. Once the wheel is revolved the individual with higher fitness is more likely to be selected. The wheel is spun every time a parent needs to be selected.

Cross-over

The cross-over operation is similar to offspring in nature. The new candidates are born from the parents. They inherit part of the genetic features of there parents. In the present work, linear combinations of the two candidates are used for cross-over as shown in the following equation. The cross-over probability α is usually 0.7.

$$\begin{cases} Children_1 = \alpha(Parent_1) + (1 - \alpha)(Parent_2) \\ Children_2 = \alpha(Parent_2) + (1 - \alpha)(Parent_1) \end{cases}$$

Mutation

Mutation alters some of the genes in a chromosome. This operation creates a new candidate (chromosome). It is used in GA to alleviate the chance of being trapped in a local optimum. A mutation probability value of 0.1 is used in this work, i.e. 10% of the population in each generation would mutate. The candidates are randomly selected and are multiplied by a random factor in such a way that the resulting value stays in the specified range of that variable.

Elitism

Usually the two best candidates of each generation are directly passed to the next generation without being manipulated by genetic operations. This is a guarantee that the best found solutions won't be neglected in the next generations.

2.4. Simplified structural model

Designing a turbine blade involves aerodynamic, structural, thermal, dynamic and vibration analyses. While doing optimization in one discipline, enough attention must be paid to other disciplines otherwise the outcome would not be practical. In practice, the aerodynamic optimization of the blade shape drags other disciplines into consideration. The aerodynamic performance improvement by modifying the blades stacking is shown later to be effective, however changing the stacking curve is a critical issue in rotor blades because of centrifugal forces. Usually the blades are stacked radially(through the CG of the individual airfoils) to reduce the centrifugal effects. However, aerodynamic redesign is suggesting different configuration of profile stacking. It is important to assess such a change in stacking line on the stresses due to centrifugal forces.

2.4.1 Structural model for blade

Rotor blade can be modeled as a rotating cantilever beam. Pressure forces exerted from flow around the blade and centrifugal forces due to rotation are the main forces applied on the blade. Pressure loadings distribution is nonlinear. For turbines, the resultant pressure forces are much smaller than the centrifugal forces since the blades are thick. Centrifugal forces are about 100 times larger than pressure forces in the cases that were tested in this thesis. Centrifugal forces generate moment around the center of gravity of the hub profile. This happens when the stacking is not radial. The

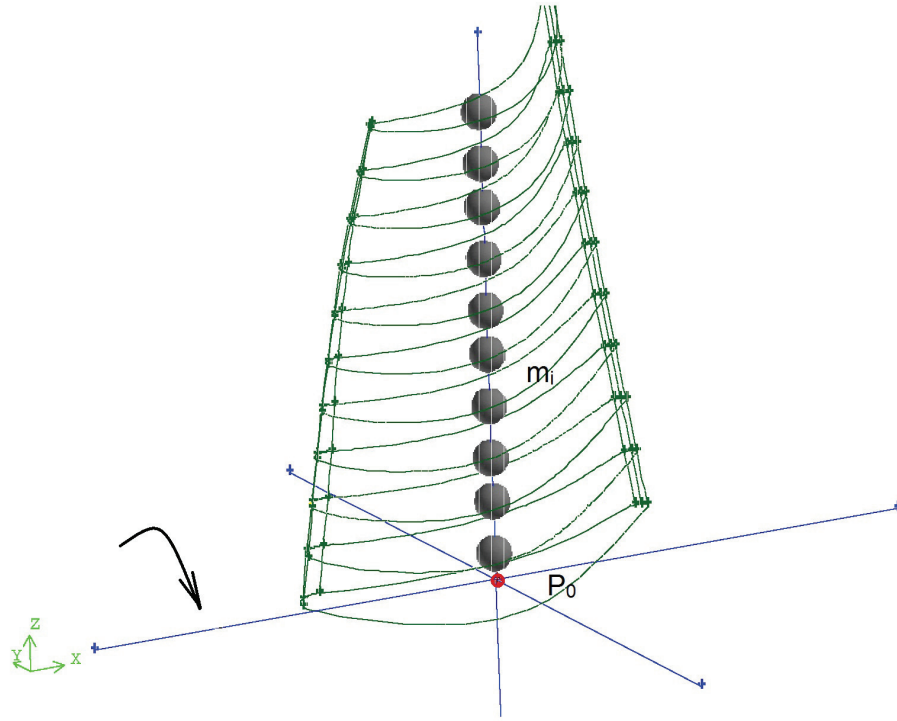


Figure 2.11: Derivation of blade volume into distributed mass

moments generated by centrifugal forces result in stresses at the hub. The centrifugal forces are also creating a tensile stress at the hub. The blade volume can be separated into several subsections as indicated in Fig. 2.11.

$$F_c = \int_{r_h}^{r_t} \rho \omega^2 A r dr \quad (2.2)$$

where

- ρ : Blade density (Kg/m^3)
- ω : Rotational speed (rad/s)
- A : Area of blade section (m^2)
- r : Radial coordinate (m)

Centrifugal forces applied to each mass are calculated according to Eq. 2.3:

$$\vec{F}_c = \sum_i^n F_i \hat{e}_i = \sum_i^n m_i r_i \omega^2 \hat{e}_i \quad (2.3)$$

where

$$\begin{aligned}
 F_i & : \text{Centrifugal force exerted to } i^{\text{th}} \text{ element (N)} \\
 \hat{e}_i & : \text{Unit vector of } F_i \text{ (rad/s)} \\
 m_i & : \text{Mass of } i^{\text{th}} \text{ element (Kg)} \\
 r_i & : \text{Radial coordinate of } i^{\text{th}} \text{ element (m)}
 \end{aligned}$$

The moment of each force around the center of gravity of the hub can be calculated as in Eq. 2.4:

$$\vec{M} = \sum_i^n \vec{l}_i \times \vec{F}_i \quad (2.4)$$

where

$$\begin{aligned}
 F_i & : \text{Vector connecting } P_0 \text{ and } m_i \\
 \hat{e}_i & : \text{Center of gravity of the hub profile}
 \end{aligned}$$

2.4.2 Bending moment: Beam with arbitrary area

A general equation for pure bending of elastic members of arbitrary cross section whose reference axes are not the principal axes is indicated in this part and is taken from [4]. The two basic requirements for equilibrium are enforced: 1) The total axial force on any cross section of a beam must be zero. 2) The external bending moment at a section must be developed by the internal stresses acting on the cross section. Hook's law is postulated for uniaxial normal strain.

Summing up all the moments around the center of gravity of hub profile, three components of the total moment are calculated. It is observed that the moment component in z direction which generates torsion is approximately two orders of magnitude less than the two other components. Therefore it is reasonable to neglect M_z . The axial and tangential components of moment, M_x and M_y , can be used to calculate the bending stress at hub profile.

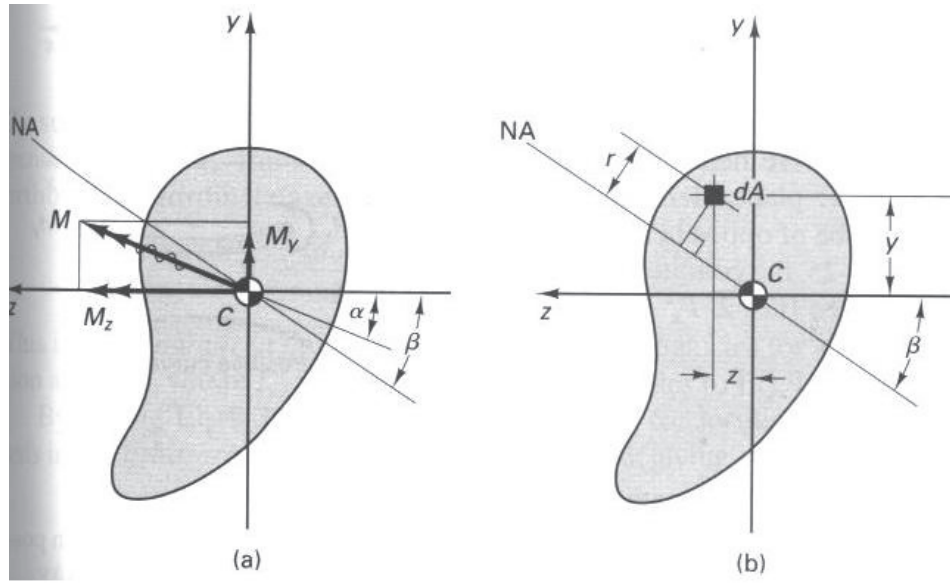


Figure 2.12: Bending of unsymmetrical cross section ([4])

Figure 2.12 indicates the general moment vector applied on an arbitrary area. The generalized flexure formula can be used to calculate the bending stress distribution as in Eq. 2.5.

$$\sigma_{bending} = -\frac{M_y I_x + M_x I_{xy}}{I_x I_y - I_{xy}^2} x + \frac{M_x I_y + M_y I_{xy}}{I_x I_y - I_{xy}^2} y \quad (2.5)$$

where

I_x, I_y : Area moment of inertia (m^4)

I_{xy} : Product of inertia (m^4)

Finally total stress is the combination of bending and tensile stresses.

$$\sigma_z = -\sigma_{bending} + \frac{F_s}{A_h} \quad (2.6)$$

where

F_s : *Spanwise component of total centrifugal force (N)*

A_h : *Hub cross section area (m²)*

2.4.3 Stress distribution computation

A C++ code was written to calculate the stress distribution on the hub section based on the above model. ANSYS-Fluent preprocessor (Gambit) is used to calculate the center of gravity of spanwise subsections of the blade as indicated in Fig. 2.11. ANSYS-Mechanical is used to calculate the area moment of inertia and product of inertia of the flat hub profile.

Chapter 3

Blade shape parameterization

This chapter describes the technique applied for parameterizing the turbine blade shape. The design parameters for optimization of the stacking line and stagger angle distribution are introduced. The sensitivity of the output parameters to the chosen design variables is presented.

3.1. Blade shape representation

Geometric shape representation is an essential part of the optimization problem. Understanding the flow physics plays an important role in developing an effective shape parameterization. Generally geometrical entities such as the coordinates of the control points are selected as the design parameters. However, it is more practical to pick up the designer's parameters for a shape optimization. Another aspect of the parameterization is the number of parameters. The number of parameters in any optimization problem is essentially important. The optimization problem gets more complicated as the number of parameters increases. This is known as the 'curse of dimensionality' in evolutionary optimization methods. In addition, the flexibility and geometric continuity strongly contribute to the effectiveness of the parameterization.

The blade shape is formed by stacking of several two dimensional airfoils in

spanwise direction according to a path which is usually called stacking line and is passing through one of the airfoils reference points. The airfoil reference point is usually the centroid for rotor blades and the leading edge for stator blades. The blade shape is obtained by wrapping a surface around the two-dimensional airfoils using e.g. the skinning technique [42]. In the present optimization work, the shape of the two-dimensional airfoils is fixed. In order to form the blade shape, the profiles are stacked according to stacking line, then they are reoriented by changing the stagger angle with respect to the profile reference point. Stagger angle variation and stacking give three degrees of freedom to each profile. Each profile can rotate with respect to radial direction, move in axial and tangential directions. Therefore ideally all possible but feasible blade shapes for the given 2D airfoil profiles can be explored. Quadratic rational Bézier curve (QRBC) was chosen as a geometric parameterization tool. It was initially used to parameterize the stacking line, it was also used to represent stagger angle distribution from hub to tip.

3.2. Quadratic rational Bézier curve (QRBC)

QRBC is a second-degree NURBS with three control points. It represents exactly a conic curve in an oblique coordinate system, it can be expressed parametrically in terms of $u \in [0, 1]$ as [42]:

$$\vec{C}(u) = \frac{(1-u)^2 w_0 \vec{P}_0 + 2u(1-u)w_1 \vec{P}_1 + u^2 w_2 \vec{P}_2}{(1-u)^2 w_0 + 2u(1-u)w_1 + u^2 w_2} \quad (3.1)$$

where $\vec{C}(u)$ gives the cartesian or cylindrical coordinates of any point on the stacking curve in terms of the parameter u , \vec{P}_i is the cartesian (or cylindrical) coordinates of control point i . The QRBC is a smooth second order curve that represents exactly any conic line e.g. an ellipse, a parabola, a circle or a hyperbola. This feature of the QRBC excludes inflection points in the profile, hence ensuring that all resulting

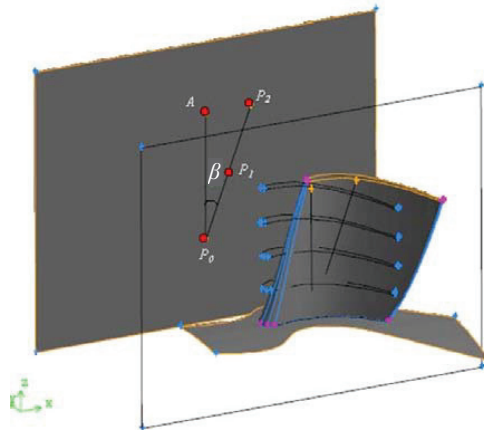
profiles are feasible, and eliminating infeasible regions of the design space.

3.3. Stacking curve parameterization

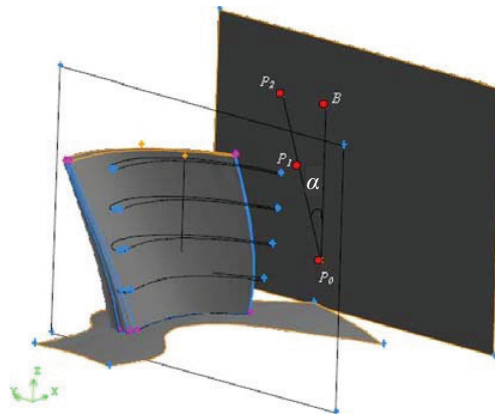
Aerodynamicists usually deal with the blade lean, sweep and bow as the set of traditional geometric design parameters to represent the blades in the hub to tip direction. These design parameters provide a physical insight into the design space. For this reason, a quadratic rational Bézier curve (QRBC) was chosen to parameterize the stacking line, not only due to its flexibility and suitability, but also due to the fact that the design parameters can be expressed directly in terms of the QRBC parameters.

Based on the QRBC representation given in Eq. 3.1, the QRBC parameters namely, P_i and w_i for $i = 1 - 3$, can be selected to parameterize the stacking curve. P_0 is fixed at some point on the hub surface (e.g. blade center of gravity or blade LE) and P_2 moves on the tip surface as shown in Fig. 3.1.a. In other words, without loss of generality, the coordinates of P_0 and the radial coordinate of P_2 are fixed. According to Fig. 3.1.a, the sweep angle is defined as β and is controlled by the axial coordinate of P_2 . Figure 3.1.b shows the lean angle α , which is set by the circumferential coordinate of P_2 . Figure 3.1.c shows the blade bowing which can be controlled by the circumferential and radial coordinates of P_1 as well as the weight w_1 . The circumferential coordinate of P_1 is controlled by angle $\widehat{P_1 P_0 B}$ as shown in Fig. 3.1.c. The lean angle is positive in the direction of the suction side and the sweep angle is positive in the axial direction. The positive sign of Θ_{P_1} makes the pressure side concave as indicated in Fig. 3.1.c and a negative value makes it convex.

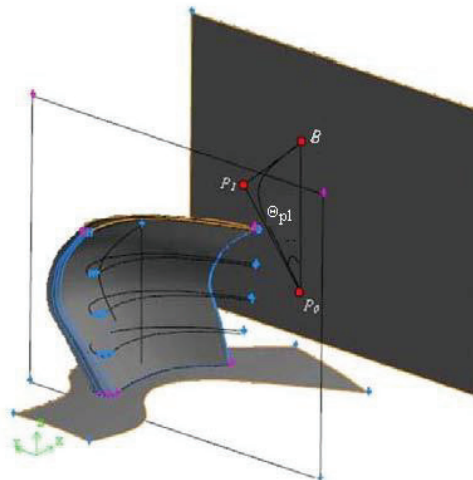
The design variables of the optimization must be wisely chosen amongst the geometrical parameters. The most influential parameters are of higher priority as keeping all can make the optimization problem too hard to solve. The following



a. Blade sweep



b. Blade lean



c. Blade bow (or compound lean)

Figure 3.1: Stacking curve parameterization with QRBC

section discusses the choice of design variables.

3.3.1 Stacking curve design variables

Designers use lean, sweep and bow for stacking of the profiles. The way these parameters are linked to the QRBC parameters makes this parameterization practical. Generally QRBC has eight parameters for stacking curve as listed in 3.1. The weights, coordinates of P_1 , the coordinates of P_2 except its radial coordinate as it has to lay on the tip surface.

These design variables are shown in the exploded views of meridional and circumferential planes in Fig. 3.2. The stacking curve is projected onto a circumferential and meridional planes that pass through P_0 in Fig. 3.2.a and b respectively.

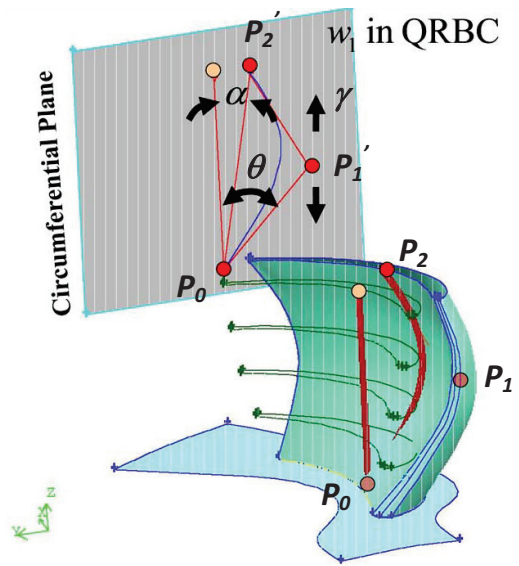
The relationship between QRBC parameters and design variables can be derived by considering a cylindrical coordinate system which its z -direction is aligned with the shaft axis of the turbine. The axial coordinate of P_0 is set at zero.

The sweep angle, β , and the compound sweep angle, λ , are related to the axial coordinates of P_2 and P_1 respectively as indicated in Eqs. 3.2 and 3.3. The axial coordinate of P_1 is assumed identical as the axial coordinate of P_0 . As the first step, this is a simple design choice. It basically means that λ is assumed zero therefore it is impossible to have compound sweep.

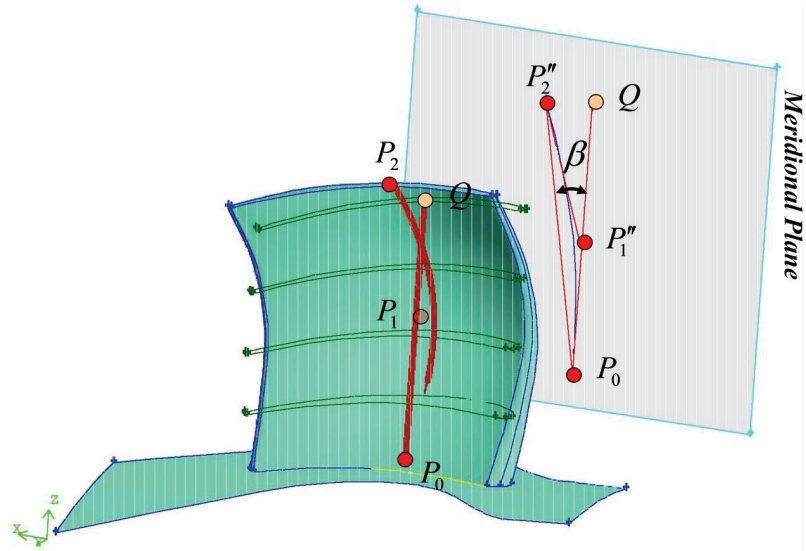
The lean angle can be related to the tangential coordinate of P_2 as shown in equation 3.4. Similarly the angle θ can be controlled with the tangential coordinate of P_1 as indicated in equation 3.5. The span ratio is a number between zero and one. The zero and one correspond to the hub and the tip respectively. The relationship between the span ratio and the radial coordinate of P_1 is indicated in 3.6.

$$z_{P_2} = (r_{p_2} - r_{p_0})\tan(\beta) \quad (3.2)$$

$$z_{P_1} = (r_{p_1} - r_{p_0})\tan(\lambda) \quad (3.3)$$



a. Tangential coordinate of P_1 , coordinates of P_2 , weight of P_1



b. Axial coordinate of P_2

Figure 3.2: Design variables for stacking curve

Table 3.1: List of QRBC parameters and possible design variables

	QRBC parameters	Related design variable	Symbol
1	Axial coordinate of P_2	sweep angle	β
2	Tangential coordinate of P_2	lean angle	α
3	Axial coordinate of P_1	compound sweep	λ
4	Tangential coordinate of P_1	compound lean	θ_{P_1}
5	Radial coordinate of P_1	span ratio	γ
6	Weight of P_0	1	w_0
7	Weight of P_1	Bowing intensity	w_1
8	Weight of P_2	1	w_2

$$\theta_{P_2} = \arcsin\left(\frac{(-r_{P_0} \cos \alpha + \sqrt{r_{P_2}^2 - r_{P_0} \sin^2 \alpha}) \sin \alpha}{r_{P_2}}\right) \quad (3.4)$$

$$\theta_{P_1} = \arcsin\left(\frac{(-r_{P_0} \cos \theta + \sqrt{r_{P_2}^2 - r_{P_0} \sin^2 \theta}) \sin \alpha}{r_{P_2}}\right) \quad (3.5)$$

$$r_{P_1} = \gamma(r_{P_2} - r_{P_0}) + r_{P_0} \quad (3.6)$$

The first derivative of the QRBC at the endpoints are shown in Equations 3.7 and 3.8 (Refer to appendix A). The slope of the curve at the end points in QRBC is not only the function of control points coordinates but also the weights. The weight w_1 influences the slope of the curve at both ends. However, the w_0 and w_2 only influence the slope at the P_0 and P_2 , respectively. Therefore, the weight w_1 was selected as the design variable while the corresponding weights of P_0 and P_2 were assigned a unit value.

$$\vec{C}'(u = 0) = \frac{2w_1}{w_0}(P_1 - P_0) \quad (3.7)$$

$$\vec{C}'(u = 1) = \frac{2w_1}{w_2}(P_2 - P_1) \quad (3.8)$$

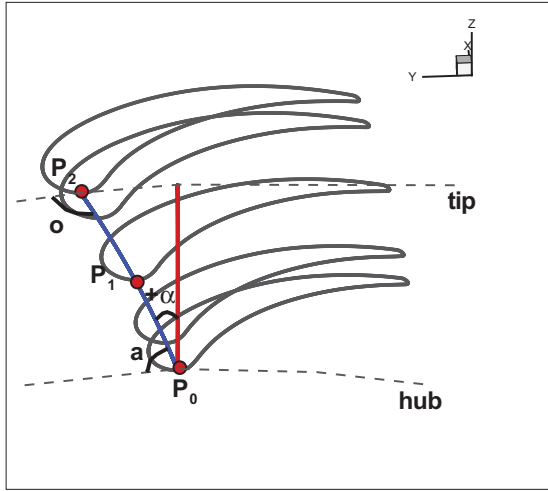
The weight w_1 is affecting the curvature of the curve as well as the slope at the end points. A zero value for w_1 makes the stacking curve a straight line connecting the two end points while increasing the value of w_1 increases the curvature of the

stacking line. Hence, it is called bowing intensity. Therefore there are five stacking curve design variables namely lean and sweep angles, compound lean, span ratio and bowing intensity.

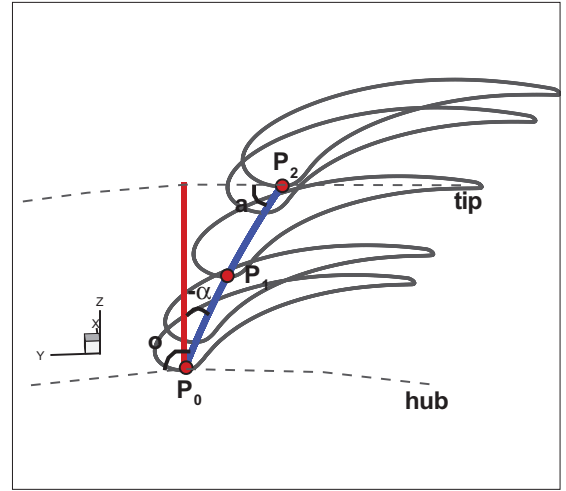
The slope of the stacking curve at the end points defines the magnitude of the lean or sweep from an aerodynamic view point. A positive lean, shown in Fig. 3.3.a makes an acute angle with the hub curve and an obtuse angle at the tip. For the negative lean, however, there is an acute angle at the tip and obtuse angle at the hub, as shown in Fig. 3.3.b. In the following chapter it will be shown that acute and obtuse angles at the end points have different implications on the pressure distribution in the end-wall region. Compound lean is introduced to produce the same type of angle (acute or obtuse) at both hub and tip. The compound lean is indicated in Figs. 3.3.c & d.

3.3.2 Stacking curve design variables range

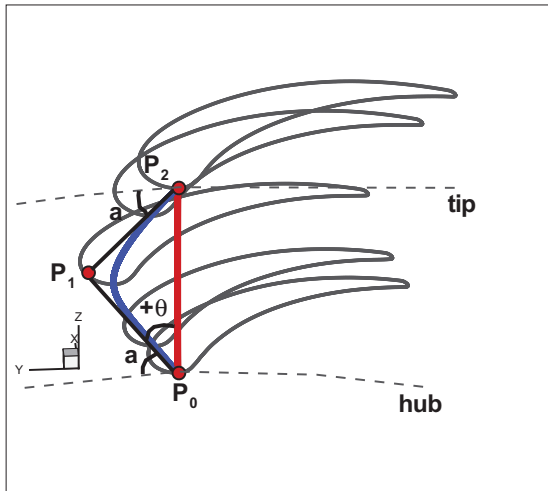
The design space must be defined after selecting the design variables. An important design concern is to keep the design space within a feasible range from a blade structural point of view and at the same time be large enough to adequately explore the aerodynamic performance. For example, leaning the blade in the direction of rotation will introduce bending moments due to centrifugal forces, but that will balance those due to aerodynamic loads [54], therefore, such blade lean will be allowed. Starting from some initial choice of design variables, preliminary results of the optimization reveal the direction in which the design space should be extended or limited. For instance, the stator lean angle of the optimum stator is always close to its lower bound. Therefore, it would be better to extend the range of the stator from its lower limit. i.e., instead of ± 20 , it is better to modify the range to $[-30, +10]$. The range of possible design variables for stator and rotor stacking curves are given in the Table 3.2.



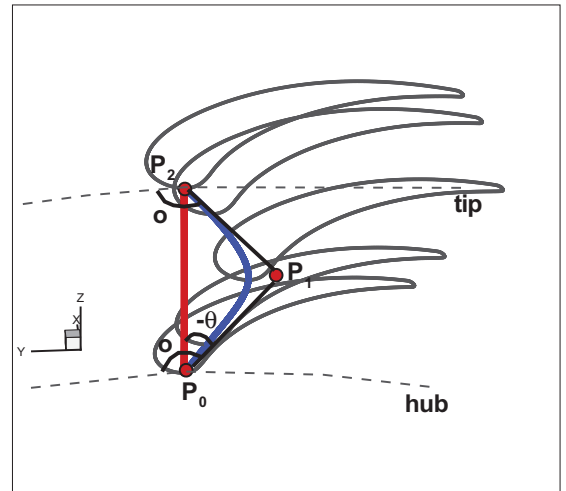
a. Positive lean



b. Negative lean



c. Compound lean (Positive bow)



d. Compound lean (Negative bow)

Figure 3.3: Illustration of lean angles and compound lean (a: acute angle, o: obtuse angle)

Table 3.2: Stacking curve design variables range for stage

	Design variables	Symbol	Min.	Max.
1	Stator sweep angle	β_s	-8	12
2	Stator lean angle	α_s	-36	0
3	Stator compound lean	$\theta_{P_{1,s}}$	-20	30
4	Stator span ratio	γ_s	0.1	0.9
5	Stator Bowing intensity	$w_{1,s}$	0	3
6	Rotor sweep angle	β_r	-10	15
7	Rotor lean angle	α_r	-5	20
8	Rotor compound lean	θ_{P_1}	-10	35
9	Rotor span ratio	γ	0.22	0.82
10	Rotor Bowing intensity	$w_{1,r}$	0	3

3.3.3 Sensitivity analysis of stacking curve design variables

Once the geometric parameterization is set up, all the parameters are used as design variable. However, not all of them have the same influence on the objective function of the optimization problem. Besides, it is easier to solve an optimization problem with less number of design variables. Therefore a sensitivity analysis was carried out to identify the influence of each design variable to the objective function.

A first order variance-based method was used, it assumes no interaction between the different design variables, hence the effect of each one on the objective function is studied one at a time. The variance of the objective function around that of the original geometry can be calculated by changing one parameter within its specified range while fixing the rest. Then all the calculated variances are normalized by total variances and a measure of importance of each parameter is calculated as a percentage.

The five introduced design variables that describe each stacking curve are used for stator and rotor blade rows parameterization. Based on the sensitivity analysis, it was found that among all five design variables, the lean and sweep angles are the most influential variables for either stator or rotor, as shown in Fig. 3.4. The bowing parameters have the least priority for this case study.

The sensitivity analysis was only applied on individual stator and rotor cases. In

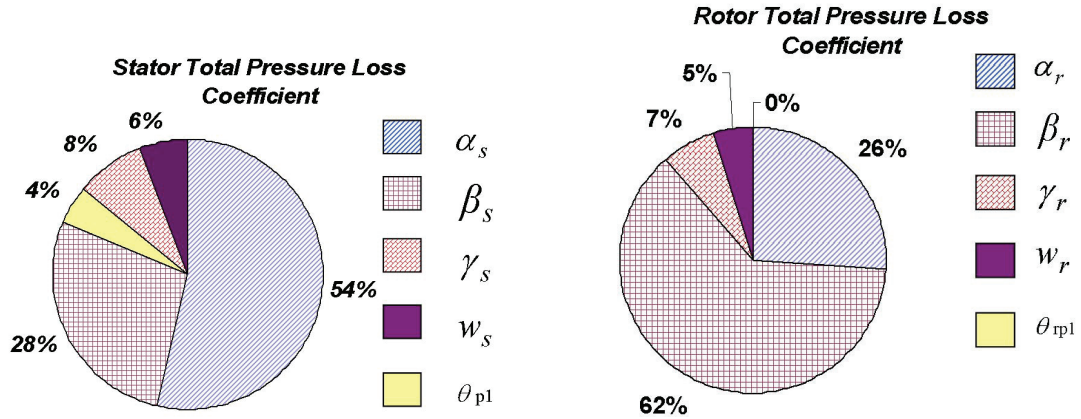


Figure 3.4: The sensitivity of the total pressure loss coefficients to the stacking curve design variables

In addition to this study, the results of a stage optimization that is presented in Chapter 4 show that the bowing is not as influential as the lean and sweep angles. The design variables of the stage optimization case are: lean and sweep angles for stator and rotor and rotor bowing intensity. It is observed that the bowing intensity for rotor is almost zero for the optimum rotor blade. Based on the sensitivity analysis and the mentioned stage optimization case, the compound lean, θ_{P1} , and the span ratio, γ , can be crossed out from the list of design variables if there is a need to reduce the number of design variables. It should be noted however that this conclusion is case dependent, e.g., if there is an aerodynamic blockage at stage inlet, this conclusion may not apply.

3.4. Blade stagger distribution parameterization

The turbine blades are highly twisted because of the variation of blade speed from hub to tip. Usually twist is measured by the stagger angle. In the absence of any additional information, the distribution of the stagger angle from hub to tip is usually assumed linear. This distribution was also included as a design variable; it was parameterized

with QRBC.

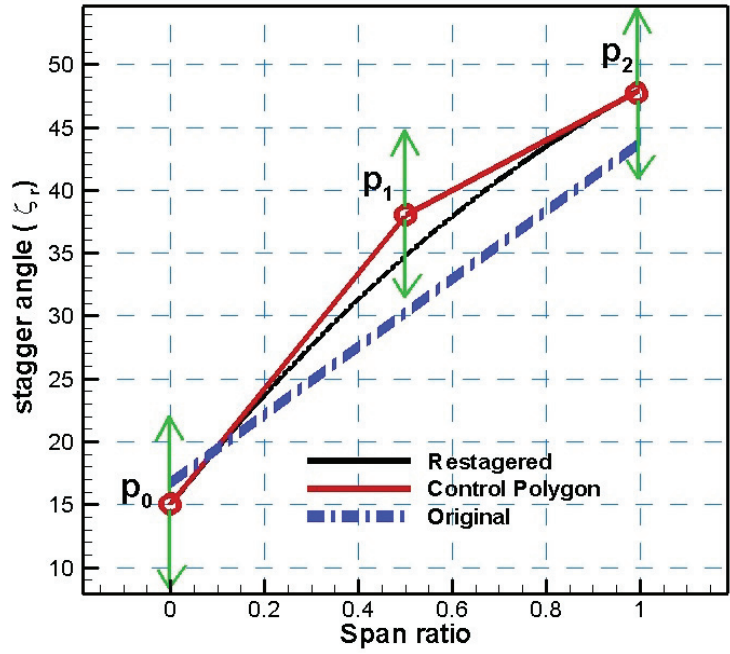
Figure 3.5 indicates the control polygons of QRBC to represent the stagger spanwise distribution for both stator and rotor. Control points P_0 , P_1 and P_2 are assigned at hub, mid-span and tip, respectively, and the design variables are given by the stagger angles at the same spanwise locations, which are the coordinates of the control points in QRBC. Therefore with only three stagger angles the spanwise distribution of blade stagger is parameterized.

In the present work, the stator stagger is taken to be varying linearly, see Fig. 3.5.b, and is represented by fixing P_1 and varying P_0 between ± 5 . This choice of stagger variation ensures that the stator throat area can be kept approximately constant so as to have a fair comparison between the original stage and the optimized one.

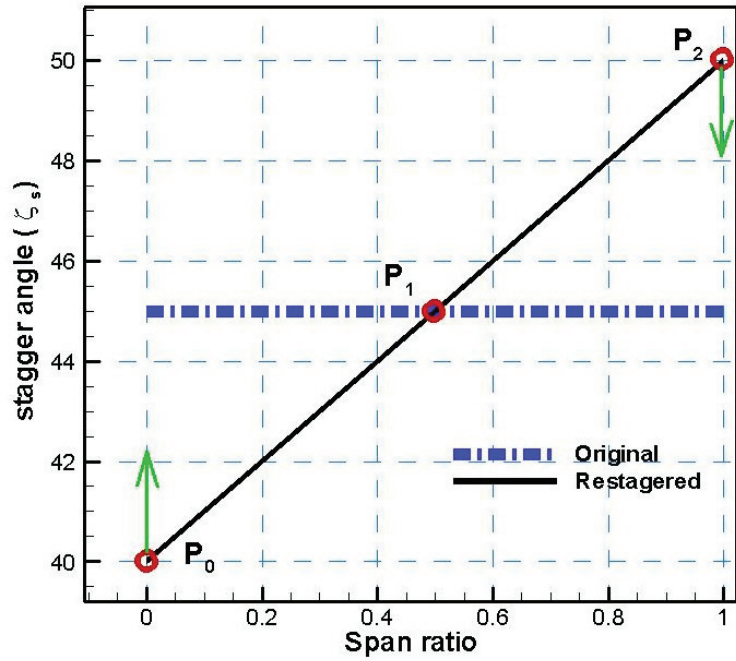
The rotor stagger angle distribution, plotted in Fig. 3.5.a, is represented with three control points that are given by the stagger angles at hub, mid-span and tip; all three angles are allowed to change during optimization. So we end up with four design variables to describe the variation of stagger for both stator and rotor.

3.4.1 Design variables range

As a preliminary step, stagger angle of a rotor mid-span is studied with 2D analysis. An initial range of variation of the stagger angle is obtained based on this analysis. A variation of ten degrees was allowed for each stagger angle. The mid-span stagger angle, ζ_m , must be between the hub and the tip stagger angles. In the present work, the range of stagger angles are assigned according to Table 3.3.



a. Rotor



b. Stator

Figure 3.5: Stagger angle parameterization with QRBC

Table 3.3: Stagger angle design variables range

	QRBC parameters	Symbol	Min. ($^{\circ}$)	Max. ($^{\circ}$)
1	Stator hub stagger angle	ζ_s	40	50
2	Rotor hub stagger angle	ζ_{rh}	12	22
3	Rotor mid-span stagger angle	ζ_{rm}	22	38
4	Rotor tip stagger angle	ζ_{rt}	38	48

Chapter 4

Single point optimization

This chapter presents the application of the present optimization methodology for improving the efficiency of an axial turbine stage at the design point. Since the stacking line is the geometric entity that is highly influential on the blade losses, it is taken as the design variable while the individual airfoil sections forming the blade shape at different spanwise locations are left unchanged. Consequently, additional improvement is suggested by the combined redesign of stacking curve and stagger angle in the last section.

4.1. E/TU-3 axial turbine stage

A low speed subsonic axial turbine stage, referred to as the E/TU-3 turbine, that is built and tested at DLR, Cologne [3] is selected for redesign. The turbine stage geometry is given as a set of x-,y- and z-coordinates of several blade sections at five spanwise locations from hub to tip. Several geometric and aerodynamic features of that stage are listed in Tables 4.1 and 4.2. The details which are available in Fottner [3], helped in building the geometry and in assessing the flow simulation tool namely ANSYS-Fluent that is used in the optimization scheme. The original stator and rotor blade profiles are sketched in Fig. 4.1.

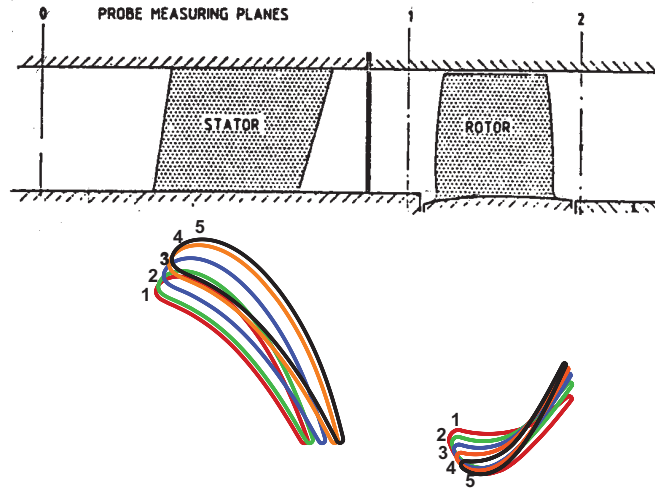


Figure 4.1: E/TU-3 single stage turbine case [3]

Table 4.1: E/TU-3 single stage turbine specifications

Data	Stator	Rotor
Number of blades	20	31
Blade aspect ratio	0.56	0.95
Blade solidity	1.56	1.51
Flow turning	69°	105°

Table 4.2: E/TU-3 single stage turbine design point specifications

Inlet total temperature (K)	346
Rotor speed (RPM)	7800
Stage pressure ratio	0.51
Reynold number	1.5×10^6
Efficiency	90%
Mid-span flow coefficient	0.74
Mid-span stage loading	1.93
Average reaction (%)	31

4.2. Optimization Objectives

There are many possible objective functions for each case. The objective function is the designer's choice. Usually for single blade rows the total pressure loss coefficient, Y , or the isentropic efficiency is chosen. The objective function for a single rotor blade row optimization is defined in Eq. 4.1 based on the rotor isentropic efficiency. Any constraints can be introduced into the objective function as a penalty term, PT .

$$F_{obj1}(X) = Min((1 - \eta_{is,r}) + PT) \quad (4.1)$$

where:

$$\eta_{is,r} = \frac{1 - \left(\frac{T_3}{T_{02r}}\right)}{1 - \left(\frac{P_3}{P_{02,r}}\right)^{\frac{\gamma-1}{\gamma}}} \quad (4.2)$$

When optimizing a turbine stage, one may choose either the total-to-total efficiency (η_{tt}) or the total-to-static efficiency (η_{ts}). In designing the last stage of a turbine, η_{ts} would be a better choice as it ensures that the exit kinetic energy is minimized. For any interior stage, the use of η_{tt} would be a better choice. These two efficiencies can be expressed as:

$$\eta_{tt} = \frac{1 - \left(\frac{T_{03}}{T_{01}}\right)}{1 - \left(\frac{P_{03}}{P_{01}}\right)^{\frac{\gamma-1}{\gamma}}} \quad (4.3)$$

$$\eta_{ts} = \frac{1 - \left(\frac{T_{03}}{T_{01}}\right)}{1 - \left(\frac{P_3}{P_{01}}\right)^{\frac{\gamma-1}{\gamma}}} \quad (4.4)$$

Therefore for the single stage turbine without exit propulsion the objective function given in Eq. 4.5, can be used. The loss parameter, $(1 - \eta_{ts})$, is minimum

when ($\eta_{ts} = 100\%$). The PT is a penalty term that can account for any mechanical, geometric or aerodynamic constraints imposed on the optimization process. In this case, the mass flow rate is allowed to vary by not more than 2.8% from its designed value otherwise, the objective function is penalized by a positive additional value.

$$F_{obj2}(X) = Min((1 - \eta_{ts}) + PT) \quad (4.5)$$

Secondary flow loss in turbines typically contributes to one third of the total aerodynamic loss. Secondary flow can be measured by the streamwise vorticity which depends on the aerodynamic inlet blockage, the flow turning and loading [55]. Therefore, the dimensionless streamwise vorticity which is denoted by Ω^* and defined in Eq. 4.6 is used as an objective function. It is non-dimensionalized with the blade rotational speed, ω .

$$\Omega^* = \frac{\vec{\Omega} \cdot \vec{V}}{2\omega |\vec{V}|} \quad (4.6)$$

Where

$$\vec{\Omega} = \nabla \times \vec{V}$$

$$F_{obj3}(X) = Min(C_1(1 - \eta_{tt})' + C_2\Omega_s^{*'} + C_3\Omega_r^{*'} + PT) \quad (4.7)$$

where $\sum_{i=1}^{i=n} C_i = 1$ and the penalty term, PT, is defined as follows:

$$PT = \begin{cases} 0 & : \frac{|\dot{m} - \dot{m}_{des}|}{\dot{m}_{des}} \leq 0.028 \\ 0.5 & : \frac{|\dot{m} - \dot{m}_{des}|}{\dot{m}_{des}} > 0.028 \end{cases}$$

To normalize all individual objective functions to vary between 0 and 1 over

the specified range for each one of them, each objective function e.g., (η_{tt}) is replaced with $((\eta_{tt})')$ where:

$$f' = \frac{f - f_{min}}{f_{max} - f_{min}} \quad f = \{\eta_{tt}, \Omega_s^*, \Omega_r^*\} \quad (4.8)$$

Two objective functions are presented for stage namely F_{obj2} and F_{obj3} . F_{obj2} , given in Eq. 4.5, is to maximize η_{ts} while constraining \dot{m} , which implies minimizing the losses and also the kinetic energy in the secondary flow at the stage exit. The F_{obj3} , given in Eq. 4.7, attempts to maximize η_{tt} and minimize Ω_s^* and Ω_r^* , while constraining \dot{m} . This choice is based on the fact that optimizing η_{tt} will minimize the viscous flow losses and minimizing Ω_s^* and Ω_r^* , will minimize the secondary flow losses. The secondary flow losses are strongly influenced by inviscid flow effects such as stretching and deforming of the incoming vortex lines and are directly related to the stage exit secondary kinetic energy. The three objectives are scaled between zero and one using their anticipated bounds according to Eq. 4.8. Once they are normalized, they can be prioritized with the coefficients, namely C_i . Optimization objective which is given by weighted sum of the individual objectives and is penalized with the constraint on \dot{m} , can be fine tuned by changing the values of C_1 , C_2 and C_3 coefficients. For instance, η_{tt} can be optimized if the coefficients are assigned the following values: $C_1 = 1$, $C_2 = 0$, $C_3 = 0$. A parametric study of different combination of coefficients was carried out before settling on the following combination of coefficients: $C_1 = 0.6$, $C_2 = 0.2$, $C_3 = 0.2$ [56].

4.3. Blade row stacking optimization

The stacking of the individual stator and rotor blades has its own implications. The stator blades are essentially cooled in a high pressure turbine. The interior cooling passages are usually straight channels which constrains bowing the stator blades. On the other hand, the rotor blades are usually stacked along a radial line that passes

through the CG. of the individual profiles. The centrifugal forces can apply bending moment at the hub if the stacking varies from the radial line. The optimization of the individual stator and then rotor blade row are presented in this section.

4.3.1 Stator optimization

The variation of the upstream stator blade shape affects the rotor performance. Therefore, stator optimization in the absence of the rotor might have a negative effect on the rotor blade and may result in a smaller stage efficiency. In other words, individual optimization of the stator blade does not guarantee an optimum stage performance and hence is not practical. Hence, the stator blade optimization is carried out within the stage environment with a frozen rotor blade shape. The objective is to maximize the stage efficiency, η_{tt} , by varying the stacking line while keeping the same airfoil shapes.

The QRBC parameters shown in Table 3.1 which are directly related to the five stator design variables listed in the Table 3.1 were picked up. Lean, sweep and bow are used as the design parameters. The range of design variables is based on the geometric and manufacturing considerations only and is shown in Table 4.3.

Twenty three candidates were selected using LHS method and were analyzed with ANSYS-Fluent. Two ANN models are trained for the efficiency and the mass flow rate each having five inputs and one output.

Between the input and output layers, there is one hidden layer composed of thirty nodes with sigmoid transfer function.

The GA with the population of fifty in each generation is used. Optimum solution is achieved after several hundred generations.

The original and optimum design variables and their objective function are shown in Table 4.3. The optimized stator increases the stage efficiency to 88.03%, an increase of 0.93%; the optimum blade has a lean of -17.2° which has shifted the

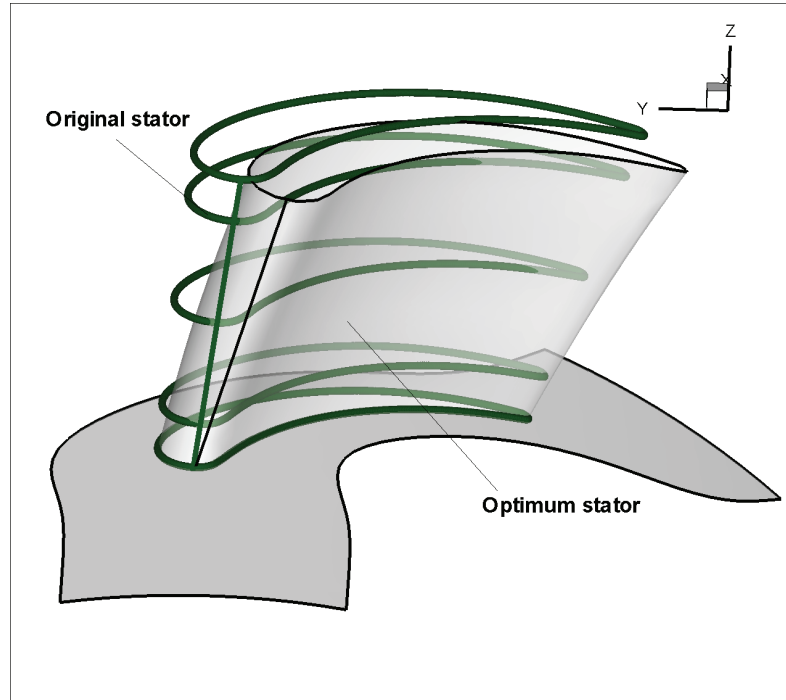


Figure 4.2: Optimum stator blade stacking

blade tip towards the PS, a sweep of -2.8° (forward sweep) and zero bowing, see Fig. 4.2. The mass flow rate is off by 1.3%.

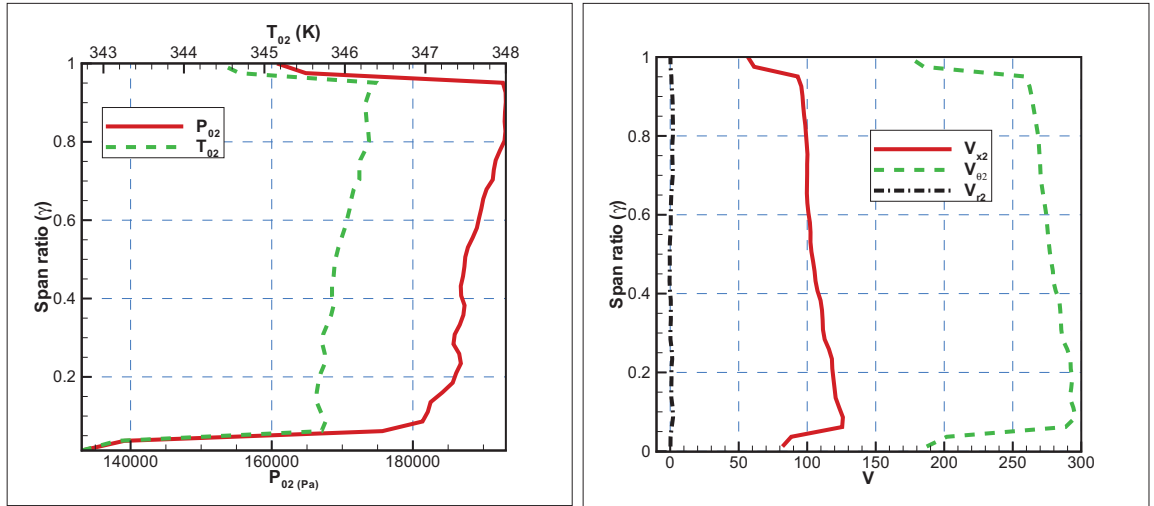
The non-uniform inlet flow, non-zero blockage, will contribute to the secondary flow. The bowing might be helpful to reduce the secondary flow strength by adjusting the loadings in the end-walls. As long as the bowing intensity is zero, the spanwise location of P_1 in QRBC (γ_{P_1}) and the compound lean (θ_{P_1}) design variables won't change the blade shape. These two design variables are not necessary if the optimum bowing remains at zero.

4.3.2 Rotor optimization

An individual rotor blade optimization case is presented, basically as an initial step to study the stacking of the rotor blade. The stage analysis is used to set up the rotor boundary conditions. The rotor inlet boundary conditions are obtained from the

Table 4.3: Stator optimization: The design variables, their range of variations and efficiency of original and optimum stages

Case	α_s	β_s	γ_{P_1}	w_1	Θ_{P_1}	η_{tt}	$\dot{m}(kg/s)$
Original	-7.3°	6.9°	0	0	0°	87.10	0.320
Optimum	-17.2°	-2.8°	0.27	0	-15°	88.03	0.336
min	-17.3°	-3°	0.10	0	-20°	—	—
max	-2.3°	17°	0.90	1.5	30°	—	—



a. Total inlet pressure and temperature profiles

b. Axial, circumferential and radial inlet velocity profiles

stator outlet station of the E/TU-3 stage analysis. The total pressure and temperature and flow angles obtained from this analysis are imposed as the rotor inlet boundary conditions. The static pressure, taken from the stage back pressure, is assigned as the rotor outlet boundary condition. The boundary conditions are indicated in Fig. 4.3. The objective is to optimize the isentropic efficiency η_{is} as defined in Eq. 4.1.

An ANN architecture similar to that of the stator optimization case was chosen for the rotor. The number of candidates in the DOE is twenty three and similar GA parameters were used.

Figure 4.3: Pressure, temperature and velocity profiles at rotor inlet boundary

Table 4.4: Rotor optimization: The design variables, their range of variations and efficiency of original and optimum rotors

Case	α_r	β_r	γ_{P_1}	w_1	Θ_{P_1}	η_{is}	\dot{m}
Original	0°	0°	0	0	0°	85.91	0.320
Optimum	9.9°	0.3°	0.39	1.5	23.3°	87.63	0.320
min	-10°	-10°	0.22	0	-10°	—	—
max	10°	10°	0.82	1.5	25°	—	—

The original and optimum rotor geometric parameters and efficiency are shown in Table 4.4. The original rotor is radially stacked through the CG of the profiles. The optimum rotor is leaned towards the SS by 9.9°. The sweep change is negligible. The bowing intensity of the optimum blade is at the max limit of bowing intensity with the value of 1.5. Also the θ_{P_1} is nearly close to its border. The stacking curve of both blades are shown in Fig. 4.4. Even though the bowing intensity is at its maximum value, this optimum blade is not significantly bowed compared with a blade such as the one given in Fig. 3.1.c. This can be explained with two facts. First, the leaning of the tip toward the SS has lightened the magnitude of bowing intensity (i.e. the curvature of the curve in particular near the tip). In other words, the angle between P_1P_2 and the casing would have been smaller if the lean angle was less. Secondly, the limits for bowing and θ_{P_1} look like tight. It seems that the optimizer tends to go beyond the imposed limits. This argument is also valid for the lean angle. Based on this observation, the design variables range for stage optimization are extended appropriately.

The optimum rotor efficiency is 87.63%, marking an increase of 1.72%. The main reason for the efficiency improvement is due to the equalization of pressure distribution in spanwise direction. This will be discussed in detail in the following sections. The mass flow rate has not changed.

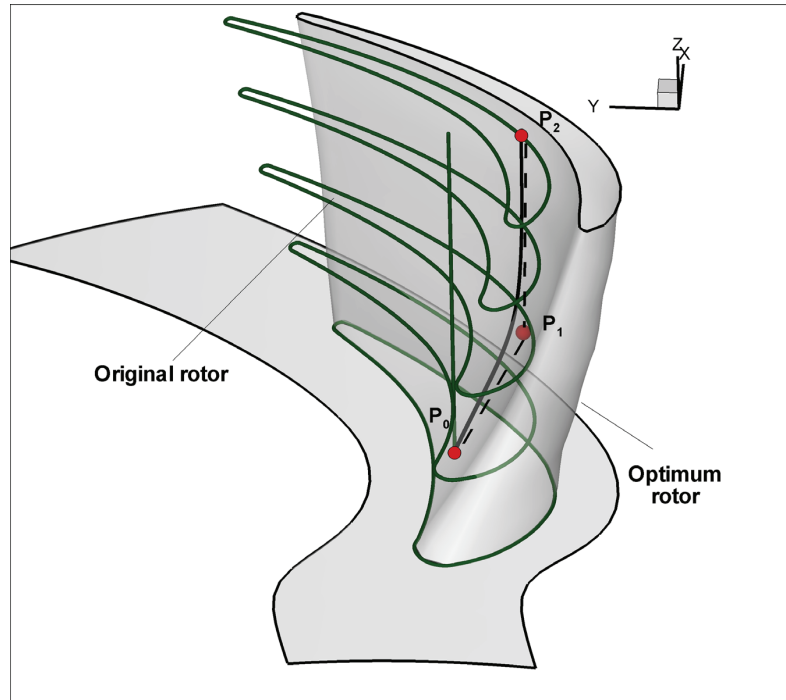


Figure 4.4: Optimum rotor blade stacking

Table 4.5: Studied cases for stress distribution

Case number	Description
1	Original blade
2	$\alpha_r = -5^\circ$
3	$\alpha_r = +20^\circ$
4	$\beta_r = -10^\circ$
5	$\beta_r = +15^\circ$
6	$w = 3$
7	Optimum blade

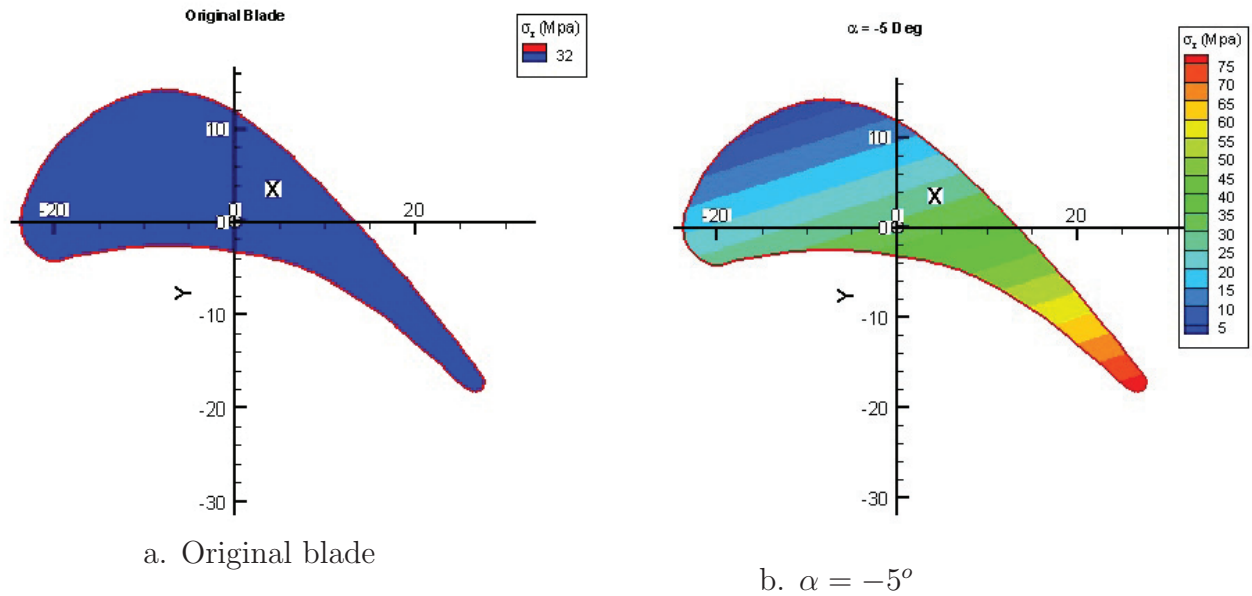


Figure 4.5: Stress contours of the listed cases in Table 4.5

4.3.3 Structural analysis of the turbine blade

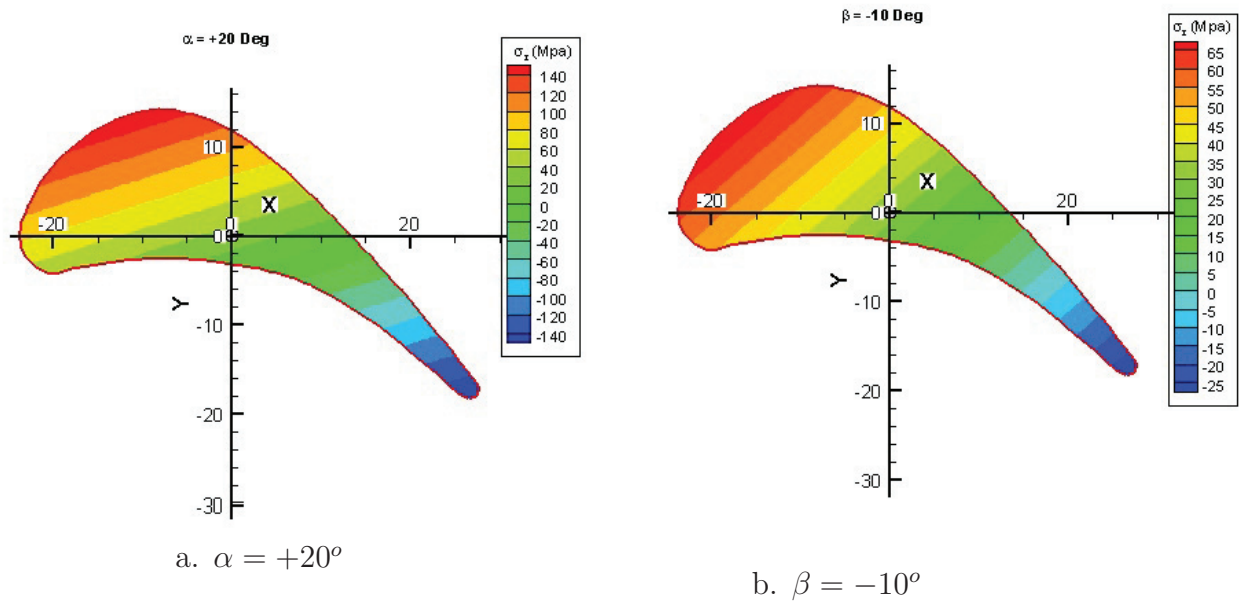
A crude stress analysis was carried out, as described in Chapter 2 to ensure that the design blades will not break due to centrifugal stresses. Assumption is that the moment in spanwise direction (M_z) which produces torsion is negligible.

Stress distribution

Some cases for calculating stress distribution are modeled and are shown in Table 4.5. There are seven blade geometries presented in Table 4.5 for stress calculation at hub. The contours in Figs. 4.5 and 4.6 indicate the stress distribution caused by bending moment due to centrifugal force. The blade radial stacking does not create any bending moment on the hub in the original blade as is shown in Fig. 4.5.a.

Stacking effect on mechanical integrity of the blade

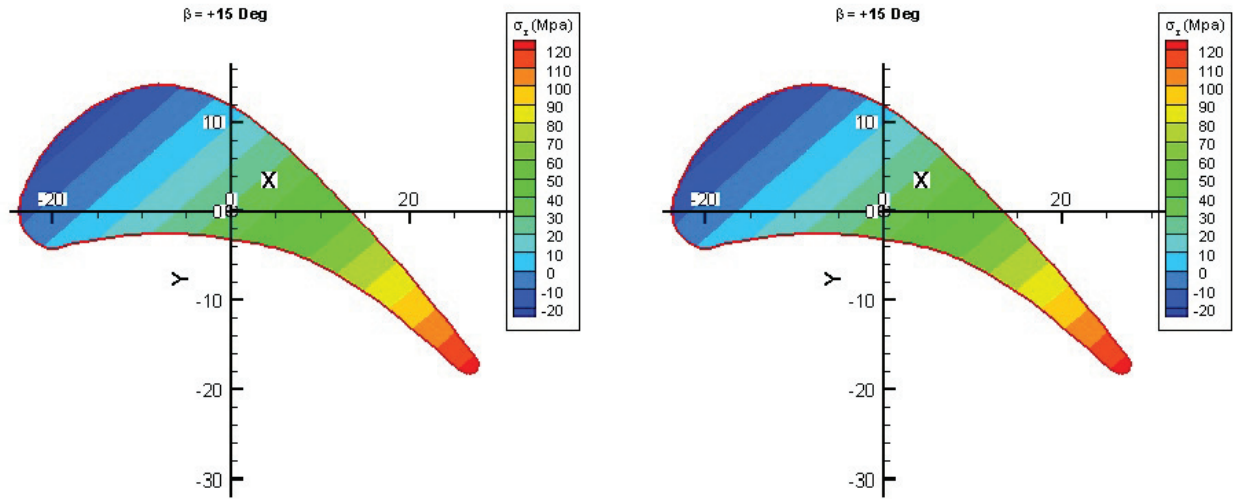
Centrifugal forces are calculated for E/TU-3 rotor blade. Bending moments of these forces are calculated around the center of gravity of hub profile which is assumed



as a flat surface. According to the cases studied, the maximum stress happens near the trailing edge and near the location of maximum thickness on the suction side. Depending on the configuration one region has tensile and the other has compressive stress. All the redesigned rotor blades are experiencing a max stress that is far less than the yield stress of Nickel-based steel alloy, which is 1035 (MPa) [4]. Since the blade is treated as a cantilever beam, the maximum stress happens at its root. So the hub region is the critical one. Therefore based on this study, the stacking curve modification within the mentioned range of design variable is not generating structural failure to the blade.

4.4. Stage optimization using stacking and stagger angle

The interaction of the stator and rotor blade rows necessitates the simultaneous optimization of the stator and rotor stacking lines. The blade profile stacking is a change of blade shape in meridional plane. It is an effective tool to control the pressure



c. $\beta = +15^\circ$

d. $w = 3$ (Bowling intensity)

Figure 4.6: Distribution of listed cases in Table 4.5

radially. This allows for to the reduction of the adverse 3D effects in the flow.

The blade stagger angle distribution is a change of blade shape in circumferential plane. It influences rather strongly the spanwise variation of mass flow, incidence angle and throat area, hence the 3D flow features.

In this section a stacking optimization of the stage, Case 1, is presented. The stacking variation alone is sometimes incapable of reducing the losses, e.g. fixing a bad incidence angle. Therefore, it is expected to gain more improvement by simultaneous optimization of stacking and stagger angle. Finally, Cases 2 and 3 present the simultaneous optimization of stacking line and stagger angle distribution with single and multiple objective optimization, respectively.

4.4.1 Case 1: Performance optimization using stacking line

The design space for the stage, as shown in Table 3.2 is different from the stator and rotor individual blade row optimizations. The application of bowing on the stator blades is not encouraged from the cooling channels point of view. It makes the

manufacturing of the stator blade more complicated. In addition, the E/TU-3 turbine case has a uniform inlet flow profile. Assuming that bowing is required mostly for non-uniform inlet flow, no bowing is considered for this stator. Therefore, the bowing intensity and hence the span ratio and compound lean are eliminated from the list of design variables. On the other hand, it was observed from the individual rotor optimization that the blade is not highly bowed. Based on this observation as well as the sensitivity analysis that was presented in Chapter 3, the design variables selected for the rotor are the lean, sweep and bowing intensity. The values of the span ratio and compound lean for both stator and rotor are set to 0.5 and 35° respectively. Hence the total number of design variables is five.

The size of the design space can be reduced and enlarged according to the optimum geometry of single blade row optimization. For instance, looking at the optimum lean angle in Table 4.4, it is realized that the lean angle range can be extended from its maximum bound. Furthermore, the range can get smaller from the minimum bound. It is huge save of time to cut off that part of the design space which dose not include any optimum solution. In a similar way, the range of each design variable is modified according to the single blade row optimization cases as shown in Table 3.2.

Twenty one candidates that distributed within the design space by means of LHS method, are analyzed using ANSYS-Fluent and are used to train and test the ANN model. The boundary condition used in CFD computations are indicated in Table 4.6. The flow properties are mass-averaged at the flow inlet and outlet stations. Hence, total-to-total efficiency and mass flow rate are calculated. Consequently, two ANN networks of five-input (for five design variables) and one-output (for $(1 - \eta_{tt})$) are trained and tested, they are then used in the optimization cycle.

The objective function consists of the $(1 - \eta_{tt})$ penalized with the \dot{m} constraint; It is given in Eq. 4.7 with coefficients being: $C_1 = 1$ and $C_2 = C_3 = 0$. There are 50

Table 4.6: Case 1: Boundary condition (Rotor profiles are given in Fig. 4.3)

	Avg. total inlet pressure (kPa)	Avg. total inlet temperature (K)	Inlet circumferential flow angle ($^{\circ}$)	Inlet meridional flow angle ($^{\circ}$)	Inlet turbulent intensity -	Inlet hydraulic diameter (m)	Outlet static pressure (kPa)
Stator	196	346	0	0	5%	0.046	95
Rotor	Profile	Profile	Profile	Profile	5%	0.046	95
Stage	196	346	0	0	5%	0.046	95

Table 4.7: Case 1: Single objective optimization of stacking in stage

Case	α_s	β_s	α_r	β_r	w_{r1}	$\eta_{tt}\%$	\dot{m}
Original	-7.3°	6.9°	0°	0°	0	87.22	10.35
Case 1 opt.	-36°	-2.5°	2.2°	-9.7°	0.05	88.56	10.64

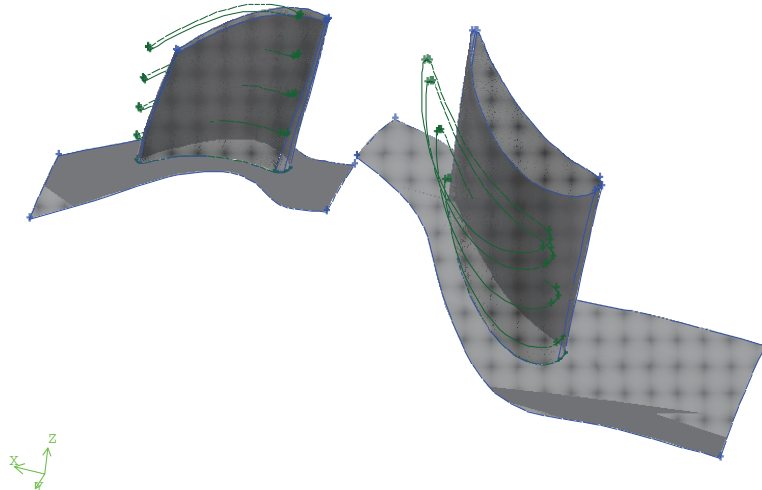


Figure 4.7: Case 1: Optimum blade stacking (wire frame depicts the original geometry)

members in each generation of GA. The cross-over and mutation probabilities are set to 0.2 and 0.7, respectively. Two elite members are kept in each generation, they are passed directly to the next generation.

The result of the optimization is shown in Table 4.7 where both rotor and stator blades have forward sweep, Fig. 4.7, while rotor blade has no bowing. The stage efficiency η_{tt} is increased from 87.5% to 88.56%.

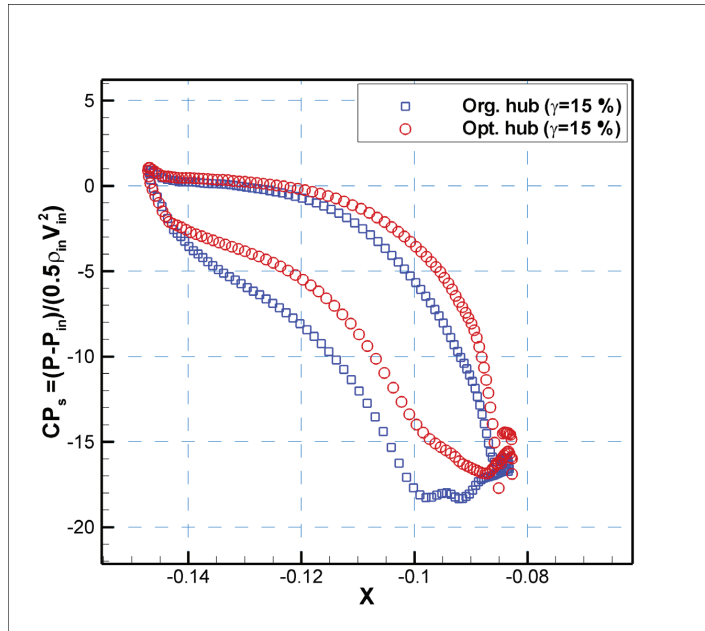
Lean and sweep are changing the blade spanwise loading. Leaning towards the blade suction side will unload the tip and put more load at hub and vice versa. This can be seen in Figs. 4.8 and 4.9 for stator and rotor blades, respectively. For instance, a stator lean of -36° increased the loading at the tip and reduced it at the hub compared to the original loading, see Fig. 4.8a. and b. The mid-span loading for both stator and rotor has not significantly changed.

The stage exit total pressure is also increased by 1.2%. Based on stator and rotor pressure loss coefficients, almost 86% of the improvement is due to the rotor blade shape optimization and only 14% improvement is due to stator blade. The reduction of stator losses caused 1.2% increase in stator exit total pressure which in turn increased the stage reaction by 3% from 0.26% to 0.29%.

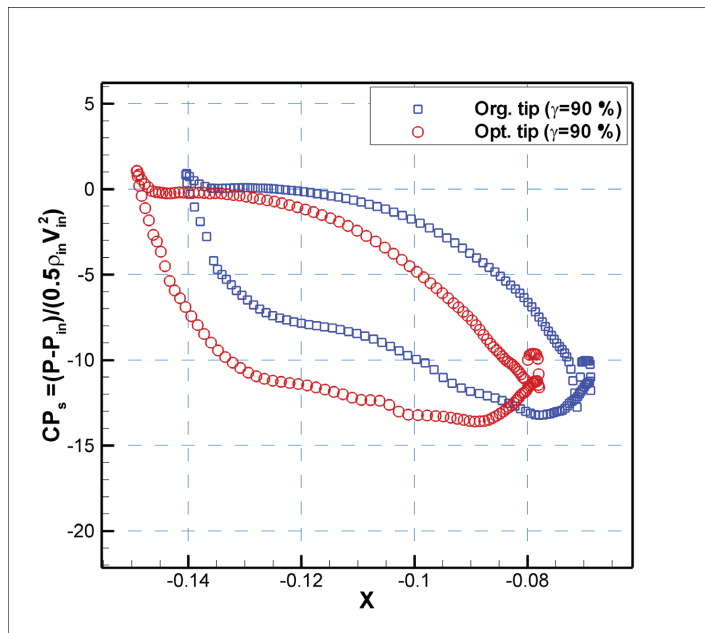
If the profiles are not changed, the flow angles are not expected to change. However, the stacking variation is also affecting the spanwise variation of the mass flux and also the flow angles. This will be discussed in detail in the following sections.

4.4.2 Case 2: Performance optimization using stacking and stagger

The stacking variation is influencing the overall spanwise pressure distribution. However, it is sometimes necessary to improve the flow characteristics locally without disturbing the flow entirely. For instance, the flow separation can be reduced by local modification of the profile. Therefore, simultaneous optimization of stacking and

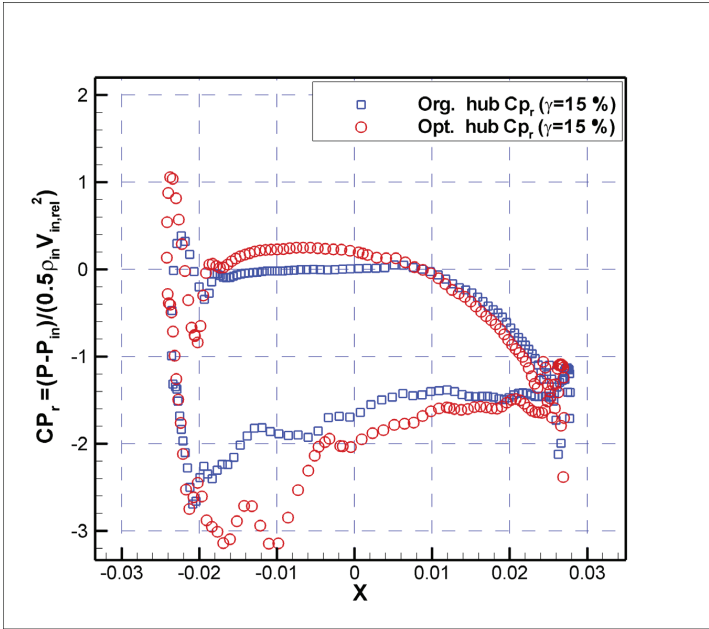


a. Stator hub

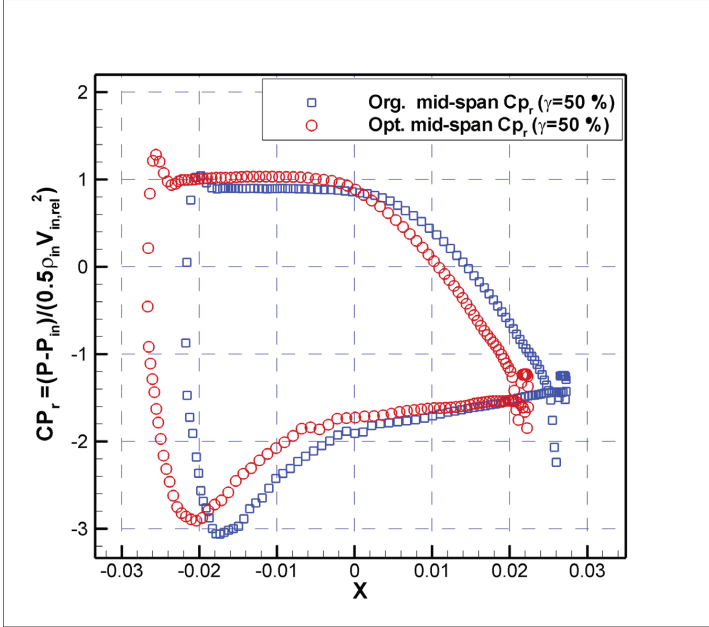


b. Stator tip

Figure 4.8: Case 1: Stator blade pressure distribution at hub and tip



a. Rotor hub



b. Rotor tip

Figure 4.9: Case 1: Rotor blade pressure distribution at hub and tip

Table 4.8: Design variables and their optimization range

Case	α_s°	β_s°	θ_{sh}°	α_r°	β_r°	θ_{rh}°	θ_{rm}°	θ_{rt}°
Org.	-7.3	6.9	45	0	0	16.8	34	43.8
Case 2 opt.	-35.1	3.6	49.8	8.6	-9.7	21.8	36.6	39.6
Case 3 opt.	-31.5	-7.9	45	10.4	2.3	20.3	35.8	46.8

stagger angle distributions is practical to control the overall as well as local loading.

Usually the blade stagger distribution varies linearly from hub to tip, however this is not necessarily the optimum distribution. In this section, the stagger angle is allowed to vary quadratically using the QRBC parameterization with four design variables described in Chapter 3. The stator stagger angle distribution is linear which is controlled by the hub stagger angle. The rotor stagger distribution is adjusted with three stagger angles namely at the hub, mid-span and tip. The range of stagger design variables are shown in Tab. 3.3. Only the lean and sweep angles are chosen for both stator and rotor stacking design variables. The range of stacking design variables are shown in Tab. 3.2. Therefore, eight design variables are considered in this optimization.

For this case, the objective function is formed of total to static efficiency and is penalized with the mass flow rate, see Eq. 4.5. The optimization is carried out assuming that the turbine maintains at the same operating conditions, i.e. fixed rotor speed, fixed inlet and exit boundary conditions; and the mass flow rate was constrained to change to within 2% of the design value.

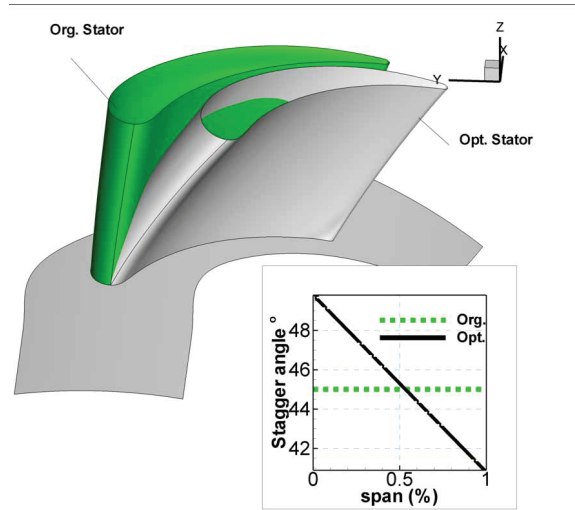
The objective and constraint are approximated using an artificial neural network (ANN) that is trained and tested using 36 CFD flow simulations. The hyperbolic tangent was deemed to be a better choice of transfer function for the efficiency network. The function sigmoid is used for the mass flow rate network. The learning rates are 90% and 2.5% for input-to-hidden and hidden-to-output layers, respectively. Then GA with the population of 50 individuals in each generation is linked to the ANN

approximations to find the optimum. The ANN-based optimum stage is finally simulated with CFD, as a high fidelity model, to check the accuracy of the ANN-based solution.

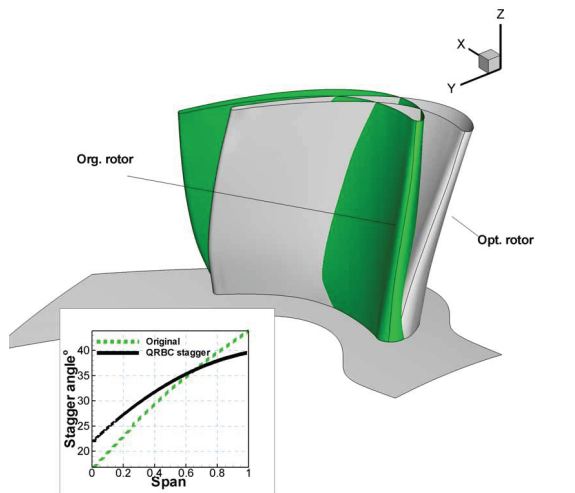
The optimum blade design variables are given in Table 4.8. Original and optimum blade shapes are shown in Fig. 4.10. Compared to the original stator, the optimum one is leaned towards the PS (negative lean) and is slightly swept forward. The stagger angle is increased near the hub and decreased by an equal amount near the tip, see Fig. 4.10.a. The rotor is leaned towards the SS (positive lean) and is swept forward. The rotor stagger angle increases from hub to nearly 75% span and decreases thereafter. The total-to-static efficiency increased from 74.44% to 76.18%, an increase of 1.74 which is significant. The streamwise vorticity at stator and rotor exits were reduced by 6.8% and 14%, respectively, although they have not been explicitly included in the objective function; this confirms the fact that η_{ts} and both Ω_s^* and Ω_r^* are interdependent.

The optimum stator blade is leaned towards the PS and swept forward (Fig. 4.10.a), which results in unloading the hub and loading the tip (Fig. 4.11) hence reducing the hub-TE separation region, see Fig. 4.13.b. On the other hand, the hub stagger angle is increased from 45° to 49.8° , which implies a smaller hub throat area and an expected drop/rise in mass flux near the hub/tip. However this mass flux redistribution did not materialize as the stator exit pressure associated with the optimum loading profile as well as the reduction in separation region were such that the exit mass flux was almost unchanged, Fig. 4.16.a.

The optimum rotor stagger angle at hub is increased while it is decreased at the tip, see Fig. 4.10. This reduces the throat area near the hub and increases it near the tip, hence mass flux passing near the hub is expected to decrease and vice versa near the tip, which is confirmed in Fig. 4.16.b. The spanwise pressure distribution of original and optimum cases are depicted in Figs. 4.11 and 4.12.

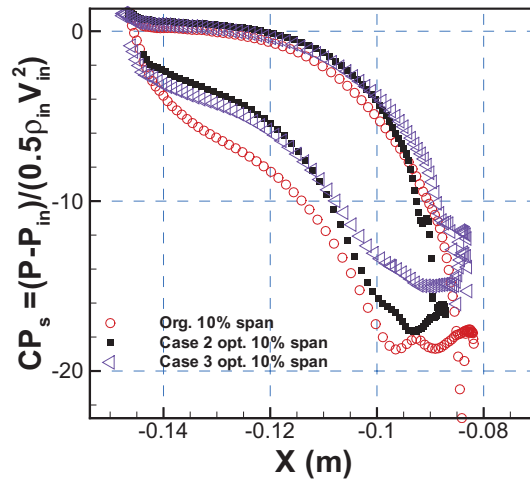


a. Stator

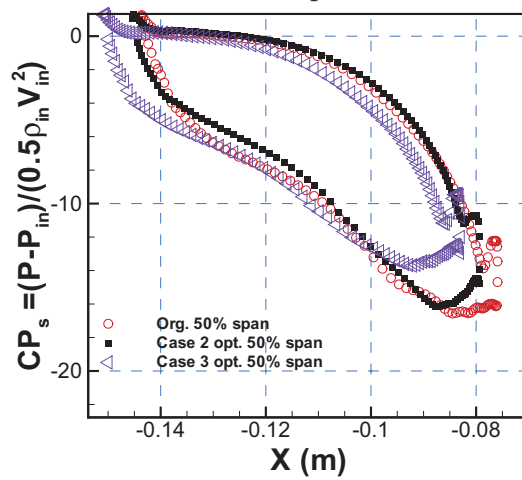


b. Rotor

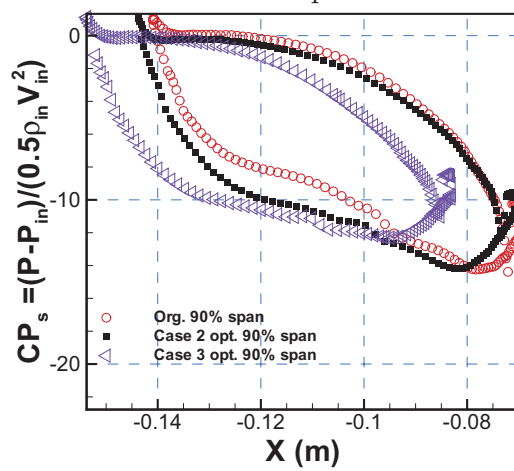
Figure 4.10: Case 2: original and optimum blade shapes



a. 10% span

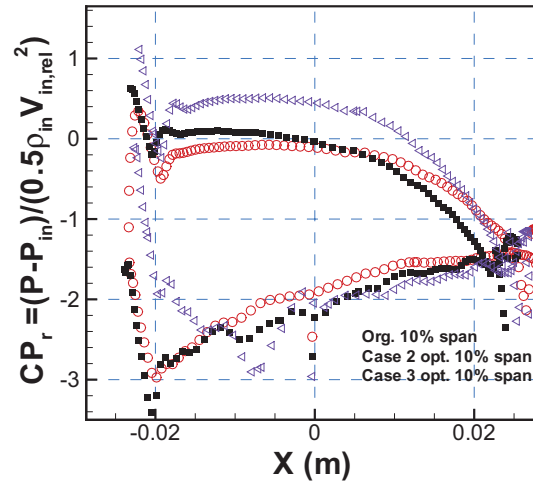


b. 50% span

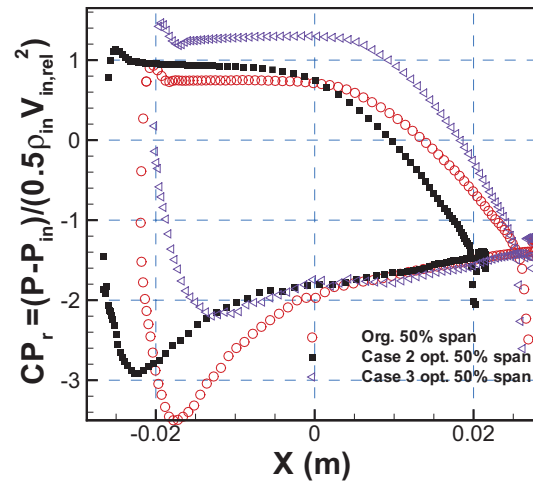


c. 90% span

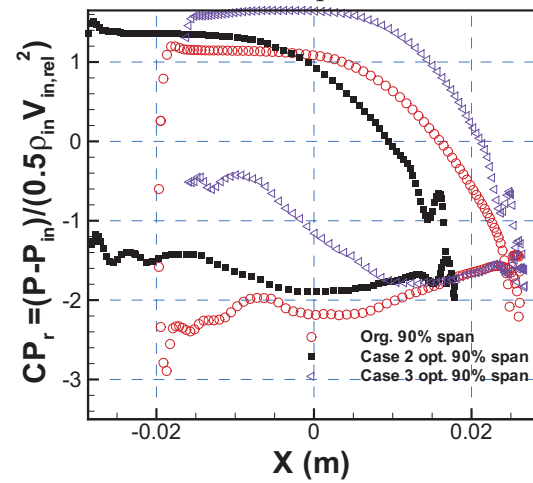
Figure 4.11: Cases 2 & 3: Stator pressure loading for the original stage



a. 10% span

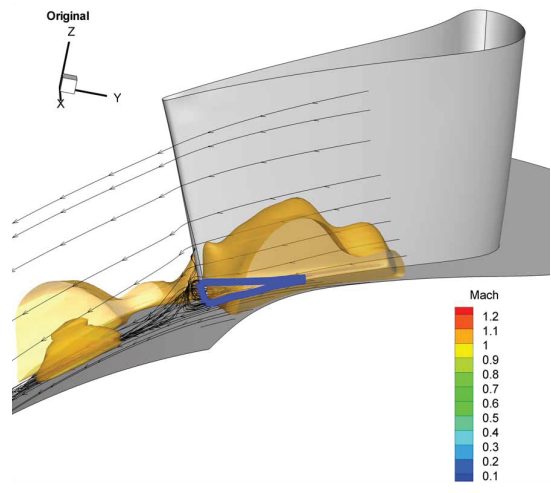


b. 50% span

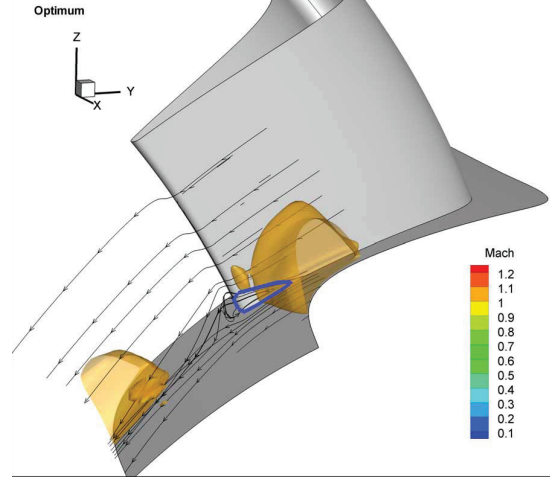


c. 90% span

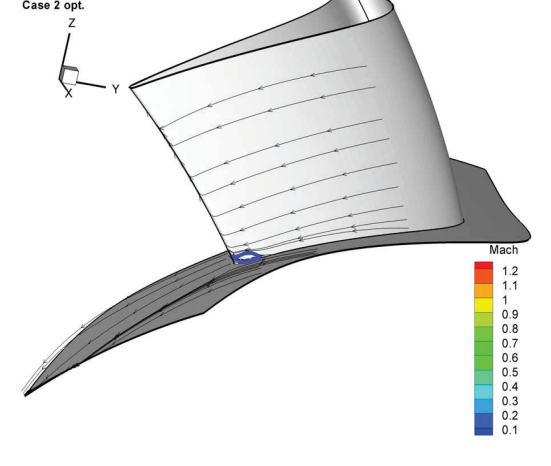
Figure 4.12: Cases 2 & 3: Rotor pressure loading for the original stage



a. Original stator



b. Case 2 stator



c. Case 3 stator

Figure 4.13: SS flow separation and sonic surface for the original and optimum stators

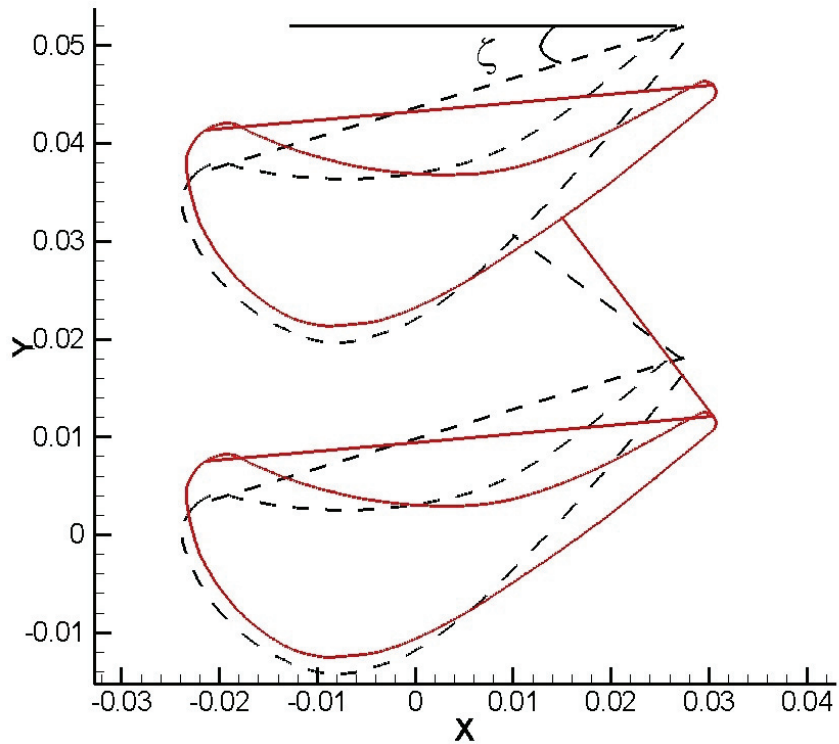


Figure 4.14: Effect of stagger angle change on the throat area

Assuming the flow angle is unchanged, the incidence angle increases as the stagger angle increases. On the other hand, a higher blade stagger angle implies a smaller throat area and hence less mass flux, see Fig. 4.14. So upon an increase in stagger angle, the axial velocity at the inlet decreases. This results in lower incidence for a turbine blade. Therefore the stagger angle increase may not necessarily mean a drastic change in incidence angle. This argument is valid in 3D flow only if the 3D effects are relatively small, which is the case for the present rotor. Although the optimum stagger angle increased at rotor hub from 16.8° to 21.8° , the incidence is slightly changed near the hub as shown in Fig. 4.18.c.

Figure 4.10 shows that the optimum rotor is leaned towards the SS (hence unloading the tip) and is swept forward (hence loading the tip), the net effect being that the pressure loading is slightly different from that of the original stage, see Fig.

Table 4.9: Original, Case 2 and 3 stage aerodynamic characteristics

Case	η_{ts}	η_{tt}	Ω_s^*	Ω_r^*	$\dot{m}(kg/s)$
Org.	74.50	87.22	1.25	3.17	10.35
Case 2	76.18	88.30	1.50	2.64	10.27
Case 3	74.55	89.09	1.35	2.833	10.54

4.12.

Stage reaction and stage loading, given in Figs. 4.19, are discussed in Sec. 4.4.4, where some comparison between the original stage and the two redesign cases: Case 2 and Case 3 are compared.

In summary, to maximize the stage total to static efficiency, the optimizer reached a combination of blade lean, sweep and stagger that reduced the stator hub loading (Fig. 4.11.c) while keeping the same mass flux distribution at stator exit (Fig. 4.16.a); this resulted in reducing the hub-TE blockage (Fig. 4.13) and the Mach number level (Fig. 4.17.a). Moreover, combination of blade lean, sweep and stagger that is reached in the rotor resulted in a more uniform spanwise distribution of max flux (Fig. 4.16.b). These changes in stator and rotor resulted in a higher stage loading (Fig. 4.19.b).

4.4.3 Case 3: Performance optimization using stacking and stagger with a different objective function

Case 3 is similar to Case 2 with except for the choice of the objective function. The optimization objective is formed of a weighted sum of total to total efficiency (η_{tt}), the streamwise vorticity downstream of the stator and rotor (Ω_s^* , Ω_r^*). Then it is augmented by a constraint on the mass flow rate, see Eq. 4.7.

These individual objectives are the total to total efficiency η_{tt} , the streamwise vorticity downstream of the stator and rotor Ω_s^* and Ω_r^* . The first objective represents the overall viscous loss while the other two represent secondary flow losses downstream

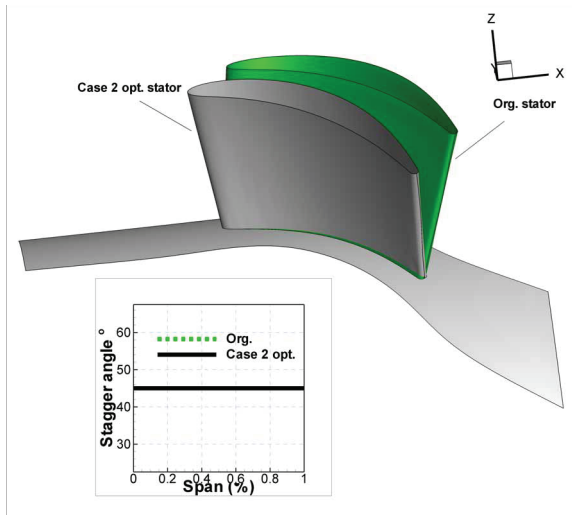
of the stator and rotor. The streamwise vorticity is directly related to secondary flow which is a major source of losses in turbines. This choice of objective would be even more useful in reducing secondary flow losses when the aerodynamic blockage is high at inlet. In turbomachinery, loss mechanisms are strongly coupled and improving one can compromise another one. For this reason, these three individual objectives were incorporated into the optimization objective, Eq. 4.7.

The optimization is carried out as described in the previous sections and the optimum design variables for this case, Case 3, are listed in Table 4.9. The original and optimized stage are plotted in Fig. 4.15. The stator is leaned towards the PS and is swept forward, while the optimum stagger distribution is equal to the original one. The rotor is leaned (positively) towards the SS with a slight backward sweep and an increase of nearly 4° in stagger angle throughout the span. The performance of this case is presented in Table 4.9. Compared to the original case, the total to total efficiency is increased from 87.18% to 89.09%, an increase of 1.91% . The streamwise vorticity downstream of the stator and rotor are reduced by 16.1% and 7.8% respectively.

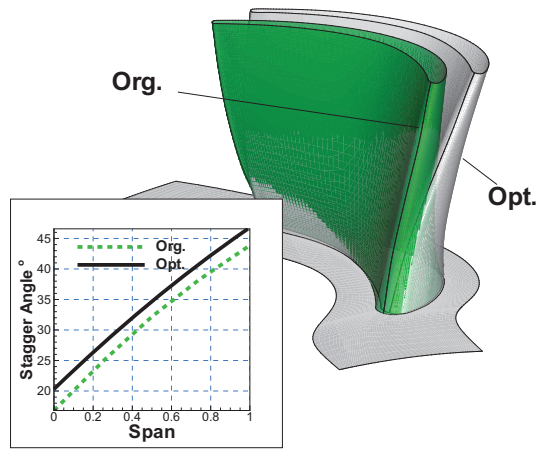
4.4.4 Physical implications of the optimized stages

The design variables namely: the blade lean and sweep (controlled by the stacking line), and the blade stagger angles affect rather strongly the spanwise loading and mass flux distributions. Lean is assumed positive when the blade tip moves towards the SS. For a given stagger distribution, positive lean unloads the tip and loads the hub [57]. In addition, a change in the stagger angle affects the spanwise variation of the throat area, mass flux and reaction.

Consider Case 3 stator, the stagger distribution is not changed from the original one. Moreover, the stator is leaned towards the PS and is swept forward, both effects contribute to unloading the hub and loading the tip, see Fig. 4.11. As a result, the



a. Stator



b. Rotor

Figure 4.15: Case 3: original and optimum blade shapes

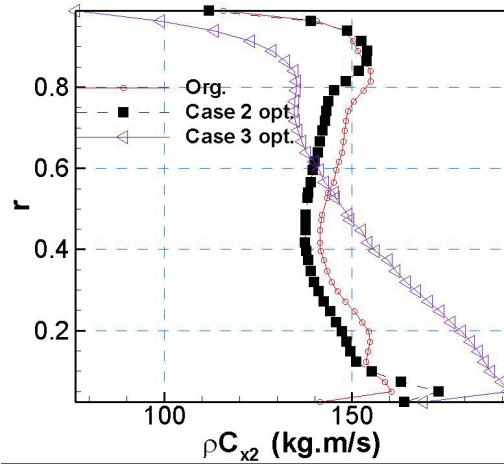
separation region near the stator hub-TE was completely eliminated, as shown in Fig. 4.13.c. In fact, Figs. 4.13 show a gradual elimination of the recirculation region as we go from the original stage to Case 2 to Case 3 redesigns, which explains the rise in stator exit static pressure as the aerodynamic blockage associated with the stalled flow region is gradually eliminated hence reducing the average spanwise Mach number, Fig. 4.17, consequently increasing the static pressure at rotor inlet. Hence the drop in pressure (and temperature) across the rotor increases since the exit static pressure is fixed. This explains the increase in stage reaction from the original stage to Case 2 to Case 3 stages, see Fig. 4.19.a.

For Case 2 rotor, Fig. 4.12 shows that the pressure levels on the PS are higher than those of the original rotor at all spanwise locations in due to the elimination of the flow blockage and shock loss that were present near the stator hub-TE region. The diffusion on the rotor SS in Case 3 is decreased compared with the other two cases at all spanwise locations particularly at rotor mid-span where it is highly reduced, as indicated in Fig. 4.12.b. Case 2 and Case 3 rotors have roughly similar geometric parameters, as shown in Table 4.8, except for sweep and tip stagger angles. Comparing Cases 1 and 2 the loading near the tip, depicted in Fig. 4.12.c, shows that Case 2 is more aft-loaded and Case 1 is more front loaded.

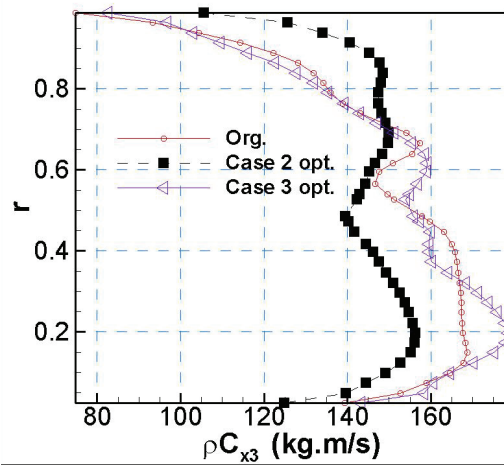
For Case 2, the mass flux distribution downstream of the optimum stator and rotor, plotted in Figs. 4.16.a and 4.16.b, shows clearly an increase in mass flux near the hub, which is due to the elimination of hub-TE flow separation.

The stage loading for all cases, given in Fig. 4.19.b, shows that Case 2 loading is slightly higher than the rest, moreover Table 4.9 shows that the streamwise vorticity downstream of the rotor is the smallest; these observations are consistent with the fact that η_{ts} is highest for Case 1. (Note that the optimization objective for Case 2 is to maximize η_{ts} .)

Figure 4.18.c shows that the trend of the rotor incidence is consistent with the

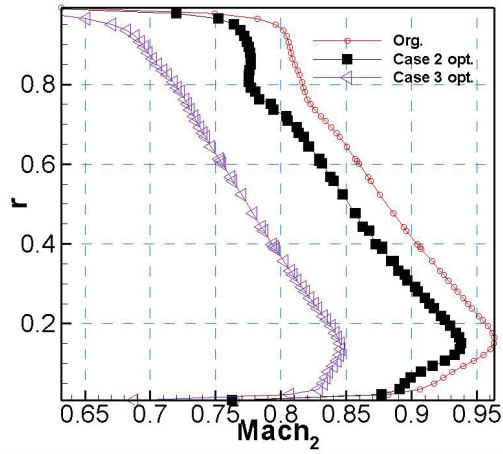


a. Stator exit mass flux

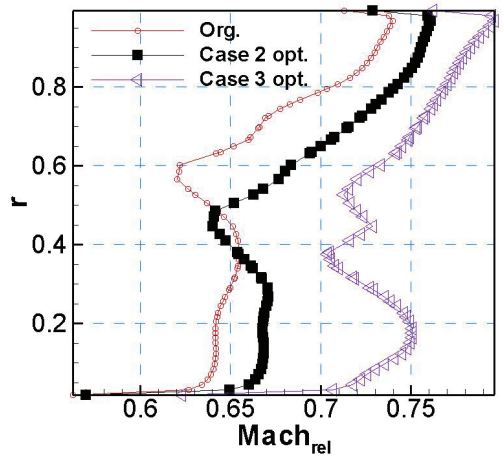


b. Rotor exit mass flux

Figure 4.16: Spanwise variation of mass flux in the original, Case 2 and Case 3 stages

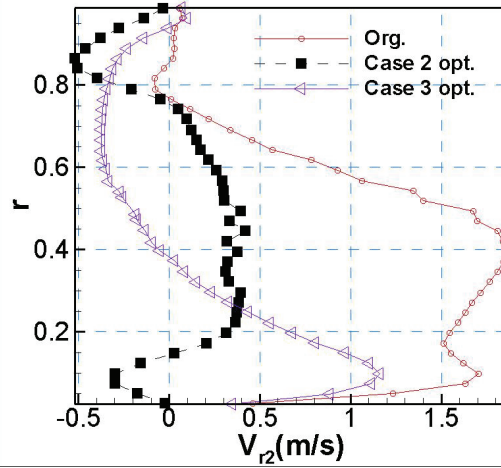


a. Absolute Mach number at stator exit

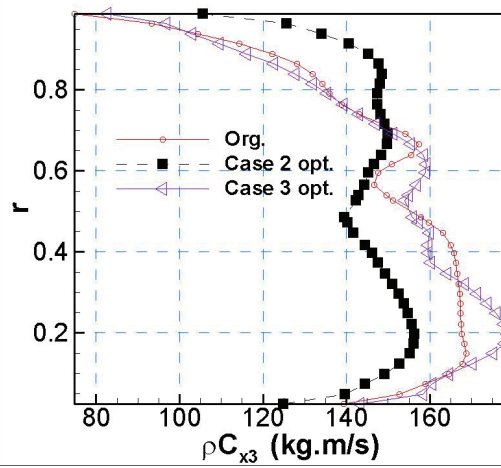


b. Relative Mach number at rotor exit

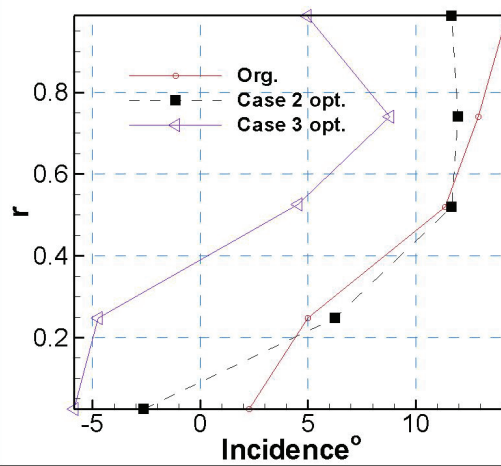
Figure 4.17: Spanwise Mach number distribution in the original stage, Case 2 and Case 3 stages



a. Radial velocity at stator exit

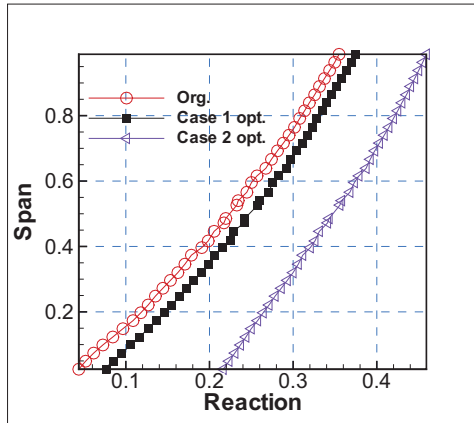


b. Radial velocity at rotor exit

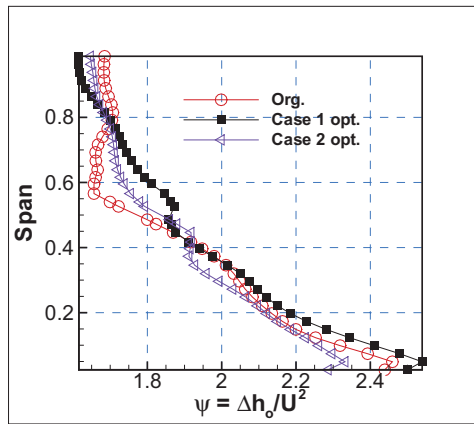


c. Rotor incidence

Figure 4.18: Spanwise radial velocity and incidence angle distribution for the original stage, Case 2 and Case 3 stages



a. Reaction



b. Stage loading

Figure 4.19: Spanwise variation of stage loading and reaction in the original stage, Case 2 and Case 3 stages

rotor loading given in Figs. 4.12. It is believed that the changes in incidence will not affect the losses in a drastic way, given that the blade LE is fairly thick.

The radial velocity of Case 2 and Case 3 are reduced at stator and rotor TE as shown in Figs. 4.18.a & b. This will reduce the radial shift of the flow hence reducing the 3D effects and making the flow more uniform.

4.5. Conclusion

This chapter presents several optimization strategies to reduce the losses in 3D axial turbine flows. Moreover, the physical implications of the design variables are discussed.

The stacking line is proved to be an important design parameter for axial turbines. It considerably influences the spanwise distribution of loading. The physical implications of lean, sweep and bow of the blades are discussed. The QRBC parameterization proved to be an effective and practical technique to reduce the source of losses in flow such as separation, secondary flow and etc. The optimization setup evolves in many aspects in the order of the presented cases in this chapter. The choice of design variables, parameterization, range of design variables, choice of objective function are modified so that better improvement are achieved. This ascending rate of improvement is clear from the indicated results.

The efficiency difference between the original and optimum stages for stator optimization case, Case 1, Case 2 and Case 3 are 0.93%, 1.34%, 1.68% and 1.87%, respectively. The simultaneous stacking and stagger optimization with the presented parameterization method is deemed to be an effective strategy to reduce the losses. The stacking would change the overall spanwise loading while stagger angle change can locally reduce losses such as separation caused by positive incidence angle.

Chapter 5

Multi-point optimization of a gas turbine stages

The design of a gas turbine results from a compromise of all requirements at design point as well as off-design points. The flow features change drastically at off-design conditions where the performance may be significantly reduced. Hence, a trade-off between performance at design and off-design conditions is crucial. To address this issue, multi-point optimization is carried out as it takes into account the performance at both design and off-design conditions. The stacking optimization proved practical to improve the performance of a gas turbine at the design point in the previous chapter. In this chapter, the turbine stage presented in the previous chapter, E/TU-3, is optimized over the full range of operation, at the design speed line.

5.1. Objective function

In this case the total-to-total efficiency and the streamwise vorticity at the stator and rotor outlets are targeted for the optimization. The optimization objective is written as a weighted sum of all individual objectives at all the operating points and

is penalized with the design constraints. The objective function is defined as:

$$\begin{aligned}
F_{obj}(X) = & Min(C_1 \sum_{i=1}^n (1 - \eta_i)' + C_2 \sum_{i=1}^n \sum_{j=1}^n |\eta_i' - \eta_j'| + \\
& C_3 \sum_{i=1}^n \Omega_s'^* + C_4 \sum_{i=1}^n \sum_{j=1}^n |\Omega_{si}'^* - \Omega_{sj}'^*| + \\
& C_5 \sum_{i=1}^n \Omega_r'^* + C_6 \sum_{i=1}^n \sum_{j=1}^n |\Omega_{ri}'^* - \Omega_{rj}'^*| + \\
& PT) \quad \text{where } i = 1, n
\end{aligned} \tag{5.1}$$

All individual objectives are normalized between 0 and 1 as follows:

$$f' = \frac{f - f_{min}}{f_{max} - f_{min}} \quad f = \{\eta_{tt}, \Omega_s^*, \Omega_r^*\}$$

Where X is the vector of design variables, which include the stator and rotor lean and sweep angles, and the rotor bowing intensity. The summation is carried out over n pre-selected operating points. Varying the back-pressure in the pre-determined range while fixing the rotor speed allows for moving along a speed line where the mass flow rate changes from minimum to maximum value, i.e. it allows for design and off-design calculations. The first, third and fifth terms in the objective function, Eq. 5.1, attempt to maximize the total to total efficiency, η_{tt} , the average streamwise vorticity at stator and rotor outlets, (Ω_s^*) and (Ω_r^*) , while the second, fourth and sixth terms terms would minimize any large difference in these objectives between any two points, which would tend to keep them constant over the entire operating range. The last term in the objective function is a penalty term (PT) that accounts for any mechanical, geometric or aerodynamic constraints imposed on the optimization process. A constraint may be the mass flow rate in a single point optimization case. For this case the mass constraint is not applied as the mass flow rate changes between different operating points. Therefore the PT term is zero. The summation is carried

Table 5.1: Different coefficients in objective function equation

F(X)	C_1	C_2	C_3	C_4	C_5	C_6
<i>Obj1</i>	1	0	0	0	0	0
<i>Obj2</i>	0	0	1	0	0	0
<i>Obj3</i>	0	0	0	0	1	0
<i>Obj4</i>	0.7	0	0.1	0	0.2	0
<i>Obj5</i>	0.5	0	0.25	0	0.25	0
<i>Obj6</i>	0.6	0	0.2	0	0.2	0
<i>Obj7</i>	0.5	0.1	0.15	0.05	.15	0.05
<i>Obj8</i>	0.16	0.16	0.16	0.16	0.16	0.16

out over n pre-selected operating points. In one of the optimization cases presented in the following section, these pre-selected points are the design point and three off-design points, i.e. $n = 4$.

The weights C_k where $k = 1 \rightarrow 6$, are prescribed by the designer; they are determined such that the different terms of the objective function have the desired influence on the optimization process. The objective function and hence the optimum solution are function of these coefficients.

The effect of the coefficients C_k on the optimum design was investigated by taking 8 different combinations, see Table 5.1 and using them to carry out optimization Case 2, given in the next section. The corresponding results are shown in Table 5.2 which is indicating the influence of weights on results. It is desired to have non-zero weights to have the influence of all designated objective function terms to the solution. The choice of weights is based on the best found efficiency which is implicitly representative of other objective functions. The combination of weights C_k given by *obj7* in Table 5.1 is eventually chosen for multi-point multi-objective optimization.

5.2. Optimization at multiple points

The single point optimization of E/TU-3 case, presented in the previous chapter, with stacking design variables showed a promising improvement. The multi-point

Table 5.2: Optimum design variables proposed by ANN

F(X)	α_s	β_s	α_r	β_r	w_{r1}	η_{tt}
<i>Obj1</i>	-33.1	-7.2	19.9	-8.0	0.2	88.57
<i>Obj2</i>	0.0	-6.6	18.6	-1.9	0.0	87.71
<i>Obj3</i>	-1.8	11.6	19.7	-9.0	1.4	87.08
<i>Obj4</i>	-32.9	-7.2	19.6	-9.6	0.0	88.67%
<i>Obj5</i>	-29.6	-4.6	19.4	-7.7	0.0	88.48%
<i>Obj6</i>	-32.0	-5.8	18.1	-9.3	0.1	88.54%
<i>Obj7</i>	-32.2	-7.0	19.1	-8.4	0.1	88.60%
<i>Obj8</i>	-0.1	-3.7	19.9	-8.8	0.1	87.70%

optimization for this case is performed at the design speed line, i.e. 7800 rpm, with a target to increase the efficiency across the whole speed line. The off-design experimental data are well documented in [3].

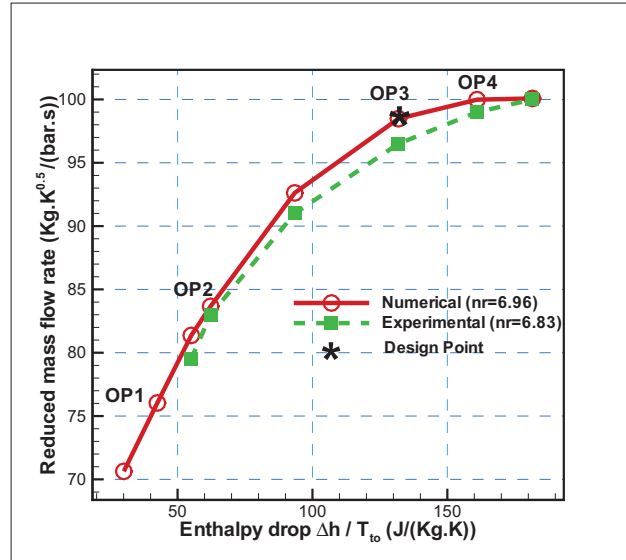


Figure 5.1: E/TU-3 turbine performance curve at design speed

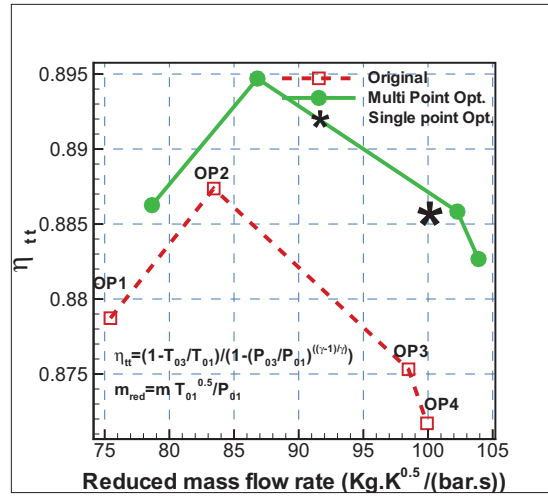
Generally all speed lines converge at choke hence limiting the mass flow rate as the back pressure is further reduced. The design point is usually close to choking conditions. The isentropic efficiency is also changing as the mass flow rate is varying while the rotational speed is fixed. At flow coefficient values lower than the design value, the rotor incidence angle decreases while, at values higher than the design

Table 5.3: Design speed line operating points

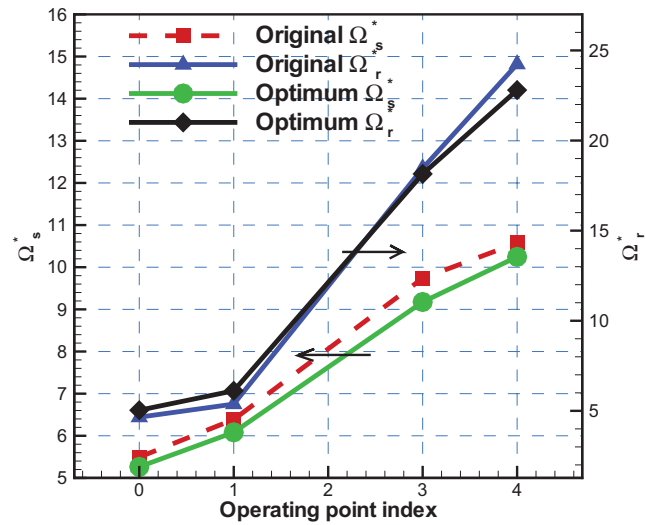
Case	OP1	OP2	OP3	OP4
$P_3(Pa)$	154023	141324	95123	75512
$\dot{m}_{red} (Kg.\sqrt{K}/bar.s)$	76.034	83.665	98.476	99.983
P_{01}/P_{03}	1.2135	1.3220	1.8357	2.1198
$\Delta h/T_{01}(J/(Kg.K))$	42.498	62.248	131.840	161.017

value the stator throat tends to choke. Given these facts, the isentropic efficiency is dropping at these two extremes. Therefore multi-point optimization is necessary to improve the performance over the entire operating range. For this purpose eight points were selected on the design speed line to study the turbine performance. To simulate the flow field at different points on the speed line, the static pressure at stage exit (which is also the boundary condition at exit) for the CFD simulation is varied while the boundary conditions at stage inlet are fixed, namely total pressure and temperature and two flow angles. The results, given in Fig. 5.1, indicate a reasonably good agreement between the numerical and experimental data. It must be mentioned that experimental data are not available for the design speed line ($n_r = 6.9679$). Therefore the closest speed line ($n_r = 6.833$) is chosen for comparison. Four points on the design speed line ($n_r = 6.9679$) are selected for optimization: points OP1, OP2, OP3, OP4 as shown in Fig. 5.1 are considered sufficient to represent different flow coefficients. OP3 is actually the design point. The stage outlet pressure, reduced mass flow and stage loading of mentioned points are listed in Table 5.3.

All the geometry candidates are analyzed using CFD at all four points to create the ANN database. Then four ANN networks are trained and tested for each objective function and for the constraint. Each ANN has six inputs and one output. The inputs include the five design variables of the stacking curve and one for the back pressure. The output corresponds to the mass flow rate and one of the variables appearing in the objective function namely the efficiency, streamwise vorticity at stator and rotor outlets.



a. Isentropic efficiency



b. Streamwise vorticity

Figure 5.2: Individual objectives at the four pre-selected points

Table 5.4: Original and optimum values of design variables and their range of variation

Case	α_s	β_s	α_r	β_r	w_{r1}
Min	-36	-8	-5	-10	0
Max	0	12	20	15	3
Original blades	-7.3	6.9	0	0	0
Optimum blades	-34.1	8.3	19.7	-9.7	0.1

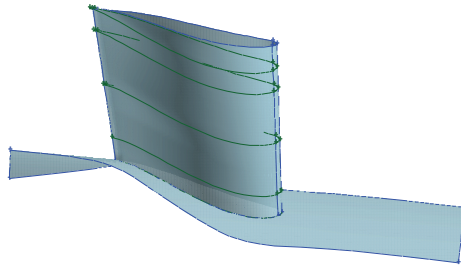
There are 50 members in each generation of GA. The cross-over and mutation probabilities are set to 0.2 and 0.7 respectively. Two elite members are kept in each generation to be passed directly to the next generation.

The ANN-based optimum stage profile is also simulated at all 4 operating points. Figure 5.2.a shows that the optimization strategy has successfully improved the stage performance at all four operating points. The design point efficiency is improved by 1.05%. The only improvement in terms of averaged streamwise vorticity is Ω_r^* at OP3 and OP4.

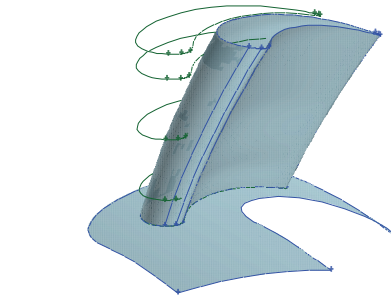
The optimum stator and rotor blade shapes are indicated in Figs. 5.3 and the optimum design variables are listed in Table 5.4. The stator blade is swept backward and the rotor blade is swept forward. Stator lean is close to the lower limit whereas rotor lean is toward the higher limit. Negative lean results in unloading the hub and loading the tip while positive lean loads the hub and unloads the tip. The proposed bowing intensity is zero. This is due to the fact that for this case the rotor inlet flow is rather uniform. Note that a non-uniform flow can produce strong secondary flows, and bowing the blade can push the end-wall flows to midspan where the flow is away from end-wall the effects.

Physical characteristics

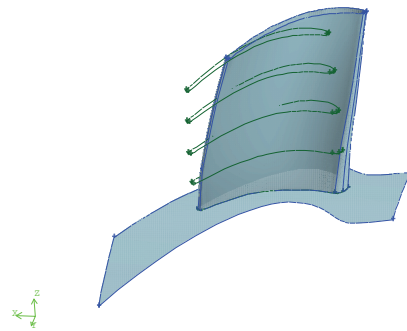
Knowing that the design point (OP3) is close to choke, the flow condition for OP4 is even more critical. The lower half-span is choked which explains the efficiency drop at OP4. The Mach iso-surfaces of the original and optimum blades, which is



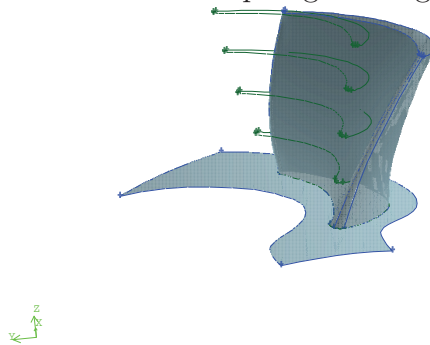
a. Stator: sweep angle change



b. Stator: lean angle change



c. Rotor: sweep angle change



d. Rotor: lean angle change

Figure 5.3: Original and optimum stator and rotor blades (wire frames refer to original geometry)

Table 5.5: Comparison of single and multipoint optimization

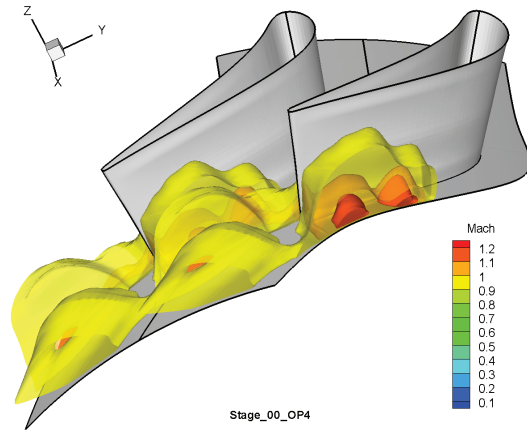
Case	α_s°	β_s°	α_r°	β_r°	w_{r1}	$\eta_{tt}\%$	\dot{m}
Original	-7.3	6.9	0	0	0	87.22	10.35
Single point opt.	-36	-2.5	2.2	-9.7	0.05	88.56	10.64
Multi-point opt.	-34.1	8.3	19.7	-9.6	0.1	88.58	10.77%

shown in Fig. 5.4 for OP4, indicates that half the suction side is supersonic for the original geometry. Whereas, in the redesign case, however, the supersonic region is significantly reduced, leading to a significant efficiency gain. Also the interaction between the supersonic region and the boundary layer caused a large corner stall at the stator hub SS-TE corner; this region is also reduced in the redesigned stator. To visualize the separation region near the stator hub, streamlines near the SS are plotted in Fig. 5.5 for the original and the redesigned stator where separation is delayed, Fig. 5.5.b.

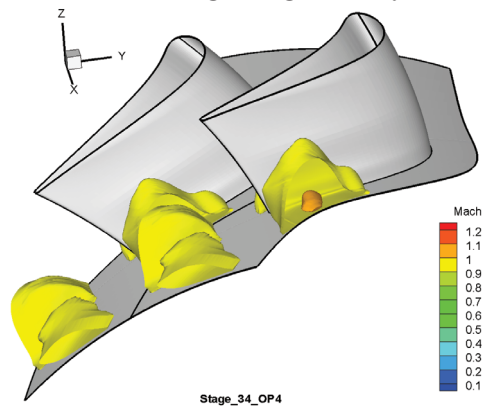
The design variables namely: the blade lean, sweep and bow, affect rather strongly the spanwise loading distribution, as can be seen in the isentropic Mach number plots at different spanwise locations of the stator blade, Fig. 5.6. In the optimum design, the tip loading is increased while the hub loading is decreased, due to the negative, see listed in Table 5.4. The separation can also be seen in Fig. 5.6.a by noting the large drop of isentropic Mach number on the SS near the TE.

The rotor blade loading given in terms of the pressure coefficient, Fig. 5.7, shows that it has increased near the hub and decreased near tip, this is due to the positive lean present in the optimum blade case.

The choice of streamwise vorticity as an optimization objective to be minimized for turbines is due to the fact that it is directly related to secondary flow which is a major source of losses in turbines. This choice of objective would be even more useful in reducing secondary flow losses when the inlet flow boundary layer or shear layer exist. Figure 5.8 show contours the dimensionless streamwise vorticity at a quarter chord downstream of the stator TE, where the maximum value of Ω_r^* is reduced in

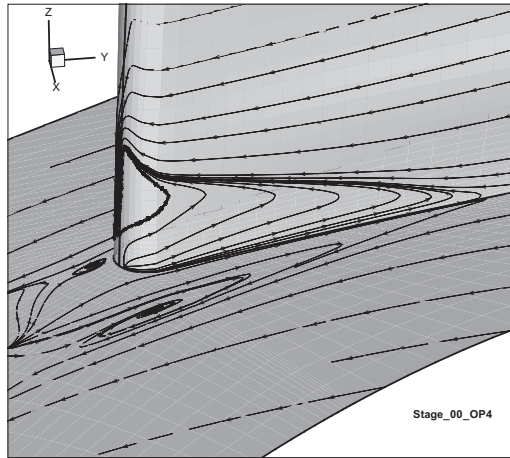


a. Original geometry

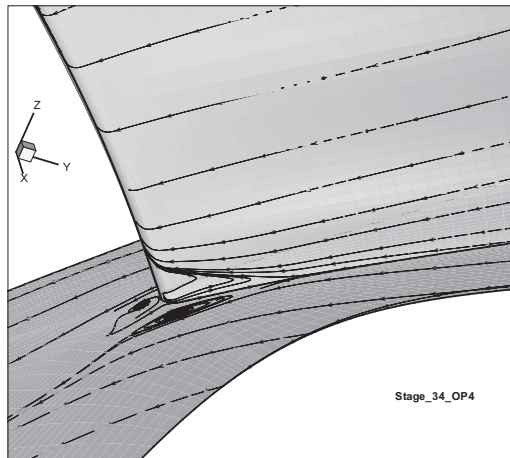


b. Multi-point optimum geometry

Figure 5.4: Mach iso-surfaces of stator blade at OP4

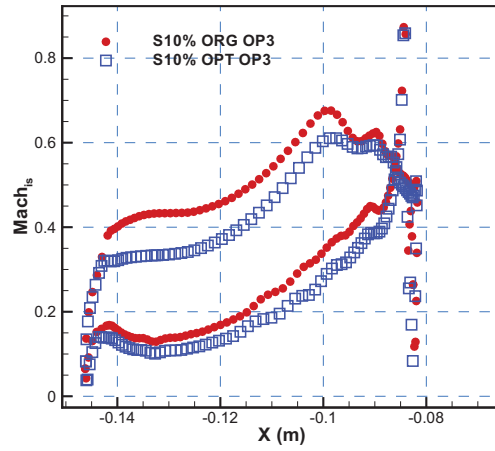


a. Original geometry

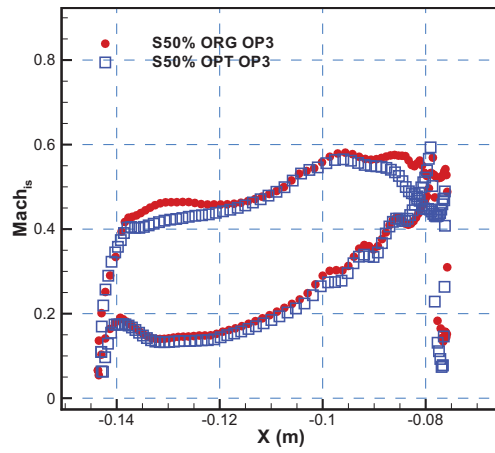


b. Multi-point optimum geometry

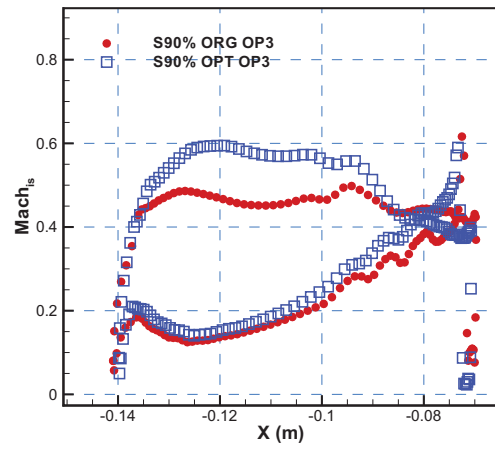
Figure 5.5: Reduction of corner stall in stator SS-TE region at OP4



a. At 10% span

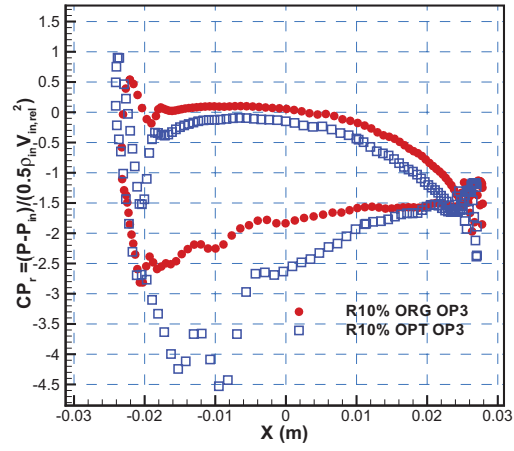


b. At 50% span

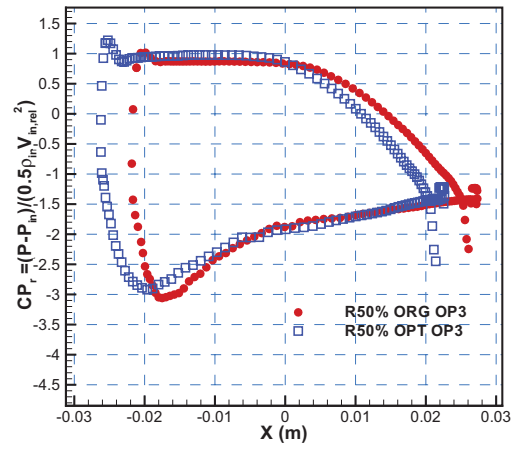


c. At 90% span

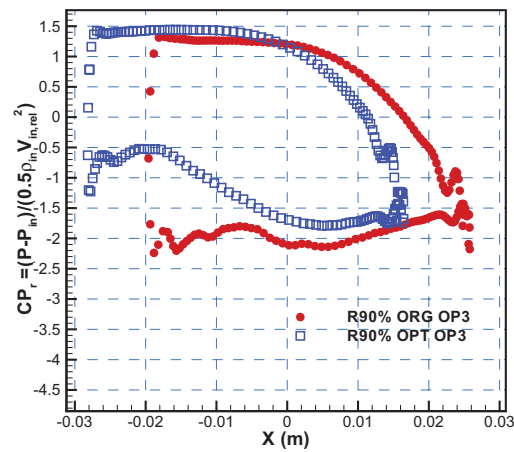
Figure 5.6: Isentropic mach across stator blade at OP3



a. At 10% span

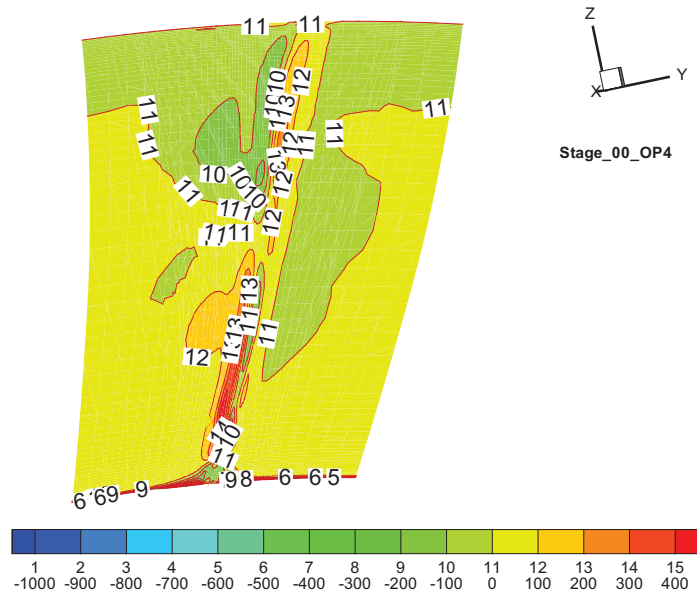


b. At 50% span

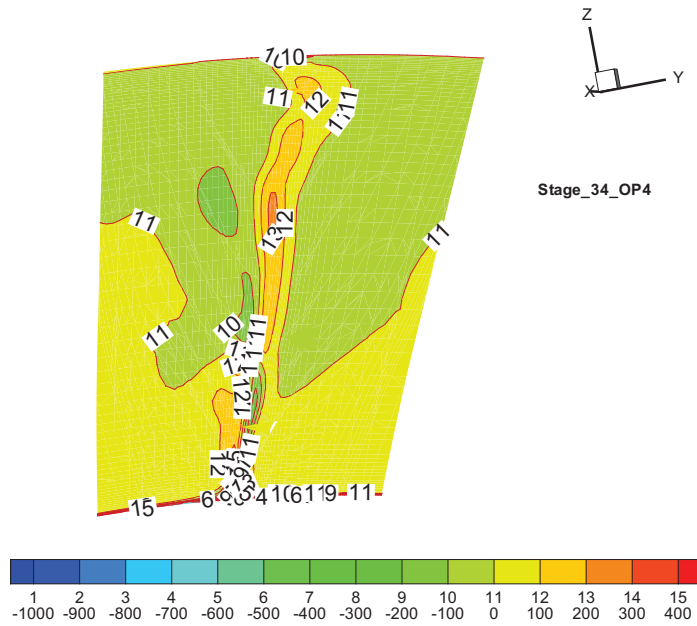


c. At 90% span

Figure 5.7: Pressure coefficient for rotor blade at OP3



a. Original geometry



b. Multi-point optimum geometry

Figure 5.8: Streamwise vorticity at rotor trailing edge at OP4

the optimum blade.

As a comparison between the single point and multi-point optimization results, the Case 1 presented in chapter 4 is compared with the multi-point optimum case in Table 5.5. The stator lean and rotor sweep are approximately identical in both cases. The main difference is in the stator sweep and rotor lean angle. The total-to-total efficiency of both cases at the design point is also nearly identical. However, mass flow rate for the multi-point optimum case changed by 4.0%.

As a concluding remark, the single-point and multi-point optimizations of a single-stage turbine were carried out using the same design variables. The optimum blade shape corresponding to single-point optimization is different from the one for multi-point optimization as indicated in Table 5.5. The efficiency improvement for single point optimization is 0.4% and 1.05% for multi-point optimization.

Chapter 6

Conclusion

6.1. Summary

Three dimensional aerodynamic shape optimization of turbine blades and stages is presented in this thesis. Despite the complexity of the loss mechanism in turbine blades, the use of genetic algorithm combined with the ANN proved to be an efficient and practical choice particularly when used with an effective blade shape parameterization method. Several optimization cases are carried out and are discussed; The cases show the effectiveness of the present methodology in the automatic optimization of turbine blades.

6.2. Concluding remarks

- The use of QRBC to parameterize the stacking line and stagger angle is a key in the successful optimization of the cases presented in this work. With the QRBC representation of the stacking curve, it can be parameterized with as low as only five design variables to vary the lean, sweep and both compound lean and sweep. The last two are referred to as bowing. The smooth hence feasible shape provided by QRBC, makes it a useful method in stacking optimization

of the blades.

- The application of GA as a global optimizer combined with ANN as low order approximation proved to be a successful and practical method for shape optimization with 3D viscous problems. The improvements made in the ANN model increased the accuracy in computing the objective function and hence reducing the overall computing time.
- When optimizing the rotor or the stator, the flow simulations should be done for the whole stage to account for the interaction between the two blade rows.
- The reduced mass flow rate and the stage reaction must be constrained in the stage optimization. Losses such as shock losses or secondary flow losses are usually proportional to the mass flow rate. Keeping a constant reduced mass flow rate ensures to have the same flow coefficient on the turbine map. This would also reduce any inconsistency for turbine and compressor matching.
- The stacking of the blade profiles is an effective way of redistributing the spanwise loading. This would basically help reduce losses associated with shock, transonic flow, secondary flow, boundary layer flow and tip clearance flow. A positive lean angle which moves the tip towards the suction side shifts the loading from the tip to the hub. The negative lean moves the loading from the hub to the tip. The compound lean or the bowing intensity, in the absence of lean and sweep results in loading or unloading the end-walls depending on its direction. The sweep also redistribute the loading. It can shift the loading in the chordwise direction. The stacking optimization can significantly improve the aerodynamic performance without even the need to redesign the individual 2D profiles. The stacking optimization for turbine rotor is tolerated from the structural point of view as the blades are sufficiently thick.

- Re-stacking can directly reduce some source of losses such as boundary layer losses, secondary flow and shock losses. Re-staggering can influence the leading and trailing edge losses. Simultaneous optimization of the re-stacking and re-staggering of the blade profiles gives more control on the losses and hence more room for improvement.

6.3. Contributions

The summary of the contributions of this work can be summarized as the following:

1. A practical stacking curve parameterization is developed by means of quadratic rational Bézier curve for turbine blades. It integrates the geometrical parameters with the design variables of stacking namely the lean angle, sweep angle and bowing of the blade. Its ability to represent the conic curves without the chance of infeasible geometry for turbine blades such as having inflexion point makes it unique.
2. Stagger angle spanwise variation is usually linear which is not necessarily optimum. A stagger angle spanwise distribution parameterization is developed differently for stator and rotor blades of turbine by means of QRBC. The parameterization is developed in a way to keep the throat area of the blade nearly constant for stator blades. The geometrical parameters are integrated with the physical design variables.
3. Streamwise vorticity is introduced in the objective function of turbine stage aerodynamic optimization to control directly the secondary flow loss which constitutes a considerable portion of the aerodynamic loss. A simple and efficient objective function is introduced which integrates the isentropic efficiency and streamwise vorticity for gas turbine blade optimization.

4. The current optimization methodology is improved with reducing the surrogate model generalization error. Early stopping and k-fold cross validation, Chapter 2, are implemented into the training process of the ANN.
5. A simplified structural model is developed to assess the order of magnitude of stress due to bending moments at the blade root while changing the blade stacking of the blade.
6. Single-point and multi-point aerodynamic optimization of a turbine stage are carried out with a developed parameterization of stacking curve and stagger angle spanwise distribution.

6.4. Future work

- The compressor blades are usually swept back to reduce the adverse effects of shocks. It would be interesting to apply the QRBC stacking parameterization to compressor and or fan blades. Also the wind turbine blades have a high twist in the spanwise direction. The use of QRBC in representing the wind turbine spanwise blade twist distribution might be helpful.
- The surrogate-based optimization is highly dependent on the accuracy of the surrogate model. The accuracy of the model can be improved during the optimization cycle by enriching the database that trains the model. The merit function is a useful method to explore and exploit the design space efficiently. It is definitely better to have it implemented in the current optimization algorithm.
- This work opened the door for aerodynamic optimization of turbine blades. however,

- This work can provide a lot of knowledge about 3D effects of stacking and twist of the blades based on the database of geometries and their physical implications. A keen designer can benefit from them and can further improve the flow features with local optimization of presented optimum cases.

Bibliography

- [1] M. V. Casey, *Turbomachinery design using CFD*. AGARD-LS-195, 1994.
- [2] J. Weiss and F. J. Kelecy, “Numerical simulation of steady-state flow through a multi-stage turbine using unstructured meshes,” *Proceedings of the 3rd ASME/JSME joint fluids engineering conference, FEDSM99:6862*, 1999.
- [3] L. Fottner, “Test cases for computation of internal flows in aero engine components,” *AGARD-AR-275*, 1990. Propulsion and Energetics Panel.
- [4] E. popov, *Engineering mechanics of solids*. Prentice-Hall Pub ,2nd ed., 1998.
- [5] B. Lakshminarayana, *Fluid dynamics and heat transfer of turbomachinery*. John Wiley & Sons, 1996.
- [6] K. Daneshkhah, *Aerodynamic inverse design of turbomachinery blading in two-dimensional viscous flow*. PhD thesis, Concordia university, 2006.
- [7] T. Verstraete, *Multidisciplinary turbomachinery component optimization considering performance, stress, and internal heat transfer*. Von Karman Institute for Fluid Dynamics, Turbomachinery and Propulsion Department, 2008.
- [8] T. Mengistu, *Aerodynamic design and optimization of turbomachinery blading*. PhD thesis, Concordia University, Mechanical and Industrial Engineering, 2005.
- [9] D. E. Goldberg, *Genetic algorithms in search, optimization and machine learning*. Addison-Wesley, 1985.

- [10] K. Deb, *Multi-objective optimization using evolutionary algorithms*. John Wiley and Sons, 2001.
- [11] R. V. den Braembussche, *Strategies for optimization and automated design of gas turbine engines*. RTO-MP-AVT-167, ISBN 978-92-837-0124-8, 2010.
- [12] T. Mengistu and W. Ghaly, “Single and multipoint shape optimization of gas turbine blade cascades,” *AIAA paper 2004-4446*, 2004.
- [13] T. Goel, R. Haftka, W. Shyy, and N. V. Queipo, “Ensemble of multiple surrogates,” *Structural and Multidisciplinary Optimization*, vol. 33(3), pp. 199–216, 2007.
- [14] A. Younis, J. Gu, and G. Li, “Trends, features, and tests of common and recently introduced global optimization methods,” *12th AIAA/ISSMO Multidisciplinary analysis and optimization conference, Canada*, 2008.
- [15] J. Vad, “Aerodynamics effects of blade sweep and skew in low-speed axial flow rotors at the design flow rate: an overview,” *Journal of Power and Energy*, vol. 222, 2008.
- [16] S. Gallimore, J. Bloger, and et. al., “The use of sweep and dihedral in multi-stage axial flow compressor blading- part 1: University research amd methods developement,” *Journal of turbomachinery*, vol. 124, pp. 521–532, Oct 2002.
- [17] J. D. Denton, A. M. Willis, D. Borthwick, J. Grant, and I. Ritchey, “The three-dimensional design of low aspect ratio 50 reaction turbines. latest advances in the aerodynamics of turbomachinery with special emphasis, upon secondary flows,” *IMechE Seminar, Dec. 9-10, Rugby, U.K. Paper S461/008/96*, 1996.
- [18] N. G. Harvey, G. R. Martin, M. D. Taylor, S. Shahpar, J. Hartland, and D. Smith, “Nonaxisymmetric turbine end wall design: Part i- three-dimensional linear design system,” *Journal of Turbomachinery*, vol. 122, p. 278, 2000.

- [19] R. Amano and C. Xu, "Blade swept effect of turbomachinery," *Aerospace Science Meeting and Exhibit*, vol. 2005-43, 2005.
- [20] I. potts, "The importance of s1 surface twist in the analysis of inviscid flow through swept linear turbine cascade," *I. Mech. Eng.*, vol. C258-87, 1987.
- [21] Sasaki and Breugelmans, "Comparison of sweep and dihedral effects on compressor cascade performance," *ASME paper 97-GT-2*, 1997.
- [22] C.-M. JANG and K.-Y. KIM, "Optimization of a stator blade using response surface method in a single stage transonic axial compressor," *J.Power and Energy, Proc.IMEchE Vol.219 Part A*, 2005.
- [23] F. Pouzadouxa, E. Taillefer, and M. Masmoudi, "Introduction of multidisciplinary optimization in compressor blade design," *12th AIAA/ISSMO*, 2008.
- [24] S. Harrison, *The influence of blade stacking on turbine losses*. PhD thesis, Cambridge University, 1989.
- [25] M. J. Atkins, "Secondary losses and end wall profiling in a turbine cascade," *In Proceedings of IMechE Conference, paper C255/87 pp. 29-42.*, 1987.
- [26] M. G. Rose, "Non-axisymmetric endwall profiling in the hp ngv's of an axial flow gas turbine," *ASME paper 94-GT-249*, 1994.
- [27] N. W. Harvey, G. Brennan, D. A. Newman, and M. G. Rose, "Improving turbine efficiency using non-axisymmetric endwalls: validation in the multi-row environment and with low aspect ratio blading," *ASME Paper GT-2002-30337*, 2002.
- [28] J. Denton and L. Xu, "The exploitation of three-dimensional flow in turbomachinery design," *Proc Instn Mech Engrs*, vol. 213 Part C, 1999.

- [29] S. Pierret, “Three-dimensional blade design by means of an artificial neural network and navier-stokes solvers.” VKI lecture series 1999-02, 1999.
- [30] D. Bagshaw, G. Ingram, D. Gregory-smith, M. Stokes, and N. Harvey, “The design of three-dimensional turbine blades combined with profiled endwalls,” *Proc. IMechE, journal of power and energy*, vol. 222 Part A, p. 278, 2008.
- [31] P. Lampart, S. Yershov, and A. Rusanov, “Increasing flow efficiency of hp and lp steam turbine stages from numerical optimization of 3d blading,” *Engineering optimization*, vol. 37, pp. 145–166, 2005.
- [32] A. M. Wallis and J. Denton, “Comparison of design intent and experimental measurements in a low aspect ratio axial flow turbine with three-dimensional blading,” *ASME paper 98-GT-516*, 1998.
- [33] S. Yershov, A. Rusanov, A. Shapochka, P. Lampart, J. Swirydczuk, and A. Gardzilewics, “Shape optimization of two turbine stage using the deformed polyhedron method and a 3d rans solver,” *J. of Power Engineering*, vol. 216-2, pp. 203–213, 2002.
- [34] P. Lampart and S. Yershov, “Direct constrained cfd-based optimization of 3d blading for the exit stage of a large power steam turbine,” *Trans. ASME J. Eng Gas Turbines Power*, vol. 125(1), pp. 385–390, 2001.
- [35] S. Harrison, “The influence of blade lean on turbine losses,” *ASME Journal of Turbomachinery*, vol. 114, pp. 184–190, 1992.
- [36] G. Singh, P. Walker, and B. Haller, “Development of three-dimensional stage viscous time marching method for optimization of short height stages,” *Proceedings of European Conf. on Turbomachinery, Fluid Dynamics and Thermodynamics Aspects*, 1995.

- [37] Z. Wang and L. Xu, “Three-dimensional theory and design method of bowed-twisted blade and its application to turbomachineries,” *VKI LS*, vol. 1999-02, 1999.
- [38] I. Akmandor and O. Oksuz, “Multi-objective aerodynamic optimization of axial turbine blades using a novel multi-level genetic algorithm,” *Proceeding of ASME Turbo Expo GT2008-50521*, 2008.
- [39] A. Clarich, G. Mosetti, V. Pediroda, and C. Poloni, “Application of evolutionary algorithms and statistical analysis in the numerical optimization of an axial compressor,” *International journal of rotating machinery*, vol. 2, pp. 143–151, 2005.
- [40] T. Mengistu, W. Ghaly, and T. Mansour, “Global and local shape aerodynamic optimization of turbine blades,” *AIAA 2006-6933*, 2006.
- [41] N. Chen, *Aerothermodynamics of turbomachinery, analysis and design*. John Wiley & Sons, 2010.
- [42] L. Piegl and W. Tiller, *The NURBS book*. Springer, 1995.
- [43] C. Hirsch, *Numerical computation of internal and external flows*. Butterworth-Heinemann, 2nd ed., 2007.
- [44] P. Spalart and S. Allmaras, “A one-equation turbulence model for aerodynamic flows,” Technical Report AIAA-92-0439, American Institute of Aeronautics and Astronautics, 1992.
- [45] www.ansys.com, *Ansys Fluent 12.0 theory guide*, 2009.
- [46] J. Denton, “Extension of the finite volume time marching method to three dimensions.” VKI lecture series, 1979-7.

- [47] R. V. chima, "Calculation of multi-stage turbomachinery using steady characteristic boundary conditions," *36th aerospace sciences meeting and exhibit, AIAA98-0968*, 1998.
- [48] J. Denton, "Computational fluid dynamics for turbomachinney design," *Proceeding of instituite of mechanical engineers*, vol. 213 Part C, pp. 107–124, 1999.
- [49] B. Tang, "Orthogonal array-based latin hypercubes," *Journal of the American Statistical Association*, vol. 88 (424), pp. 1392–1397, 1993.
- [50] S. Haykin, *Neural networks: A comprehensive foundation*. 2nd Edition, Prentice-Hall, 1999.
- [51] V. Sivashanmugam, "Three dimensional aero-structural shape optimization of turbomachinery blades," Master's thesis, Concordia university, 2011.
- [52] R. H. Myers and D. C. Montgomery, *Response surface methodology-process and product optimization using designed experiments*. John Wiley & Sons, New York, 1995.
- [53] T. Mengistu and W. Ghaly, "Aerodynamic design of gas turbine cascades using global optimizers and artificial neural networks," *ICCFD3*, Jul 2004.
- [54] H. Saravanamuttoo, G. Rogers, and H. Cohen, *Gas turbine theory*. Prentice-Hall, 2001.
- [55] J. Denton, "Loss mechanisms in turbomachines," *Journal of turbomachinery*, vol. 115, pp. 621–656, 1993.
- [56] M. Arabnia and W. Ghaly, "A strategy for multi-point shape optimization of turbine stages in three-dimensional flow," *Proceedings of Turbo Expo 2009, GT2009-59708*, 2009.

- [57] M. Arabnia and W. Ghaly, “A strategy for multi-objective optimization of turbine stages in three-dimensional flow,” *AIAA-2008-5808*, 2008.
- [58] Ansys, *Ansys-Fluent user manual*. Ansys, USA, 12.0.16 ed., 2009. See also URL <http://www.ansys.com>.

Appendix A

Quadratic rational Bézier curve (QRBC)

In this appendix, QRBC and its derivative are derived. Some features of the curve are mentioned.

A.1. Definition

The rational Bézier curve adds adjustable weights to provide closer approximations to arbitrary shapes. The numerator is a weighted Bernstein-form Bézier curve and the denominator is a weighted sum of Bernstein polynomials. Rational Bézier curves can, among other uses, be used to represent segments of conic sections exactly. Given $n + 1$ control points P_i , the rational Bézier curve can be described by [42]:

$$\vec{C}(u) = \frac{\sum_{i=0}^n \binom{n}{i} u^i (1-u)^{n-i} P_i w_i}{\sum_{i=0}^n \binom{n}{i} u^i (1-u)^{n-i} w_i} \quad (\text{A.1})$$

QRBC is a second degree NURBS curve with three control points defined as follows:

$$\vec{C}(u) = \frac{(1-u)^2 w_0 \vec{P}_0 + 2u(1-u)w_1 \vec{P}_1 + u^2 w_2 \vec{P}_2}{(1-u)^2 w_0 + 2u(1-u)w_1 + u^2 w_2} \quad (\text{A.2})$$

The first derivative of the QRBC is:

$$\begin{aligned} \vec{C}'(u) = \frac{1}{A^2} [2(1-u)A - A'(1-u)^2] P_0 w_0 + [(2-4u)A - 2A'u(1-u)] P_1 w_1 + \\ [2uA - u^2 A'] P_2 w_2 \end{aligned} \quad (\text{A.3})$$

where:

$$A(u) = ((1-u)^2 w_0 + 2u(1-u)w_1 + u^2 w_2) \quad (\text{A.4})$$

Therefore the first derivatives at the end points are as follow:

$$C'(u) = \begin{cases} \frac{2w_1}{w_0} (P_1 - P_0) & u=0, \\ \frac{2w_1}{w_2} (P_2 - P_1) & u=1. \end{cases} \quad (\text{A.5})$$

The slope of the curve at the end points is the function of the control points and the weights as shown in the above equation. In fact the slope of the curve at end points is the blade slope in the spanwise direction at hub and tip.

Appendix B

Governing equations

In this section, the governing equations used in simulating the 3D viscous flow in the turbine stage are briefly summarized. The flow motion of compressible viscous fluid is governed by the (Reynolds averaged Navier-Stokes equations). Spalart-Almaras turbulent model due to its simplicity and accuracy is chosen.

All the governing equations and turbulence model equations used for this research work are solved by Ansys-Fluent CFD package. They are presented in the following sections [58]

B.1. Reynolds averaged Navier-Stokes equations

The equations are derived from the conservation of mass (continuity), momentum and energy. The equations of motion are derived from Newton's second law for compressible, viscous and Newtonian fluid.

In Reynolds averaging, the solution variables in the instantaneous (exact) Navier-Stokes equations are decomposed into the mean (ensemble-averaged for unsteady flow or time-averaged for steady flow) and fluctuating components. For the velocity components:

$$u_i = \bar{u}_i + u_i' \quad (\text{B.1})$$

Where \bar{u}_i and u_i' are the mean and fluctuating velocity componenets (i=1,2,3). Likewise, for the pressure and other scalar quantities:

$$u_i = \bar{\phi} + \phi' \quad (\text{B.2})$$

where ϕ denotes a scalar such as pressure, temperature, ...

Substituting expressions of this form for the flow variables into the instantaneous continuity and momentum equations and taking a time average (or ensemble) and dropping the overbar on the mean velocity, \bar{u} yields the ensemble-averaged momentum equations. They can be written in Cartesian tensor form as:

$$\frac{\partial \rho}{\partial t} + \frac{\partial}{\partial x_i}(\rho u_i) = 0 \quad (\text{B.3})$$

$$\frac{\partial}{\partial t}(\rho u_i) + \frac{\partial}{\partial x_j}(\rho u_i u_j) = -\frac{\partial p}{\partial x_i} + \frac{\partial}{\partial x_j}[\mu(\frac{\partial u_i}{\partial x_j} + \frac{\partial u_j}{\partial x_i} - \frac{2}{3}\delta_{ij}\frac{\partial u_l}{\partial x_l})] + \frac{\partial}{\partial x_j}(-\rho\overline{u_i' u_j'}) \quad (\text{B.4})$$

$$\frac{\partial}{\partial t}(\rho E) + \nabla \cdot (\vec{v}(\rho E + p)) = \nabla \cdot (k_{eff}\nabla T - \sum_j h_j \vec{J}_j + (\overline{\tau_{eff}} \cdot \vec{v})) \quad (\text{B.5})$$

where E is the total enthalpy and k_{eff} is the effective conductivity and τ_{eff} is effective viscosity for viscous dissipation term.

Equations B.3 and B.4 are called Reynolds-averaged Navier-Stokes (RANS) equations. They have the same general form as the instantaneous Navier-Stokes

equations, with the velocities and other solution variables now representing ensemble-averaged (or time-averaged) values. Additional terms now appear that represent the effects of turbulence. These Reynolds stresses, $\overline{u_i u_j}$, must be modeled in order to close Equation B.4 . For variable-density flows, Equations B.3 and B.4 can be interpreted as Favre-averaged Navier-Stokes equations, with the velocities representing mass-averaged values. As such, Eq. B.3 and B.4 can be applied to density-varying flows.

Equation B.5 is the energy equation. k_{eff} is the effective conductivity ($k + k_t$), where k_t is the turbulent thermal conductivity defined in turbulence model. \vec{J}_j is the diffusion flux of species j . The first three terms on the right hand side of the Eq. B.5 represent energy transfer by conduction, species diffusion and viscous dissipation, respectively.

B.2. Spalart-Almaras turbulence model

A brief overview of Spalart-Almaras turbulence model is given in this section. The Spalart-Almaras turbulence model was developed

B.2.1 Description of the model

The transported variable in the Spalart-Allmaras model, $\tilde{\nu}$, is identical to the turbulent kinematic viscosity except in the near-wall (viscosity-affected) region. The transport equation for $\tilde{\nu}$ is:

$$\frac{\partial}{\partial t}(\rho\tilde{\nu}) + \frac{\partial}{\partial x_i}(\rho\tilde{\nu}u_i) = G_\nu + \frac{1}{\sigma_{\tilde{\nu}}}\left[\frac{\partial}{\partial x_j}\left((\mu + \rho\tilde{\nu})\frac{\partial\tilde{\nu}}{\partial x_j}\right) + C_{b2}\rho\left(\frac{\partial\tilde{\nu}}{\partial x_j}\right)^2\right] - Y_\nu + S_i \quad (\text{B.6})$$

where G_ν is the production of turbulent viscosity, and Y_ν is the destruction of turbulent viscosity that occurs in the near-wall region due to wall blocking and viscous damping. $\sigma_{\tilde{\nu}}$ and C_{b2} are two constants and ν is the molecular kinematic

viscosity. $S_{\bar{\nu}}$ is a user-defined source term. Note that the turbulence kinetic energy, κ , is not calculated in the Spalart-Allmaras model.

The Reynolds-averaged approach to turbulence modeling requires that the Reynolds stresses in Eq. B.4 be appropriately modeled. A common method employs the Boussinesq hypothesis to relate the Reynolds stresses to the mean velocity gradients as shown in Eq. B.2.1:

$$-\overline{\rho u_i' u_j'} = \mu_t \left(\frac{\partial u_i}{\partial x_j} + \frac{\partial u_j}{\partial x_i} \right) - \frac{2}{3} \left(\rho \kappa + \mu_t \frac{\partial u_k}{\partial x_k} \right) \delta_{ij} \quad (\text{B.7})$$

The Boussinesq hypothesis is used in the Spalart-Allmaras model. The advantage of this approach is the relatively low computational cost associated with the computation of the turbulent viscosity, μ_t . Only one additional transport equation (representing turbulent viscosity) is solved. The disadvantage of Boussinesq hypothesis is the assumption of isotropic scalar turbulent viscosity.

Appendix C

Some notes on surrogate modeling

In this appendix the universal approximation theory is stated. This is an important statement which sets the theoretical background for approximation with artificial neural networks. Two generic function that usually used for validation are defined.

C.1. Universal approximation theory

The universal approximation theory for single layer network states [50]:

”Let $\varphi(\cdot)$ be a nonconstant, bounded and monotone-increasing continuous function. Let I_{m_0} denote the m_0 -dimensional unit hypercubic $[0, 1]^{m_0}$. The space of continuous functions on I_{m_0} is denoted by $C(I_{m_0})$. Then, given any function $f \in C(I_{m_0})$ and $\epsilon > 0$, there exist an integer m_1 and sets of real constant α_i , b_i and w_{ij} where $i = 1, \dots, m_1$ and $j = 1, \dots, m_0$ such that we may define:

$$F(x_1, \dots, x_{m_0}) = \sum_{i=1}^{m_1} \alpha_i \varphi\left(\sum_{j=1}^{m_0} w_{ij} x_j + b_i\right) \quad (\text{C.1})$$

as an approximate realization of the function $f(\cdot)$; that is,

$$|F(x_1, \dots, x_{m_0}) - f(x_1, \dots, x_{m_0})| < \epsilon \quad (\text{C.2})$$

for all x_1, x_2, \dots, x_{m_0} that lie in the input space.”

C.2. Used generic functions

The following generic functions [8] are normally used in surrogate modeling as test functions.

Rosenbrock function:

$$f(X) = \sum_{i=1}^{n-1} [(1 - x_i)^2 + 100(x_{i+1} - x_i^2)^2] \quad (\text{C.3})$$

Speed reducer function:

$$\begin{aligned} f(X) = & 0.78x_1x_2^2(3.33x_3^2 + 14.93 * x_3 - 43.09) - \\ & 1.5 * x_1 * (x_6^2 + x_7^2) + 7.47 * (x_6^3 + x_7^3) + \\ & 0.78 * (x_4 * x_6^2 + x_5 * x_7^2) \end{aligned} \quad (\text{C.4})$$

C.3. ANN accuracy

All the explained techniques and improvements explained in Chapter 2 for the ANN training code are applied for training the Rosenbrock function. The Rosenbrock function has been selected and modeled by ANN back propagation with a 2-31-1 architecture of the network which contains 2 input nodes (n=2), 31 hidden nodes

Table C.1: Rosenbrock function approximation with ANN: Predicted value vs. actual value of testing sample points

Cases	Actual value	Target value	% Error
1	190.58	202.53	6.3
2	355.24	350.13	1.4
3	144.40	131.35	9.0
4	18.82	26.58	41.3
5	646.38	613.48	5.1
6	405.01	382.16	5.6
7	1585.90	1560.40	1.6
8	782.45	793.28	1.4
9	91.46	84.88	7.2
10	548.71	595.38	8.5
11	505.72	523.77	3.6
12	193.22	173.01	10.5
13	1153.90	1159.35	0.5
14	94.10	95.46	1.5
15	352.18	321.95	8.6
16	328.82	321.03	2.4
17	763.54	735.83	3.6
18	21.10	23.17	9.8
19	205.30	260.01	26.6
20	33.28	29.83	10.4

and 1 output node where x_i varies between ± 2.0 . The approximation was done using the 100 representative sample points selected using the Latin-Hypercube method over the specified domain. Then 80 sample points are used for training. The hyperbolic tangent function is chosen as a transfer function.

When all the modifications and improvements described in Section 2.3.3 are implemented into the ANN model, the results thus obtained show a significant improvement over the model that we started with namely, Mengistu [8]. The average and the maximum relative errors were reduced from 23% and 58% using the original implementation of Mengistu [8] to 8% and 41% respectively, using the current ANN model.